2017

IMPEDANCE-TO-SCATTERING MATRIX METHOD FOR LARGE SILENCER ANALYSIS

Peng Wang
University of Kentucky, bryanwangwp@gmail.com
Digital Object Identifier: https://doi.org/10.13023/ETD.2017.463

STUDENT AGREEMENT:

I represent that my thesis or dissertation and abstract are my original work. Proper attribution has been given to all outside sources. I understand that I am solely responsible for obtaining any needed copyright permissions. I have obtained needed written permission statement(s) from the owner(s) of each third-party copyrighted matter to be included in my work, allowing electronic distribution (if such use is not permitted by the fair use doctrine) which will be submitted to UKnowledge as Additional File.

I hereby grant to The University of Kentucky and its agents the irrevocable, non-exclusive, and royalty-free license to archive and make accessible my work in whole or in part in all forms of media, now or hereafter known. I agree that the document mentioned above may be made available immediately for worldwide access unless an embargo applies.

I retain all other ownership rights to the copyright of my work. I also retain the right to use in future works (such as articles or books) all or part of my work. I understand that I am free to register the copyright to my work.

REVIEW, APPROVAL AND ACCEPTANCE

The document mentioned above has been reviewed and accepted by the student's advisor, on behalf of the advisory committee, and by the Director of Graduate Studies (DGS), on behalf of the program; we verify that this is the final, approved version of the student's thesis including all changes required by the advisory committee. The undersigned agree to abide by the statements above.

Peng Wang, Student

Dr. Tingwen Wu, Major Professor

Dr. Haluk Karaca, Director of Graduate Studies

IMPEDANCE-TO-SCATTERING MATRIX METHOD FOR LARGE SILENCER ANALYSIS

DISSERTATION

A dissertation submitted in partial fulfillment of the requirements for the degree of Doctor of Philosophy in the College of Engineering at the University of Kentucky

By

Peng Wang

Lexington, Kentucky

Director: Dr. Tingwen Wu, Professor of Mechanical Engineering

Lexington, Kentucky

2017

ABSTRACT OF DISSERTATION

Impedance-to-Scattering Matrix Method for Large Silencer Analysis

Large silencers used in the power generation industry usually have a very large cross section at the inlet and outlet. Higher-order modes will populate the inlet and outlet even at very low frequencies. Although the silencer itself is often modeled by a three-dimensional analysis tool such as the boundary element method (BEM) or finite element method (FEM), a direct computation of the transmission loss (TL) from the BEM or FEM model can be challenging without incorporating certain forms of modal expansion.

A so-called “impedance-to-scattering matrix method” is proposed to extract the modes at the inlet and outlet from the BEM impedance matrix based on the point collocation method. The BEM impedance matrix relates the sound pressures at the inlet and outlet to the corresponding particle velocities, while the scattering matrix relates the modes at the inlet and outlet. Normally there are more boundary elements than the total number of modes at the inlet and outlet, and a least-squares procedure is used to condense the element-based impedance matrix to the mode-based scattering matrix. The TL computation will follow if a certain form of the incident wave is assumed and the outlet is non-reflective. Several commonly used inlet/outlet configurations are considered in this dissertation, which include axisymmetric, non-axisymmetric circular, and rectangular inlet/outlet shapes. In addition to the single inlet and outlet silencers, large multi-inlet and multi-outlet silencers are also investigated.

Besides the collocation-based impedance-to-scattering matrix method, an integral-based impedance-to-scattering matrix method based on the reciprocal identity is also proposed for large silencer analysis. Although it may be more time-consuming to perform the additional numerical integration, an integral-based method is free of any uncertainties associated with collocation points. The computational efficiency, accuracy and stability are compared between two proposed methods.

One bonus effect of producing the scattering matrix is that it can also be used to combine subsystems in series connection. The Redheffer’s star product is introduced to combine scattering matrices of subsystems.

In the design stage, rapid assessment of the silencer performance is always preferred. However, the existing analytical approaches are only suitable for simple

dissipative silencers such as straight lined ducts. A two-dimensional first-mode semi-analytical solution is developed to quickly evaluate the performance of tuned dissipative silencers below the cut-off frequency. The semi-analytical solution can also serve as a validation tool for the BEM.

KEYWORDS: Impedance matrix, scattering matrix, large silencers, boundary element method, transmission loss

Peng Wang

Student's Signature

11/17/2017

Date

IMPEDANCE-TO-SCATTERING MATRIX METHOD FOR LARGE SILENCER ANALYSIS

By

Peng Wang

Tingwen Wu
_____
Director of Dissertation

Haluk Karaca
_____
Director of Graduate Studies

11/17/2017
_____
Date

ACKNOWLEDGEMENTS

First of all, I would like to express my deepest appreciation to my major advisor, Dr. Tingwen Wu, for his valuable suggestions and insightful guidance for my Ph.D. study. It has always been enjoyable to have discussion with him to complete my all challenging projects. His encouragement, caring, patience helped me overcome many difficulties I have been facing through my research and finish this dissertation. I would also like to thank my co-advisor, Dr. David W. Herrin, for his support and help to develop my background in the field of noise and vibration control engineering.

I would also like to thank Dr. John Baker and Dr. Qiang Ye for being my committee members and providing helpful suggestions. Thanks also go to Dr. Lance Delong, who served as the Outside Examiner for my final doctoral examination.

I want to thank my colleagues, Connor Campbell, Huangxing Chen, Jonathan Chen, Keyu Chen, Gong Cheng, Shujian He, Aihua Huang, Xin Hua, Caoyang Li, Jundong Li, Jiazhu Li, Wanlu Li, Weiyun Liu, Kangping Ruan, Shishuo Sun, Robert Wick, Ruimeng Wu, Xin Yan, Nan Zhang, Yitian Zhang, Hao Zhou and Limin Zhou, for making my life enjoyable in Kentucky. I also want to thank Zeguang Tao, for his kind help and friendship. My appreciation goes to Rui Pan, for encouraging and inspiring me.

Finally, and most importantly, I would like to appreciate Mike&Tina Pepper and my parents, for their love and support.

TABLE OF CONTENTS

LIST OF TABLES

LIST OF FIGURES

Chapter 1 INTRODUCTION

1.1 Background

The power generation industry is the mainstay of the modern society, which supplies essential energy to the industrial development and our everyday life. However, a loud noise will be generated during the operation of the power plants, and noise complaints often arise from the nearby residents if it cannot be addressed appropriately. The combustion exhaust noise from the gas turbine is one of the major noise sources. To attenuate the sound level of the exhaust noise, large dissipative silencers are widely used in the power generation industry, such as the parallel-baffle silencers, round silencers, and rectangular lined ducts, as shown in Figure 1.1.

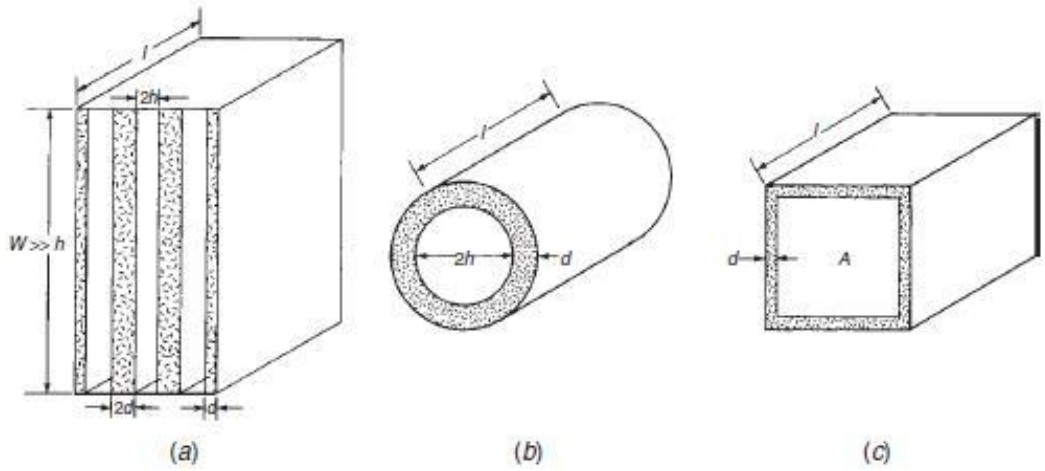

Figure 1.1 Geometry of typical dissipative silencer types: (a) parallel-baffle silencer; (b) round silencer; (c) rectangular lined duct. (Beranek and Vér, 2006)

1.1.1 Silencers

Silencers are the commonly used noise control devices for internal combustion engines, gas turbines, air-conditioning and ventilation systems (Munjal, 2014).

There are two different types of silencers: reactive silencers and dissipative silencers. Dissipative silencers shown in Figure 1.1 convert the acoustic energy to heat by using sound absorbing materials, and are suited to addressing medium to high frequency broadband noise because of the frequency characteristics of the absorbing materials (Wallin et al., 2012). Reactive silencers do not use sound absorbing materials but instead employ geometric design principles (Harris, 1991). By providing the impedance mismatch due to the sudden area change, noise is attenuated by reflection and cancellation of sound waves. Therefore, reactive silencers are normally used to abate sound consisting of discrete tones, especially in the low frequency region (Wallin et al., 2012). A typical reactive silencer is shown in Figure 1.2.

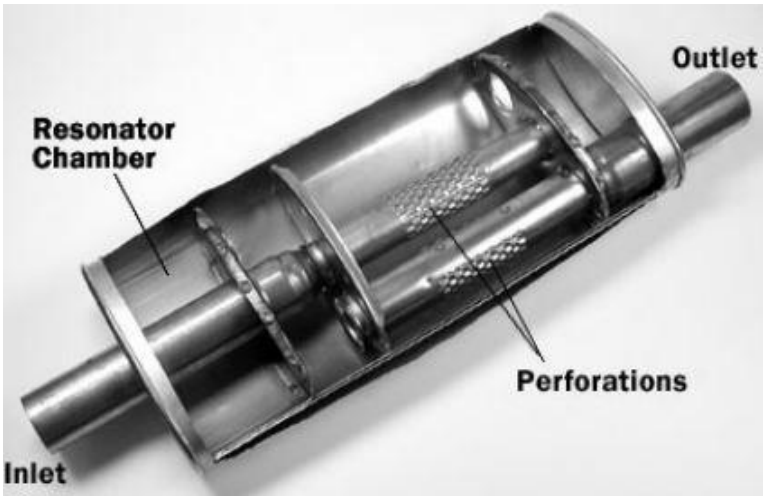

Figure 1.2 Typical reactive silencer. (Potente, 2005)

1.1.2 Acoustic performance criteria of silencers

The insertion loss (IL), transmission loss (TL) and noise reduction (NR) are three commonly used metrics to evaluate the acoustic performance of silencers (Munjal, 2014).

Insertion loss (IL) is defined as the change in the radiated sound pressure level (SPL) at a certain point resulting from the insertion of the silencer when compared to a straight pipe output without the silencer (Beranek and Vér, 2006).

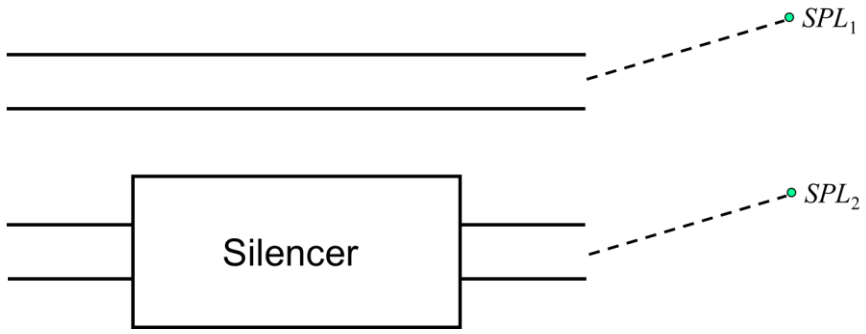

Figure 1.3 Definition of insertion loss of a silencer.

With reference to Figure 1.3, the insertion loss is defined by

$$IL = SPL_1 - SPL_2 = 20 \log_{10} \left| \frac{p_1}{p_2} \right| \quad (1.1)$$

Transmission loss (TL) is defined as the difference between the incident sound power level and the transmitted sound power level with an anechoic termination (Munjal, 2014).

Figure 1.4 Definition of transmission loss of a silencer.

With reference to Figure 1.4, the transmission loss is defined by

$$TL = 10 \log_{10} \frac{W_i}{W_t} \quad (1.2)$$

Noise reduction (NR) is the difference in sound pressure levels at two points one upstream and one downstream (Munjal, 2014), which is demonstrated in Figure 1.5.

Figure 1.5 Definition of noise reduction of a silencer.

Equation 1.3 is the mathematical expression of the noise reduction

$$NR = SPL_1 - SPL_2 = 20 \log_{10} \left| \frac{p_1}{p_2} \right| \quad (1.3)$$

Of the three performance parameters introduced above, insertion loss is clearly the most direct metric to indicate the performance of silencer since it represents the loss in the radiated sound power level due to the insertion of the silencer between the noise source and the receiver (Munjal, 2014). Insertion loss is easy to measure but difficult to simulate because it requires the knowledge of the source impedance and the termination condition when sound exits the outlet pipe and radiates into the surrounding environment. Similar to the insertion loss, noise reduction also depends on the property of the termination condition and the locations of the two measurement points. Unlike insertion loss and noise reduction, transmission loss is the property of the silencer itself because it does

not take the source impedance into consideration and it also assumes the outlet has an anechoic termination. Due to its simplicity, transmission loss has been used as the main indicator of silencer performance in the research community. It should be noted that for large dissipative silencers used in power generation, most sound waves are absorbed by the sound-absorbing materials and all three performance metrics (IL, NR, and TL) produce very similar results.

1.1.3 Traditional methods for TL calculation

In general, there are two commonly used methods for determining TL numerically: the four-pole matrix method (Wu et al, 1998; Munjal, 2014), and the wave decomposition method (Wu and Wan, 1996; Selamet and Radavich, 1997).

Four-pole matrix method

Based on the plane-wave theory (Pierce, 1981), a silencer with an inlet and outlet shown in Figure 1.6 can be represented by a linear acoustic four-pole network below the cut-off frequency at the inlet/outlet:

$$\begin{Bmatrix} p_1 \\ v_1 \end{Bmatrix} = \begin{bmatrix} A & B \\ C & D \end{bmatrix} \begin{Bmatrix} p_2 \\ v_2 \end{Bmatrix} \tag{1.4}$$

Figure 1.6 Four-pole method for TL calculation.

where p_1 and v_1 are the sound pressure and normal particle velocity at the inlet, and p_2 and v_2 are the sound pressure and normal particle velocity at the outlet,

respectively. The four-pole matrix can be obtained by 1-D transfer matrix method if the analytical four-pole matrices for all attenuating elements are available, or calculated by a 3D numerical tool, such as the finite element method (FEM) or the boundary element method (BEM). In the BEM model, a negative sign on v_2 is added because the normal vector at the outlet is opposite to the normal at the inlet, and the four-pole parameters, A, B, C and D can be obtained from

$$A = \left.\frac{p_1}{p_2}\right|_{v_2=0, v_1=1} \qquad B = \left.\frac{p_1}{-v_2}\right|_{p_2=0, v_1=1} \tag{1.5a, 1.5b}$$

$$C = \left.\frac{v_1}{p_2}\right|_{v_2=0, v_1=1} \qquad D = \left.\frac{v_1}{-v_2}\right|_{p_2=0, v_1=1} \tag{1.5c, 1.5d}$$

The TL of the silencer can be then calculated by Equation 1.6,

$$TL = 20\log_{10}\left(\frac{1}{2}\left|A + \frac{B}{\rho c} + \rho c C + D\right|\right) + 10\log_{10}\frac{S_i}{S_o} \tag{1.6}$$

where S_i and S_o are the cross-sectional areas of the inlet and outlet tubes, respectively. Wu et al (1998) proposed an improved four-pole method that calculates the impedance matrix first, and then converts the impedance matrix into the four-pole matrix. The advantage of the improved method is that it speeds up the computation time by 50%.

Wave decomposition method

The acoustic wave in the duct is the superposition of the forward and backward moving waves (Munjal, 2014). Based on the plane-wave theory, the sound pressure at the at the location x of the inlet duct is expressed below,

$$p(x) = Ae^{-jkx} + Be^{jkx} \tag{1.7}$$

where A is the complex amplitude of incident wave, B is the complex amplitude of reflected wave, and k is the wavenumber.

Because of the anechoic termination assumption at the outlet for the TL calculation, only the outgoing wave exists, and the sound pressure at the location x of the outlet duct is,

$$p(x) = Ce^{-jkx} \tag{1.8}$$

Therefore, the TL of the silencer can be calculated in terms of A and C, as shown in Equation 1.9.

$$TL = 20\log_{10}\frac{|A|}{|C|} + 10\log_{10}\frac{S_i}{S_o} \tag{1.9}$$

In order to obtain the wave amplitudes of A and B, the three-point method (Wu and Wan, 1996) is one of the popular approaches. As shown in Figure 1.7, x_1 and x_2 are the longitudinal coordinates of the two selected points at the inlet duct. The sound pressures of these two points p_1 and p_2 can be written as

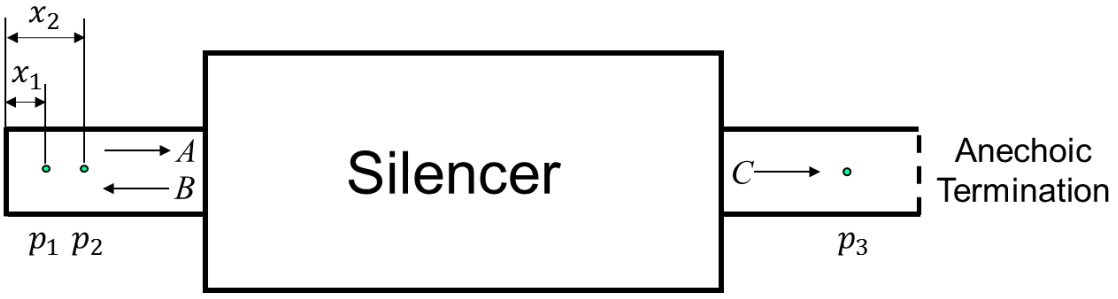

Figure 1.7 Three-point method for TL calculation.

$$p_1 = Ae^{-jkx_1} + Be^{jkx_1} \tag{1.10a}$$

$$p_2 = Ae^{-jkx_2} + Be^{jkx_2} \tag{1.10b}$$

The incident wave amplitude A can be obtained after solving Equation 1.10a and 1.10b,

$$A = \frac{p_1 e^{+jkx_2} - p_2 e^{+jkx_1}}{2j\sin\big(k(x_2 - x_1)\big)} \tag{1.11}$$

provided that $\sin\big(k(z_2 - z_1)\big) \neq 0$. Since $|C| = |p_3|$, the point of p_3 can be selected anywhere in the outlet duct. The TL can be then calculated by Equation 1.9.

1.1.4 BEM substructuring technique

The BEM substructuring technique (Lou et al, 2003) is an efficient tool for large silencer analysis, since it may not be possible to analyze a very large silencer in one single BEM model on a desktop computer. Thanks to the direct mixed-body BEM theory, which can handle complex internal components (Wu et al, 1998 and Wu and Wan, 1996) as well as multiple bulk-reacting materials (Wu et al, 2002 and Jiang et al, 2010) in one single BEM domain without resorting to the tedious multi-domain BEM, a large silencer can be divided into several smaller substructures at any cross sections along with the axial direction of the silencer. Continuity of sound pressures and particle velocities at junctions is automatically enforced when the BEM impedance matrices are merged by a synthesis procedure (Wu et al, 2002). After all the impedance matrices of the substructures are merged, the resulting impedance matrix of the silencer can be used to calculate the TL. As demonstrated in Figure 1.8, a tuned dissipative silencer, also known as the “pine-tree” silencer

because of its internal structural shape, can be divided into three small substructures A, B and C to fit within the memory limitation of a desktop computer. For substructure B, only one small template needs to be modeled, and its impedance matrix can be used repeatedly downstream. To speed up the computation, multiple desktop computers can be used simultaneously for different substructures as each substructure calculation is independent of one another. Finally, with the impedance matrices of all substructures available, the impedance matrix of the large silencer can be formed by using the impedance matrix synthesis.

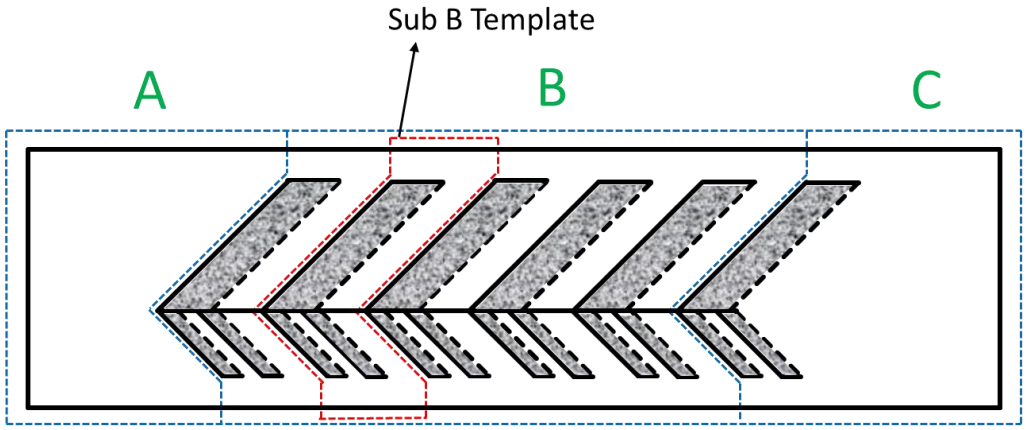

Figure 1.8 A tuned dissipative silencer divided into three small substructures with the second substructure as a repeating template.

1.2 Motivation

In general, silencers used in the power generation usually have very large dimensions. Even a single unit isolated from an array of bar silencers or tuned-dissipative silencers may still have a large cross section at the inlet and the outlet (Cummings and Astley, 1996, Mechel, 2002 and Wang and Wu, 2015). The plane-

wave cutoff frequency of the inlet and outlet ducts of such silencers can be less than a few hundred Hz, and the frequency range of interest normally goes up to 8000 Hz or above. Due to the low cutoff, the conventional four-pole transfer matrix is not valid, and more importantly the anechoic termination can no longer be represented by the characteristic impedance boundary condition. Although the silencer itself is often modeled by a three-dimensional analysis tool such as BEM (Cheng and Seybert, 1987; Wu and Wan, 1996; Wu et al. 2002; Ji, 2010) or FEM (Peat, 1982; Peat and Rathi, 1995; Tsuji et al., 2002; Barbieri, 2006), a direct computation of the TL from the BEM or FEM model can be challenging without incorporating certain forms of modal expansion.

Since the 1990s, approximate analytical solutions are available for large lined duct silencers. Cummings and Sormaz (1993), Ingard (1994) and Kakoty and Roy (2002) proposed a two-dimensional analytical solution for an infinitely long lined duct. By assuming no reflected waves in the lined duct, the attenuation of an incident plane wave can be obtained after solving the characteristic equation numerically. However, this approach is strictly restricted to very simple and uniform structures.

Kirby and his co-workers (2003, 2005, 2006, 2009, and 2014) used a hybrid FEM to study the acoustical performance of large dissipative silencers. To apply the hybrid technique, the 2D FEM is first employed to extract the eigenvalues and the associated eigenvectors of an axially uniform cross section. These 2D transversal modes are then used in the modal expansion along the axial direction if the cross section remains the same. To determine the unknown amplitudes in the modal

expansion, either a point collocation method or a mode matching scheme is adopted to enforce the continuity of sound pressure and particle velocity at both ends where the uniform section meets the flanges or any irregular junctions. The higher-order modes, including the evanescent modes, are considered in the modal expansion because the evanescent modes are still important at the flanges or irregular junctions. Since the FEM is mainly used on a 2D cross section to extract the modes, the hybrid FEM is a very efficient numerical technique for silencers with a very long axially uniform section.

On the BEM side, Zhou et al. (2012, 2013 and 2016) recently proposed a reciprocal identity method in conjunction with the BEM impedance matrix to extract the higher-order modes at the inlet and outlet. Each reciprocal identity couples the analytical modal expansion in the inlet and outlet ducts to a BEM solution with a random boundary condition set. The modal expansion assumes a certain form of the incident wave in the inlet duct, and an anechoic termination at the outlet. The unknown modal amplitudes are the reflected waves in the inlet duct and the transmitted waves in the outlet duct. Depending on how many modes can propagate to the inlet and outlet at a given frequency, a minimum number of BEM solutions are needed for the reciprocal identity coupling. The BEM impedance matrix can naturally provide more than enough such solutions since each column of the impedance matrix represents a BEM solution corresponding to a unique boundary condition set. A least-squares procedure is then used to solve for the unknown modal amplitudes. The reciprocal identity method can be regarded as an

indirect post-processing filter whose sole function is to extract the modes at the inlet and outlet from the BEM impedance matrix.

In this dissertation, a so-called “impedance-to-scattering matrix method” is developed to extract the modes at the inlet and outlet from the BEM impedance matrix for the large silencer analysis (Wang and Wu, 2014, 2015 and 2016). Compared to the reciprocal identity method (Zhou et al., 2012, 2013 and 2016), the proposed method is a more efficient approach that directly converts the BEM impedance matrix into the scattering matrix for TL computation. The BEM impedance matrix relates the sound pressures at the inlet and outlet to the corresponding particle velocities (Lou et al., 2003; Marburg and Nolte, 2008), while the scattering matrix relates the modes at the inlet and outlet. Each sound pressure and particle velocity can be expanded in terms of the duct modes at the centroid of each constant boundary element. These point-wise expansions are then related by the BEM impedance matrix, and the scattering matrix can be obtained after a few matrix operations. Normally there are more boundary elements than the total number of modes at the inlet and outlet, and a least-squares procedure is used to condense the element-based impedance matrix to the mode-based scattering matrix. The TL computation will follow if a certain form of the incident wave is assumed and the outlet is non-reflective. Figure 1.9 demonstrates the complete TL computation procedure of the large silencer.

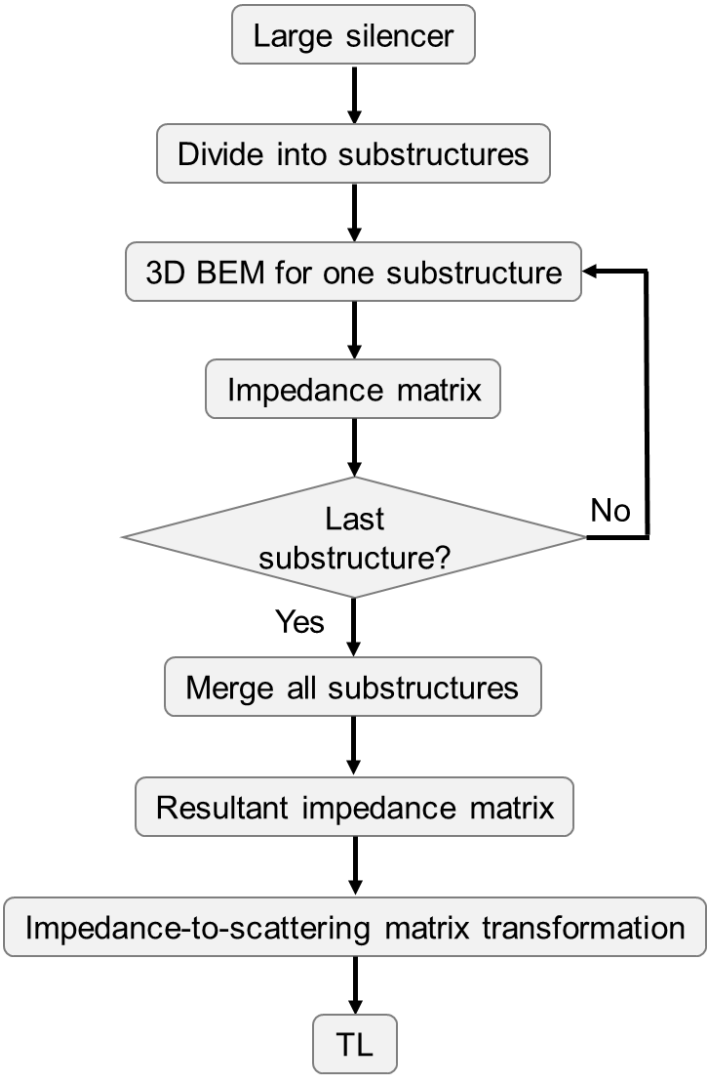

Figure 1.9 Flowchart of the procedure for large silencer analysis.

The concept of scattering matrix was introduced in the past in electromagnetics (Dicke, 1947) and acoustics (Åbom, 1991) below the plane-wave cutoff frequency. In other words, only the first mode was considered in those early scattering matrix applications. With the introduction of the BEM impedance matrix (Lou et al, 2003), all higher-order propagating modes along with the evanescent modes can be extracted from the BEM impedance matrix and incorporated into the scattering matrix. One bonus effect of producing the scattering matrix is that it can also be

used to combine subsystems in series connection. Unlike the traditional 4-pole transfer matrix, the higher-order modes are now included in the scattering matrix. Although the BEM impedance matrix may also be used to combine subsystems (Lou et al, 2003), it should be noted that the impedance matrix must be always associated with a particular BEM mesh due to its element-based nature, but the scattering matrix is a system property that does not rely on any mesh. Therefore, it is easier to store scattering matrices in the database, and thus it is a better approach for combining subsystems in series connection.

1.3 Organization

The dissertation is organized as follows:

Chapter 2 first introduces the impedance matrix and the scattering matrix for large silencers, and then details the derivation of the transformation from the impedance matrix to the scattering matrix. Test cases are presented to validate the proposed method.

Chapter 3 extends the proposed method to large multi-inlet and multi-outlet silencers. The current techniques to calculate the TL of multi-inlet and multi-outlet silencers are reviewed first. Then the transformation from the impedance matrix to scattering matrix for large three-port silencers is detailed. The BEM TL solution is validated by an equivalent IL solution using the automatically matched layer (AML) in the FEM.

In Chapter 2 and 3, a direct point collocation approach is used to convert the BEM impedance matrix into the scattering matrix for TL computation. Chapter 4

presents an integral-based impedance-to-scattering matrix method based on the recently developed reciprocal identity method (Zhou et al, 2016). The computational efficiency, accuracy and stability are compared between the collocation-based and integral-based methods.

Chapter 5 first extends the impedance-to-scattering matrix method to large silence with irregular inlet and outlet configurations analysis, and then introduces the Redheffer's star product (Redheffer, 1962) to combine scattering matrices of subsystems and methods for determination of TL in one-third octave and octave band.

Chapter 6 presents an important case study on the tuned dissipative silencers. A semi-analytical solution is also developed to evaluate the BEM solution.

Chapter 7 includes summary, conclusions and suggestions for future work.

Chapter 2 COLLOCATION-BASED IMPEDANCE-TO-SCATTERING MATRIX METHOD FOR LARGE SILENCER ANALYSIS

2.1 Introduction

As discussed in Chapter 1, silencers used in power generation usually have very large dimensions. The plane-wave cutoff frequency of the inlet and outlet ducts of such silencers can be less than a few hundred Hz, while the frequency range of interest normally goes to 8000 Hz or above. Although the BEM is a truly 3D analysis tool, and in theory it should be valid at any high frequencies as long as the BEM mesh is fine enough, the conventional method to calculate TL has been relying on the 1-D four-pole transfer matrix. When the frequency goes above the plane-wave cutoff of the inlet and outlet ducts, higher-order modes begin to emerge at the inlet and outlet, and the conventional four-pole transfer matrix is no longer valid. Therefore, a different method that considers the higher-order modes must be developed to compute the TL for large silencers.

In this chapter, a so-called collocation-based impedance-to-scattering matrix method is proposed to extract the higher-order modes at the inlet and outlet from the BEM impedance matrix for TL computation. Later in Chapter 4, an integral-based impedance-to-scattering matrix method is also introduced as an alternative to the collocation-based method. Comparison between these two methods is presented in Chapter 4.

2.2 BEM impedance matrix

The BEM impedance matrix **Z** is defined by

$$\begin{pmatrix} p_{11} \\ p_{12} \\ \cdot \\ \cdot \\ \cdot \\ p_{1q} \\ \cdots \\ p_{21} \\ p_{22} \\ \cdot \\ \cdot \\ \cdot \\ p_{2l} \end{pmatrix} = \begin{bmatrix} Z_{1,1} & \cdots & Z_{1,q+l} \\ \vdots & \ddots & \vdots \\ Z_{q+l,1} & \cdots & Z_{q+l,q+l} \end{bmatrix} \begin{pmatrix} v_{11} \\ v_{12} \\ \cdot \\ \cdot \\ \cdot \\ v_{1q} \\ \cdots \\ v_{21} \\ v_{22} \\ \cdot \\ \cdot \\ \cdot \\ v_{2l} \end{pmatrix} \tag{2.1}$$

where p and v denote the sound pressure and particle velocity at the inlet and outlet. For p and v, the first subscript 1 represents the inlet and 2 the outlet; the second subscript represents the boundary element numbering (q constant elements at inlet and l constant elements at outlet). The impedance matrix can be obtained by "tuning on" v = 1 on each element at the inlet and outlet successively, one at a time. Although there are a total of $q + l$ velocity boundary condition sets, they all share the same BEM coefficient matrix. Therefore only one matrix inverse (or decomposition) is needed at each frequency. Equation 2.1 can be re-written in a more compact vector form

$$\begin{pmatrix} \mathbf{p_1} \\ \mathbf{p_2} \end{pmatrix} = \begin{bmatrix} \mathbf{Z_{11}} & \mathbf{Z_{12}} \\ \mathbf{Z_{21}} & \mathbf{Z_{22}} \end{bmatrix} \begin{pmatrix} \mathbf{v_1} \\ \mathbf{v_2} \end{pmatrix} \tag{2.2}$$

where 1 and 2 denote the inlet and the outlet, respectively, and the element numbering index is dropped.

2.3 Scattering matrix

The scattering matrix **S** relates the modal amplitudes at the inlet and outlet:

$$\begin{pmatrix} P_{20}^{+} \\ P_{21}^{+} \\ \vdots \\ P_{2(N-1)}^{+} \\ P_{10}^{-} \\ P_{11}^{-} \\ \vdots \\ P_{1(N-1)}^{-} \end{pmatrix} = \begin{bmatrix} S_{1,1} & \cdots & S_{1,2N} \\ \vdots & \ddots & \vdots \\ S_{2N,1} & \cdots & S_{2N,2N} \end{bmatrix} \begin{pmatrix} P_{10}^{+} \\ P_{11}^{+} \\ \vdots \\ P_{1(N-1)}^{+} \\ P_{20}^{-} \\ P_{21}^{-} \\ \vdots \\ P_{2(N-1)}^{-} \end{pmatrix} \tag{2.3}$$

where P denotes the wave amplitude of a particular mode. The superscript + on P represents the right-traveling wave and – the left-traveling wave; the first subscript 1 denotes the inlet and 2 the outlet; the second subscript denotes the order of the mode. Assume that there are N modes (n = 0 to N-1) in the inlet duct and the outlet duct as well. The N modes may include evanescent modes, but normally one evanescent mode beyond the last propagating mode is enough because most evanescent modes are insignificant when they reach the inlet and outlet locations. In fact, the exponential decay rate of any evanescent mode can be analytically assessed at a given frequency. Equation 2.4 can be re-written in a more compact vector form

$$\begin{pmatrix} \mathbf{P_2^+} \\ \mathbf{P_1^-} \end{pmatrix} = \begin{bmatrix} \mathbf{S_{11}} & \mathbf{S_{12}} \\ \mathbf{S_{21}} & \mathbf{S_{22}} \end{bmatrix} \begin{pmatrix} \mathbf{P_1^+} \\ \mathbf{P_2^-} \end{pmatrix} \tag{2.4}$$

It is noted that in Equation 2.4 the transmitted wave amplitudes at the outlet $\mathbf{P_2^+}$ and the reflected wave amplitudes at the inlet $\mathbf{P_1^-}$ are placed on the left-hand side, while the incident wave amplitudes at the inlet $\mathbf{P_1^+}$ and the reflected wave amplitudes at the outlet $\mathbf{P_2^-}$ are placed on the right-hand side. Since the TL is defined based on

an anechoic termination, $\mathbf{P_2^-}$ is clearly a zero vector. As for $\mathbf{P_1^+}$, a single incident plane wave without any higher-order modes is assumed in this study for simplicity, although the three different source models suggested by Mechel (Mechel, 1990) may also be adopted. In other words, we let $\mathbf{P_1^+} = [1, 0, 0, \dots, 0]^{\mathrm{T}}$, where the superscript T denotes the transpose. If the scattering matrix **S** is available, both $\mathbf{P_2^+}$ and $\mathbf{P_1^-}$ may be solved from Equation 2.4.

2.4 TL above the plane-wave cutoff frequency of the inlet/outlet

In Chapter 1, the traditional TL calculation methods are introduced. However, the results are only valid below the plane-wave cutoff at the inlet/outlet since the plane-wave theory is used in those methods. In this section, by including the higher-order modes at the inlet and outlet ducts, the TL computation is valid at all frequencies.

The sound pressure and particle velocity of the incident wave at any point i in the inlet duct can be expressed in the general modal expansion form,

$$p_{1i}^{+} = \sum_{n=0}^{N-1} \Phi_{1n}^{i} P_{1n}^{+} \, \mathrm{e}^{-\mathrm{j}k_{1z,n}z} \tag{2.5}$$

$$v_{1i}^{+} = \frac{1}{\rho\omega} \sum_{n=0}^{N-1} k_{1z,n} \Phi_{1n}^{i} P_{1n}^{+} \, \mathrm{e}^{-\mathrm{j}k_{1z,n}z} \tag{2.6}$$

where z is the axial coordinate along the inlet duct, P_{1n}^{+} is the modal amplitude corresponding to the right-traveling wave of order n, k_{1z} represents the wavenumber in the z direction, Φ_{1n}^{i} denotes the eigenfunction value at the point i.

For a circular or rectangular cross section, the eigenfunctions can be obtained analytically. For convenience, z=0 is set right at the inlet cross section.

The intensity of the incident wave then can be calculated

$$I_{1i} = \frac{1}{2} Re(p_{1i}^{+}(v_{1i}^{+})^{*}) \tag{2.7}$$

where $*$ denotes the conjugant and $Re(\cdot)$ denotes the real part of a complex number.

The sound power is the integration of the intensity over the cross-sectional area of the inlet

$$W_1 = \int_{S_1} I_{1i}\, dS \tag{2.8}$$

where S_1 is the cross-sectional area of the inlet.

Based on assumption of the single incident plane-wave, $\mathbf{P_1^+} = [1, 0, 0, \dots, 0]^{\mathrm{T}}$, the incident sound power is simply

$$W_1 = \frac{S_1}{2\rho c} \tag{2.9}$$

At the outlet, by simply switching the first subscript 1 to 2 in Equation 2.5 to Equation 2.8, the transmitted sound power is the summation of sound power from different modes:

$$W_2 = \int_{S_2} \frac{1}{2\rho\omega} \sum_{n=0}^{N-1} Re\left(\Phi_n^i P_{2n}^+ (k_{z,n} \Phi_n^i P_{2n}^+)^*\right) \, dS \tag{2.10}$$

where the transmitted modal amplitudes P_{2n}^+ can be calculated from Equation 2.4 once the BEM impedance matrix **Z** is converted into the scattering matrix **S**. The TL is defined as the difference between the incident and transmitted sound power level,

$$TL \; = \; 10 \log_{10} \frac{W_1}{W_2} \tag{2.11}$$

2.5 Impedance-to-Scattering matrix method for axisymmetric silencers

2.5.1 Transformation from the impedance matrix to scattering matrix

The simplest way to demonstrate the impedance-to-scattering matrix method is to begin with the axisymmetric configuration. For an axisymmetric silencer, the modal expansion of sound pressure in the inlet/outlet duct is

$$p(r,z) = \sum_{n=0}^{\infty} J_0\left(k_{r,n} r\right)\left[P_n^+ \, \mathrm{e}^{-\mathrm{j}k_{z,n}z} + P_n^- \mathrm{e}^{\mathrm{j}k_{z,n}z}\right] \tag{2.12}$$

where $k_{r,n}$ is the radial wavenumber associated with the *n*-th mode, and $k_{z,n}$ is the corresponding axial wavenumber, J_0 is the Bessel function of the first kind of order zero, and the superscripts + and – represent the incident and reflected waves, respectively. The n = 0 mode is the plane-wave mode with $k_{r,0}$ = 0. The two wavenumbers are related by

$$k_{r,n}^2 = k^2 - k_{z,n}^2 \tag{2.13}$$

where $k = \omega/c$, ω is the circular frequency and *c* is the speed of sound. The radial wavenumber $k_{r,n}$ has to satisfy the rigid-wall boundary condition

$$J_0'(k_{r,n}a) = 0 \tag{2.14}$$

where a is the radius of the inlet/outlet duct.

For convenience, $z = 0$ is locally set at the inlet cross section. Therefore, sound pressures of the *q* boundary elements at the inlet can be expressed in the matrix form

$$\begin{pmatrix} p_{11} \\ p_{12} \\ \vdots \\ p_{1q} \end{pmatrix} = \begin{bmatrix} J_0(k_{r,0}r_{11}) & \cdots & J_0(k_{r,N-1}r_{11}) & J_0(k_{r,0}r_{11}) & \cdots & J_0(k_{r,N-1}r_{11}) \\ \vdots & \ddots & \vdots & \vdots & \ddots & \vdots \\ J_0(k_{r,0}r_{1q}) & \cdots & J_0(k_{r,N-1}r_{1q}) & J_0(k_{r,0}r_{1q}) & \cdots & J_0(k_{r,N-1}r_{1q}) \end{bmatrix} \begin{pmatrix} P_{10}^+ \\ P_{11}^+ \\ \vdots \\ P_{1(N-1)}^+ \\ P_{10}^- \\ P_{11}^- \\ \vdots \\ P_{1(N-1)}^- \end{pmatrix} \tag{2.15}$$

where r_{1i} is the radial coordinate of the centroid of the i^{th} boundary element at the inlet. Equation 2.15 can be re-written in a more compact vector form

$$\mathbf{p_1} = \mathbf{M_{11}} \begin{pmatrix} \mathbf{P_1^+} \\ \mathbf{P_1^-} \end{pmatrix} \tag{2.16}$$

where the "modal matrix" $\mathbf{M_{11}}$ relates sound pressures at the inlet cross section to the modal amplitudes at the inlet. Similarly, sound pressures at the outlet (where $z = 0$ is also locally set) is

$$\mathbf{p_2} = \mathbf{M_{21}} \begin{pmatrix} \mathbf{P_2^+} \\ \mathbf{P_2^-} \end{pmatrix} \tag{2.17}$$

The particle velocity expression corresponding to the sound pressure in Equation 2.12 is

$$v(r,z) = \frac{1}{\rho\omega} \sum_{n=0}^{\infty} k_{z,n} J_0\left(k_{r,n} r\right) \left[P_n^+ \, \mathrm{e}^{-\mathrm{j}k_{z,n}z} - P_n^- \mathrm{e}^{\mathrm{j}k_{z,n}z}\right] \tag{2.18}$$

Express the particle velocities of the q boundary elements at the inlet (where $z = 0$) in terms of the modal amplitudes at the inlet to get

$$\begin{pmatrix} v_{11} \\ v_{12} \\ \vdots \\ v_{1q} \end{pmatrix} = \begin{bmatrix} \frac{k_{z,1}}{\rho\omega} J_0(k_{r,0} r_{11}) & \cdots & \frac{k_{z,N-1}}{\rho\omega} J_0(k_{r,N-1} r_{11}) \\ \vdots & \ddots & \vdots \\ \frac{k_{z,1}}{\rho\omega} J_0(k_{r,0} r_{1q}) & \cdots & \frac{k_{z,N-1}}{\rho\omega} J_0(k_{r,N-1} r_{1q}) \end{bmatrix}$$

$$\begin{bmatrix} -\frac{k_{z,1}}{\rho\omega} J_0(k_{r,0} r_{11}) & \cdots & -\frac{k_{z,N-1}}{\rho\omega} J_0(k_{r,N-1} r_{11}) \\ \vdots & \ddots & \vdots \\ -\frac{k_{z,1}}{\rho\omega} J_0(k_{r,0} r_{1q}) & \cdots & -\frac{k_{z,N-1}}{\rho\omega} J_0(k_{r,N-1} r_{1q}) \end{bmatrix} \begin{pmatrix} P_{10}^+ \\ P_{11}^+ \\ \vdots \\ P_{1(N-1)}^+ \\ \cdots \\ P_{10}^- \\ P_{11}^- \\ \vdots \\ P_{1(N-1)}^- \end{pmatrix} \tag{2.19}$$

or in a more compact vector form

$$\mathbf{v_1} = \mathbf{M_{12}} \begin{pmatrix} \mathbf{P_1^+} \\ \mathbf{P_1^-} \end{pmatrix} \tag{2.20}$$

Similarly, the particle velocities at the outlet can be written as

$$\mathbf{v_2} = \mathbf{M_{22}} \begin{pmatrix} \mathbf{P_2^+} \\ \mathbf{P_2^-} \end{pmatrix} \tag{2.21}$$

Substitute Equations 2.16, 2.17, 2.20, 2.21 into Equation 2.2 to get

$$\mathbf{M_{11}} \begin{pmatrix} \mathbf{P_1^+} \\ \mathbf{P_1^-} \end{pmatrix} = \mathbf{Z_{11}M_{12}} \begin{pmatrix} \mathbf{P_1^+} \\ \mathbf{P_1^-} \end{pmatrix} + \mathbf{Z_{12}M_{22}} \begin{pmatrix} \mathbf{P_2^+} \\ \mathbf{P_2^-} \end{pmatrix} \tag{2.22}$$

$$\mathbf{M_{21}} \begin{pmatrix} \mathbf{P_2^+} \\ \mathbf{P_2^-} \end{pmatrix} = \mathbf{Z_{21}M_{12}} \begin{pmatrix} \mathbf{P_1^+} \\ \mathbf{P_1^-} \end{pmatrix} + \mathbf{Z_{22}M_{22}} \begin{pmatrix} \mathbf{P_2^+} \\ \mathbf{P_2^-} \end{pmatrix} \tag{2.23}$$

The above two equations are combined into one matrix form

$$\begin{bmatrix} \mathbf{M_{11} - Z_{11}M_{12}} \\ \mathbf{Z_{21}M_{12}} \end{bmatrix} \begin{pmatrix} \mathbf{P_1^+} \\ \mathbf{P_1^-} \end{pmatrix} = \begin{bmatrix} \mathbf{Z_{12}M_{22}} \\ \mathbf{M_{21} - Z_{22}M_{22}} \end{bmatrix} \begin{pmatrix} \mathbf{P_2^+} \\ \mathbf{P_2^-} \end{pmatrix} \tag{2.24}$$

It should be noted that all the inlet wave amplitudes (with subscript 1) are on one side and all the outlet wave amplitudes (with subscript 2) are on the other side of Equation 2.24. Although this may look like a “transfer scattering matrix” that relates the inlet directly to the outlet, matrix inverse should not be performed at this stage because Equation 2.24 does not represent a well-posed boundary value problem. A well-posed boundary value problem should have a known condition at the inlet and another known condition at the outlet. For example, to find the TL, a certain incident wave ($\mathbf{P_1^+}$) should be given at the inlet and the outlet is assumed anechoic ($\mathbf{P_2^- = 0}$). To split the matrix contributions into the incident and reflected waves in Equation 2.24, let

$$\begin{bmatrix} \mathbf{M_{11}} - \mathbf{Z_{11}M_{12}} \\ \mathbf{Z_{21}M_{12}} \end{bmatrix} = [\mathbf{N_{11}} \quad \mathbf{N_{12}}] \tag{2.25}$$

$$\begin{bmatrix} \mathbf{Z_{12}M_{22}} \\ \mathbf{M_{21}} - \mathbf{Z_{22}M_{22}} \end{bmatrix} = [\mathbf{N_{21}} \quad \mathbf{N_{22}}] \tag{2.26}$$

and re-arrange Equation 2.24 to obtain

$$[\mathbf{N_{21}} \quad -\mathbf{N_{12}}] \begin{pmatrix} \mathbf{P_2^+} \\ \mathbf{P_1^-} \end{pmatrix} = [\mathbf{N_{11}} \quad -\mathbf{N_{22}}] \begin{pmatrix} \mathbf{P_1^+} \\ \mathbf{P_2^-} \end{pmatrix} \tag{2.27}$$

Equation 2.27 is now "well-posed" because it has both inlet and outlet components on each side. Since there are always more boundary elements than the number of propagating modes, a least-squares matrix inverse can be performed on Equation 2.27 to get the scattering matrix **S**,

$$\begin{pmatrix} \mathbf{P_2^+} \\ \mathbf{P_1^-} \end{pmatrix} = \begin{bmatrix} \mathbf{S_{11}} & \mathbf{S_{12}} \\ \mathbf{S_{21}} & \mathbf{S_{22}} \end{bmatrix} \begin{pmatrix} \mathbf{P_1^+} \\ \mathbf{P_2^-} \end{pmatrix} \tag{2.28}$$

The unknowns $\mathbf{P_2^+}$ and $\mathbf{P_1^-}$ can be then obtained if the scattering matrix is available and a single incident plane wave and the anechoic termination are assumed.

At this point, the scattering matrix **S** can also be rearranged to obtain a so-called "transfer scattering matrix" **S***,

$$\begin{pmatrix} \mathbf{P_1^+} \\ \mathbf{P_1^-} \end{pmatrix} = \begin{bmatrix} \mathbf{S_{11}^*} & \mathbf{S_{12}^*} \\ \mathbf{S_{21}^*} & \mathbf{S_{22}^*} \end{bmatrix} \begin{pmatrix} \mathbf{P_2^+} \\ \mathbf{P_2^-} \end{pmatrix} \tag{2.29}$$

The transfer scattering matrix relates the modes at the inlet to the modes at the outlet. As such, it may be used in the same way as the traditional four-pole transfer matrix to combine subsystems in series connection.

2.5.2 Axisymmetric Test Case

An axisymmetric round bar silencer shown in Figure 2.1 is used as the test case for the above formulation. The bar is made of polyester, serving as the sound absorbing material. The characteristic impedance Z' and complex wavenumber k' are the bulk-reacting properties of the sound absorbing material, and there are several different empirical models for the bulk-reacting properties of fibrous materials (Allard and Atalla, 2009). One of the most popular empirical models proposed by Delany and Bazley (1970) is shown below:

$$Z' = Z_0(1 + 0.0571X^{-0.754} - j0.087X^{-0.732}) \tag{2.30}$$

$$k' = k_0(1 + 0.0978X^{-0.7} - j0.0189X^{-0.595}) \tag{2.31}$$

where Z_0 is the characteristic impedance of air and k_0 the wavenumber in the air, and X is a dimensionless parameter in terms of density of air ρ, frequency f and the flow resistivity of the material R:

$$X = \frac{\rho f}{R} \tag{2.32}$$

The flow resistivity for polyester at room temperature is $R = 16000$ Rayl/m. The fibrous material is normally protected by a perforated facing sheet, which can be modeled by a transfer impedance. In this study, a simple empirical formula by Sullivan and Crocker (1978) is used. That is

$$\xi = (6.0 \times 10^{-3} + j4.8 \times 10^{-5} f)/\sigma \tag{2.33}$$

where ξ is the normalized transfer impedance of the perforated facing sheet, f is frequency, and σ is the porosity. In this test case, we use $\sigma = 30\%$.

Due to the size and length of the silencer, the bar silencer is divided into three small substructures with the second substructure being a small template. As shown in Figure 2.1, the template substructure represents 1/9 of the axially uniform middle section, and its impedance matrix can be repeatedly used 9 times in the impedance matrix synthesis procedure. The analytical solution for the axisymmetric bar silencer can be obtained by using a method similar to the one proposed by Selamet et al. (2004) for lined expansion chambers except that the bulk-reacting material is now placed in the middle instead of on the wall and all higher-order modes are included in the TL computation. With reference to Table 1, there are 16 propagating modes up to 8000 Hz at room temperature. To account for any residual contributions from the evanescent modes that may manage to survive at the inlet and outlet, one evanescent mode is included in the modal expansion. In other words, N =17 is used. The BEM mesh using at least 8 constant elements per wavelength and 1/45 rotational symmetry has 690 constant elements at the inlet and another group of 690 elements at the outlet. This results in a 1380×1380 impedance matrix at each frequency. Figure 2.2 compares the BEM solution using N = 17 to the analytical solution. It should be noted that our analytical solution code based on the method in by Selamet et al. (2004) fails to find the correct characteristic roots after 4000 Hz. Nonetheless, we still present the BEM solution up to 8000 Hz. It is seen that the BEM solution compares very

well with the analytical solution up to the frequency for which the analytical solution is valid.

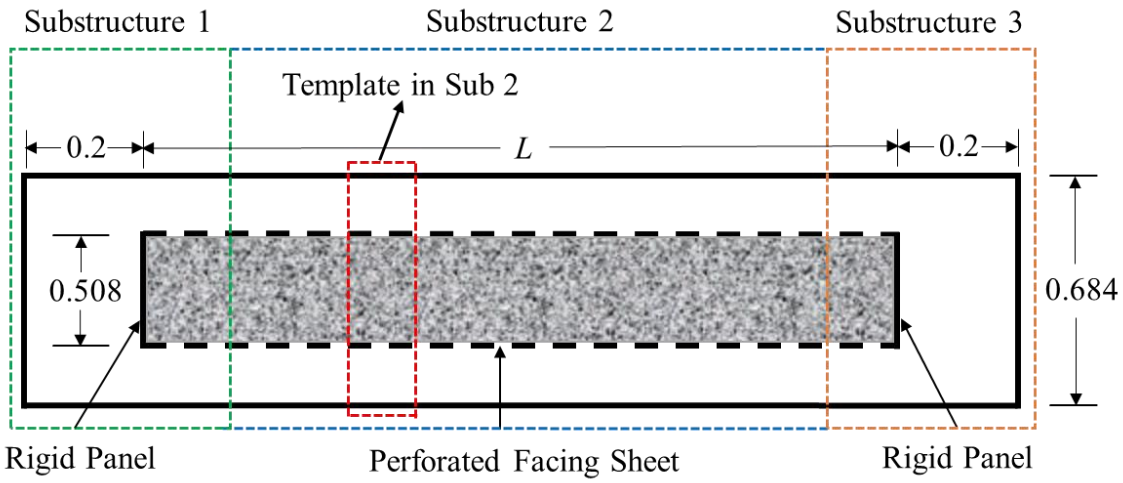

Figure 2.1 An axisymmetric round bar silencer with three substructures (Unit: m; L = 6 m).

Table 2.1 Cut-on Frequencies at Inlet/Outlet of the Bar Silencer.

Cut-on Frequency (Hz)	Total Number of Propagating Modes
612	2
1120	3
1624	4
2127	5
2629	6
3131	7
3633	8
4135	9
4637	10
5138	11
5640	12
6141	13
6643	14
7145	15
7646	16
8148	17

To test the convergence of using more modes, we increase the number of modes to $N = 30$. Figure 2.3 compares the solution of $N = 17$ to the solution of $N = 30$. We can see that adding more evanescent modes barely changes the TL curve.

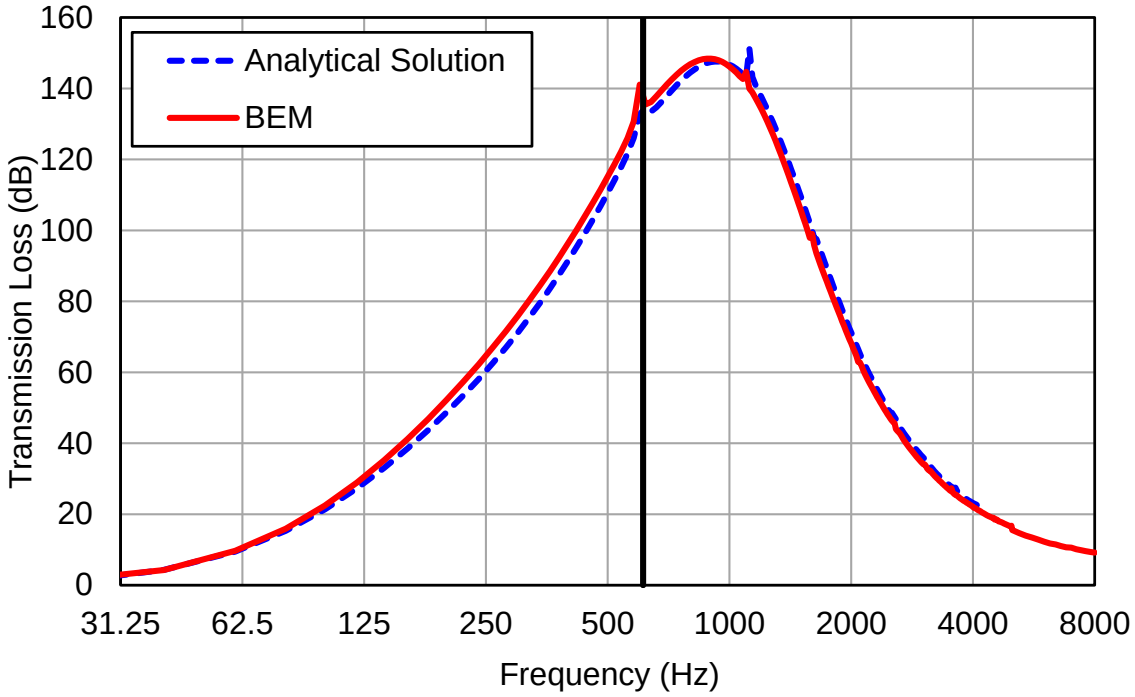

Figure 2.2 TL comparison between the BEM and the analytical solution.

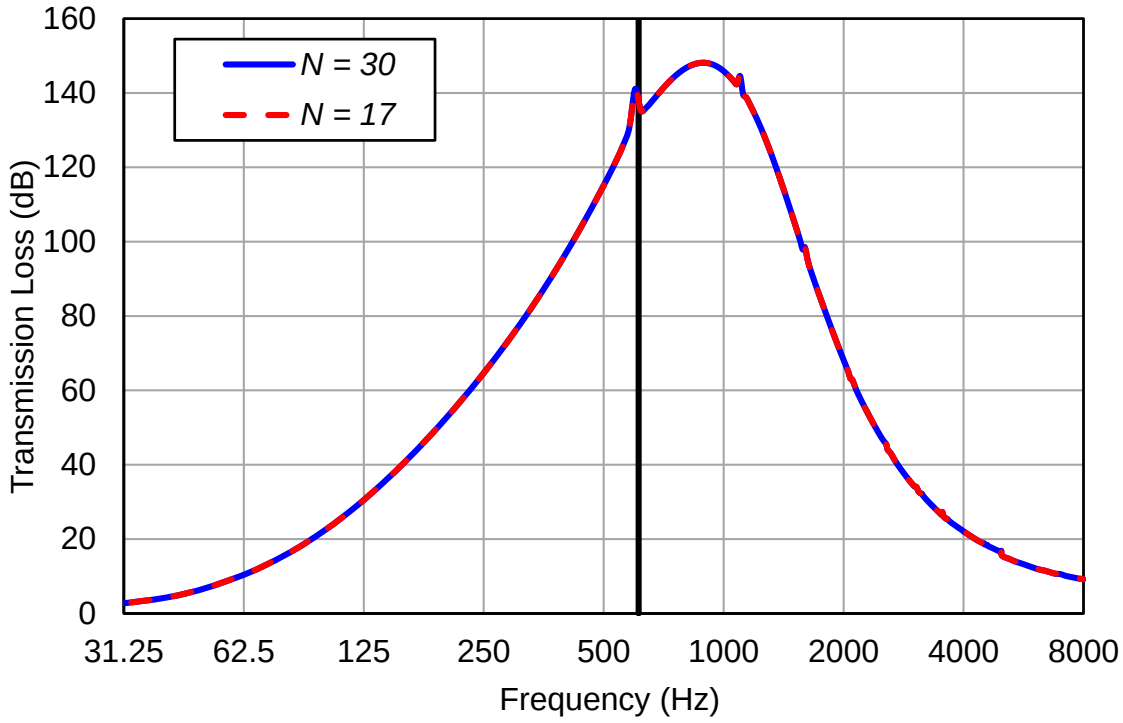

Figure 2.3 TL of the axisymmetric bar silencer using N = 17 and N = 30.

2.6 Impedance-to-Scattering matrix method for a non-axisymmetric circular inlet/outlet

2.6.1 Transformation from the impedance matrix to the scattering matrix

The modal expansion of sound pressure in a circular duct with a non-axisymmetric solution is

$$p(r,\theta,z) = \sum_{n=0}^{\infty} J_0\left(k_{r,0,n}r\right)\left[A_{0n}\mathrm{e}^{-\mathrm{j}k_{z,0,n}z} + B_{0n}\mathrm{e}^{\mathrm{j}k_{z,0,n}z}\right] + \sum_{m=1}^{\infty}\sum_{n=0}^{\infty} J_m\left(k_{r,m,n}r\right)\left[\left(A_{mn}^{+}\mathrm{e}^{-\mathrm{j}m\theta} + A_{mn}^{-}\mathrm{e}^{\mathrm{j}m\theta}\right)\mathrm{e}^{-\mathrm{j}k_{z,m,n}z} + \left(B_{mn}^{+}\mathrm{e}^{-\mathrm{j}m\theta} + B_{mn}^{-}\mathrm{e}^{\mathrm{j}m\theta}\right)\mathrm{e}^{\mathrm{j}k_{z,m,n}z}\right] \quad (2.34)$$

where $k_{r,m,n}$ is the radial wavenumber associated with the (*m*, *n*) mode, and $k_{z,m,n}$ is the corresponding axial wavenumber. The two wavenumbers are related by

$$k_{r,m,n}^2 = k^2 - k_{z,m,n}^2 \tag{2.35}$$

where *k* is the wavenumber. The radial wavenumber $k_{r,m,n}$ has to satisfy the rigid-wall boundary condition

$$J_m'(k_{r,m,n}a) = 0 \tag{2.36}$$

where a is the radius of the inlet/outlet duct, and the prime denotes the derivative. If $z = 0$ is locally set at the inlet cross section, sound pressures of the *q* boundary elements at the inlet can be expressed in the matrix form

$$\begin{pmatrix} p_{11} \\ p_{12} \\ \cdot \\ \cdot \\ \cdot \\ p_{1q} \end{pmatrix} = [\boldsymbol{MPA_{0n}}, \boldsymbol{MPA_{mn}^{+}}, \boldsymbol{MPA_{mn}^{-}}, \boldsymbol{MPB_{0n}}, \boldsymbol{MPB_{mn}^{+}}, \boldsymbol{MPB_{mn}^{-}}] \begin{pmatrix} \boldsymbol{A_{0n}} \\ \boldsymbol{A_{mn}^{+}} \\ \boldsymbol{A_{mn}^{-}} \\ \boldsymbol{B_{0n}} \\ \boldsymbol{B_{mn}^{+}} \\ \boldsymbol{B_{mn}^{-}} \end{pmatrix} \tag{2.37}$$

where

$$\boldsymbol{MPA_{0n}} = \boldsymbol{MPB_{0n}} = \begin{bmatrix} J_0(k_{r,0,0}r_{11}) & \cdots & J_0(k_{r,0,N-1}r_{11}) \\ \vdots & \ddots & \vdots \\ J_0(k_{r,0,0}r_{1q}) & \cdots & J_0(k_{r,0,N-1}r_{1q}) \end{bmatrix}_{q\times N} \tag{2.38}$$

Let

$$\boldsymbol{MP\theta^{+}}(m) = \begin{bmatrix} J_m(k_{r,m,0}r_{11})\mathrm{e}^{-\mathrm{j}*m*\theta_{11}} & \cdots & J_m(k_{r,m,N-1}r_{11})\mathrm{e}^{-\mathrm{j}*m*\theta_{11}} \\ \vdots & \ddots & \vdots \\ J_m(k_{r,m,0}r_{1q})\mathrm{e}^{-\mathrm{j}*m*\theta_{1q}} & \cdots & J_m(k_{r,m,N-1}r_{1q})\mathrm{e}^{-\mathrm{j}*m*\theta_{1q}} \end{bmatrix}_{q\times N} \tag{2.39}$$

$$\boldsymbol{MP\theta}^{-}(m)=\begin{bmatrix} J_m(k_{r,m,0}r_{11})\mathrm{e}^{\mathrm{j}*m*\theta_{11}} & \cdots & J_m(k_{r,m,N-1}r_{11})\mathrm{e}^{\mathrm{j}*m*\theta_{11}} \\ \vdots & \ddots & \vdots \\ J_m(k_{r,m,0}r_{1q})\mathrm{e}^{\mathrm{j}*m*\theta_{1q}} & \cdots & J_m(k_{r,m,N-1}r_{1q})\mathrm{e}^{\mathrm{j}*m*\theta_{1q}} \end{bmatrix}_{q\times N} \tag{2.40}$$

where m =1, 2,……, *M*-1. Therefore

$$\boldsymbol{MPA}^{+}_{\boldsymbol{mn}}=\boldsymbol{MPB}^{+}_{\boldsymbol{mn}}=[\boldsymbol{MP\theta}^{+}(1),\boldsymbol{MP\theta}^{+}(2),\dots,\boldsymbol{MP\theta}^{+}(M-1)\,]_{q\times[(M-1)*N]} \tag{2.41}$$

$$\boldsymbol{MPA}^{-}_{\boldsymbol{mn}}=\boldsymbol{MPB}^{-}_{\boldsymbol{mn}}=[\boldsymbol{MP\theta}^{-}(1),\boldsymbol{MP\theta}^{-}(2),\dots,\boldsymbol{MP\theta}^{-}(M-1)\,]_{q\times[(M-1)*N]} \tag{2.42}$$

The details of the right-hand side vector of Equation 2.37 are

$$\boldsymbol{A}_{\boldsymbol{0n}}=\begin{pmatrix} P^{+}_{10} \\ P^{+}_{11} \\ \cdot \\ \cdot \\ \cdot \\ P^{+}_{1(N-1)} \end{pmatrix} \quad \boldsymbol{A}^{+}_{\boldsymbol{mn}}=\begin{pmatrix} P^{+}_{1N} \\ P^{+}_{1(N+1)} \\ \cdot \\ \cdot \\ \cdot \\ P^{+}_{1(M*N)} \end{pmatrix} \quad \boldsymbol{A}^{-}_{\boldsymbol{mn}}=\begin{pmatrix} P^{+}_{1(M*N+1)} \\ P^{+}_{1(M*N+2)} \\ \cdot \\ \cdot \\ \cdot \\ P^{+}_{1[(2M-1)*N]} \end{pmatrix} \tag{2.43}$$

$$\boldsymbol{B}_{\boldsymbol{0n}}=\begin{pmatrix} P^{-}_{10} \\ P^{-}_{11} \\ \cdot \\ \cdot \\ \cdot \\ P^{-}_{1(N-1)} \end{pmatrix} \quad \boldsymbol{B}^{+}_{\boldsymbol{mn}}=\begin{pmatrix} P^{-}_{1N} \\ P^{-}_{1(N+1)} \\ \cdot \\ \cdot \\ \cdot \\ P^{-}_{1(M*N)} \end{pmatrix} \quad \boldsymbol{B}^{-}_{\boldsymbol{mn}}=\begin{pmatrix} P^{-}_{1(M*N+1)} \\ P^{-}_{1(M*N+2)} \\ \cdot \\ \cdot \\ \cdot \\ P^{-}_{1[(2M-1)*N]} \end{pmatrix} \tag{2.44}$$

Equation 2.37 can be re-written in a more compact vector form same as Equation 2.16:

$$\mathbf{p_1}=\mathbf{M_{11}}\begin{pmatrix}\mathbf{P_1^{+}}\\ \mathbf{P_1^{-}}\end{pmatrix} \tag{2.45}$$

Similarly, sound pressures at the outlet (where $z=0$ is also locally set) is

$$\mathbf{p_2} = \mathbf{M_{21}}\begin{pmatrix}\mathbf{P_2^+}\\ \mathbf{P_2^-}\end{pmatrix} \tag{2.46}$$

The particle velocity expression corresponding to the sound pressure in Equation 2.34 is

$$\begin{aligned} v(r,\theta,z) = \frac{1}{\rho\omega}\Bigg\{ & \sum_{n=0}^{\infty} J_0\left(k_{r,0,n}r\right)\left[A_{0n}\mathrm{e}^{-\mathrm{j}k_{z,0,n}z} - B_{0n}\mathrm{e}^{\mathrm{j}k_{z,0,n}z}\right] \\ & + \sum_{m=1}^{\infty}\sum_{n=0}^{\infty} J_m\left(k_{r,m,n}r\right)\left[\left(A_{mn}^{+}\mathrm{e}^{-\mathrm{j}m\theta} + A_{mn}^{-}\mathrm{e}^{\mathrm{j}m\theta}\right)\mathrm{e}^{-\mathrm{j}k_{z,m,n}z}\right. \\ & \left. - \left(B_{mn}^{+}\mathrm{e}^{-\mathrm{j}m\theta} + B_{mn}^{-}\mathrm{e}^{\mathrm{j}m\theta}\right)\mathrm{e}^{\mathrm{j}k_{z,m,n}z}\right]\Bigg\} \end{aligned} \tag{2.47}$$

Express the particle velocities of the q boundary elements at the inlet (where $z = 0$) in terms of the modal amplitudes at the inlet cross section to get

$$\begin{pmatrix} v_{11} \\ v_{12} \\ \cdot \\ \cdot \\ \cdot \\ v_{1q} \end{pmatrix} = [\boldsymbol{MVA_{0n}}, \boldsymbol{MVA_{mn}^{+}}, \boldsymbol{MVA_{mn}^{-}}, \boldsymbol{MVB_{0n}}, \boldsymbol{MVB_{mn}^{+}}, \boldsymbol{MVB_{mn}^{-}}] \begin{pmatrix} \boldsymbol{A_{0n}} \\ \boldsymbol{A_{mn}^{+}} \\ \boldsymbol{A_{mn}^{-}} \\ \boldsymbol{B_{0n}} \\ \boldsymbol{B_{mn}^{+}} \\ \boldsymbol{B_{mn}^{-}} \end{pmatrix} \tag{2.48}$$

where

$$\boldsymbol{MVA_{0n}} = -\boldsymbol{MVB_{0n}} = \begin{bmatrix} \frac{k_{z,0,0}}{\rho\omega}J_0(k_{r,0,0}r_{11}) & \cdots & \frac{k_{z,0,N-1}}{\rho\omega}J_0(k_{r,0,N-1}r_{11}) \\ \vdots & \ddots & \vdots \\ \frac{k_{z,0,0}}{\rho\omega}J_0(k_{r,0,0}r_{1q}) & \cdots & \frac{k_{z,0,N-1}}{\rho\omega}J_0(k_{r,0,N-1}r_{1q}) \end{bmatrix}_{q\times N} \tag{2.49}$$

Let

$$\boldsymbol{MV\theta}^{+}(m)=\begin{bmatrix}\frac{k_{z,m,0}}{\rho\omega}J_m\left(k_{r,m,0}r_{11}\right)\mathrm{e}^{-\mathrm{j}*m*\theta_{11}} & \cdots & \frac{k_{z,m,N-1}}{\rho\omega}J_m\left(k_{r,m,N-1}r_{11}\right)\mathrm{e}^{-\mathrm{j}*m*\theta_{11}}\\ \vdots & \ddots & \vdots\\ \frac{k_{z,m,0}}{\rho\omega}J_m\left(k_{r,m,0}r_{1q}\right)\mathrm{e}^{-\mathrm{j}*m*\theta_{1q}} & \cdots & \frac{k_{z,m,N-1}}{\rho\omega}J_m\left(k_{r,m,N-1}r_{1q}\right)\mathrm{e}^{-\mathrm{j}*m*\theta_{1q}}\end{bmatrix}_{q\times N} \tag{2.50}$$

$$\boldsymbol{MV\theta}^{-}(m)=\begin{bmatrix}\frac{k_{z,m,0}}{\rho\omega}J_m(k_{r,m,0}r_{11})\mathrm{e}^{\mathrm{j}*m*\theta_{11}} & \cdots & \frac{k_{z,m,N-1}}{\rho\omega}J_m(k_{r,m,N-1}r_{11})\mathrm{e}^{\mathrm{j}*m*\theta_{11}}\\ \vdots & \ddots & \vdots\\ \frac{k_{z,m,0}}{\rho\omega}J_m(k_{r,m,0}r_{1q})\mathrm{e}^{\mathrm{j}*m*\theta_{1q}} & \cdots & \frac{k_{z,m,N-1}}{\rho\omega}J_m(k_{r,m,N-1}r_{1q})\mathrm{e}^{\mathrm{j}*m*\theta_{1q}}\end{bmatrix}_{q\times N} \tag{2.51}$$

where m =1, 2,……, *M*-1. Therefore

$$\boldsymbol{MVA}^{+}_{\boldsymbol{mn}}=-\boldsymbol{MVB}^{+}_{\boldsymbol{mn}}=[\boldsymbol{MV\theta}^{+}(1),\boldsymbol{MV\theta}^{+}(2),\ldots,\boldsymbol{MV\theta}^{+}(M-1)\,]_{q\times[(M-1)*N]} \tag{2.52}$$

$$\boldsymbol{MVA}^{-}_{\boldsymbol{mn}}=-\boldsymbol{MVB}^{-}_{\boldsymbol{mn}}=[\boldsymbol{MV\theta}^{-}(1),\boldsymbol{MV\theta}^{-}(2),\ldots,\boldsymbol{MV\theta}^{-}(M-1)\,]_{q\times[(M-1)*N]} \tag{2.53}$$

or in a more compact vector form same as Equation 2.20:

$$\mathbf{v_1}=\mathbf{M_{12}}\begin{pmatrix}\mathbf{P_1^{+}}\\ \mathbf{P_1^{-}}\end{pmatrix} \tag{2.54}$$

Similarly, particle velocities at the outlet is

$$\mathbf{v_2}=\mathbf{M_{22}}\begin{pmatrix}\mathbf{P_2^{+}}\\ \mathbf{P_2^{-}}\end{pmatrix} \tag{2.55}$$

The rest of the derivation is the same as Equations 2.22-2.28.

2.6.2 Test Cases

The first test case is an axisymmetric simple expansion chamber as shown in Figure 2.4. In this case, we will ignore the symmetry and treat the problem as a non-axisymmetric problem to see if the more general formulation would still produce the correct result. Like the axisymmetric round bar silencer, the analytical

solution used for comparison is also based on the method by Selamet et al. (2004) except that the transmitted sound power for the TL calculation now includes higher-order modes. The plane-wave cutoff frequency of the 0.418 m diameter inlet/outlet is 1000 Hz at room temperature. Table 2.2 lists all the cut-on frequencies up to the 4^{th} mode. Since the TL is negligible after 1000 Hz for this simple expansion chamber, we only run the test up to 4000 Hz, which is high enough for validation purposes. According to Table 2, there are 5 propagating modes in the inlet and outlet ducts at 4000 Hz, and the next propagating mode will not emerge until 4302 Hz, which is far away from the 4000 Hz target. Therefore, five propagating modes in the radial direction will be enough without having to include any evanescent modes in that direction. At the same time, we randomly select the first 5 modes in the angular direction, although there is really no angular variation in this axisymmetric test case. In other words, we select $M = N = 5$ in the modal expansion to form the scattering matrix. The BEM mesh used has 684 elements at the inlet and another group of 684 elements at the outlet. This results in a 1368x1368 impedance matrix at each frequency. The TL comparison between the BEM solution and analytical solution is shown in Figure 2.5. It is seen that the non-axisymmetric formulation does produce a very accurate result for this axisymmetric test case.

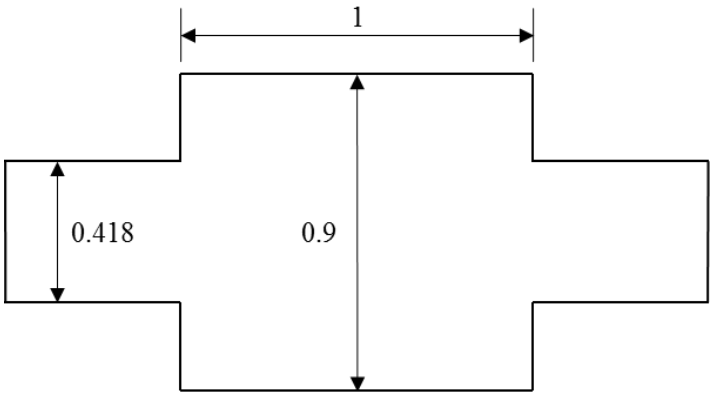

Figure 2.4 Simple expansion chamber (Unit: m).

Table 2.2 Cut-on Frequencies at Inlet/Outlet of the Simple Expansion Chamber.

Cut-on Frequency (Hz)	Total Number of Propagating Modes
1000	2
1832	3
2657	4
3480	5
4302	6

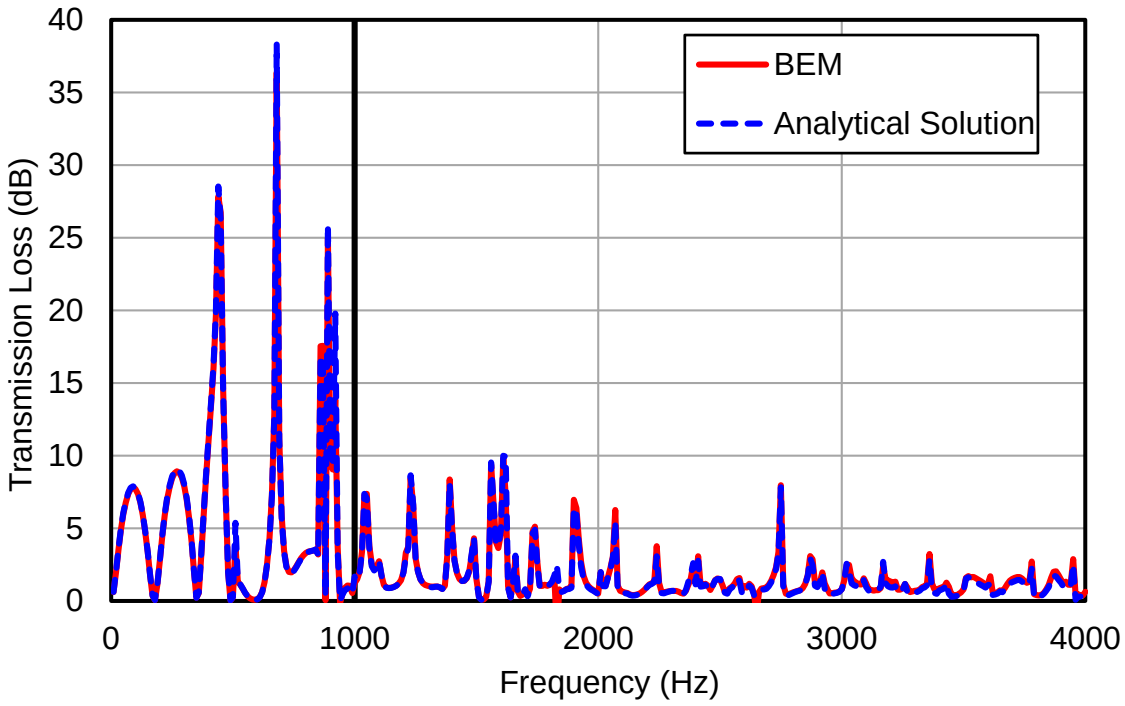

Figure 2.5 TL comparison between the BEM and the analytical solution for the simple expansion chamber test case.

The second test case is a non-axisymmetric expansion chamber as shown in Figure 2.6. The expansion chamber has a small inlet and a small outlet so that its TL can be reliably obtained as a benchmark solution by using the conventional BEM up to the cutoff frequency of the inlet and outlet.

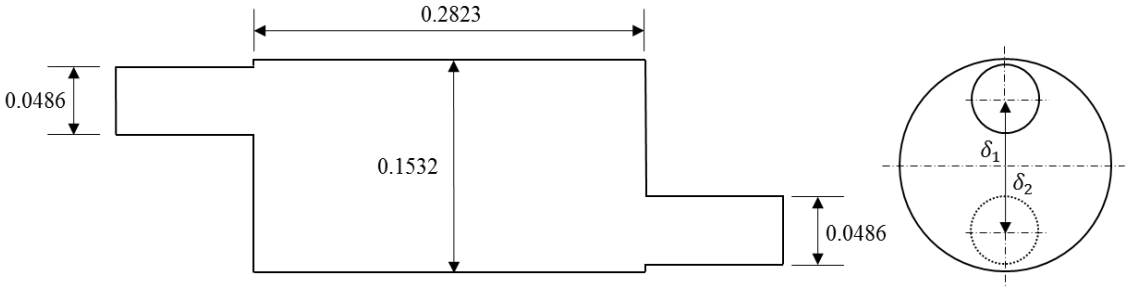

Figure 2.6 Non-axisymmetric expansion chamber (Unit: m; $\delta_1 = \delta_2$= 0.051 m).

To validate the scattering matrix formulation, we intentionally divide the muffler into two subsystems as shown in Figure 2.7, so that each subsystem would have either a large inlet or a large outlet. The transfer scattering matrix of each subsystem can be individually obtained, and then the two matrices are multiplied together to form the resultant transfer scattering matrix:

$$\mathbf{S}^* = \mathbf{S}_1^* \mathbf{S}_2^* \tag{2.56}$$

The resultant transfer scattering matrix $\mathbf{S}^*$ is then converted back to a resultant scattering matrix **S** for the final TL computation.

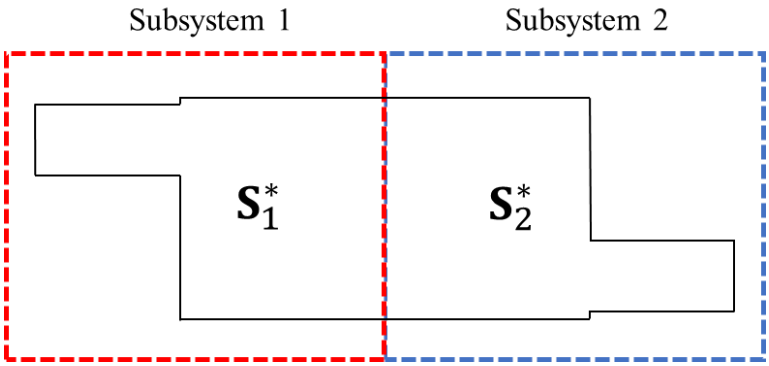

Figure 2.7 Demonstration of two subsystems.

By comparing the TL to the benchmark solution, we can indirectly verify the scattering matrix formulation without having to find the analytical solution of a non-axisymmetric expansion chamber with a large inlet and a large outlet. Table 2.3 lists the cut-on frequencies associated with different (m, n) modes at room temperature. To ensure that all the modes are covered in the frequency range that we are interested in, which is up to 3000 Hz, we select M = 4 and N = 2. The BEM mesh for subsystem 1 has 116 elements at the inlet and 220 elements at the outlet, while subsystem 2 has 220 elements at the inlet and 116 elements at the outlet.

Figure 2.9 compares the two BEM solutions, one from the two-subsystem transfer scattering matrix approach and the other from the conventional single-structure BEM (the benchmark solution). Also shown in Figure 2.8 is the measurement data from Selamet, Ji and Radavich (1998). It is observed that two BEM solutions are identical to each other and both agree very well with the experimental data.

Table 2.3 Cut-on Frequencies at the Chamber of the Non-axisymmetric Simple Expansion Chamber.

m / *n*	0	1	2
0	0	2731	5000
1	1312	3800	6084
2	2177	4779	7105
3	2994	5712	8086
4	3790	6615	9038

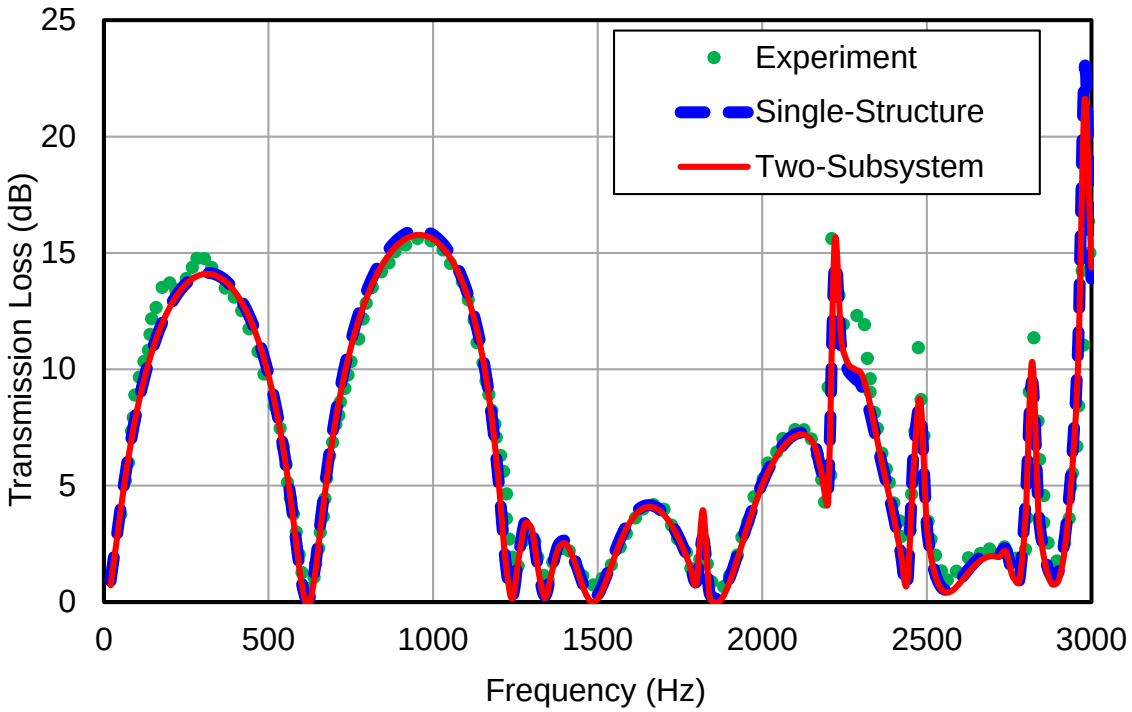

Figure 2.8 Comparison between conventional single-structure BEM, two-subsystem transfer scattering matrix approach, and experiment.

2.7 Impedance-to-Scattering matrix method for a rectangular inlet/outlet

2.7.1 Transformation from the impedance matrix to scattering matrix

The modal expansion of sound pressure inside a rectangular duct is

$$p(x,y,z)=\sum_{m=0}^{\infty}\sum_{n=0}^{\infty}\cos\frac{m\pi x}{b}\cos\frac{n\pi y}{h}\left[A_{mn}\,\mathrm{e}^{-\mathrm{j}k_{z,m,n}z}+B_{mn}\mathrm{e}^{\mathrm{j}k_{z,m,n}z}\right] \tag{2.57}$$

where $k_{z,m,n}$ is the wavenumber associated with the (m, n) mode, which is given by

$$k_{z,m,n}^2=k^2-\left(\frac{m\pi}{b}\right)^2-\left(\frac{n\pi}{h}\right)^2 \tag{2.58}$$

If $z = 0$ is locally set at the inlet cross section, sound pressures of the q boundary elements at the inlet can be expressed in the matrix form

$$\begin{pmatrix} p_{11} \\ p_{12} \\ \cdot \\ \cdot \\ \cdot \\ p_{1q} \end{pmatrix} = [\boldsymbol{MPA}(0), \boldsymbol{MPA}(1), \dots, \boldsymbol{MPA}(M-1), \boldsymbol{MPB}(0), \boldsymbol{MPB}(1), \dots, \boldsymbol{MPB}(M-1)] \begin{pmatrix} \boldsymbol{A}(0) \\ \boldsymbol{A}(1) \\ \vdots \\ \boldsymbol{A}(M-1) \\ \boldsymbol{B}(0) \\ \boldsymbol{B}(1) \\ \vdots \\ \boldsymbol{B}(M-1) \end{pmatrix} \tag{2.59}$$

where

$$\boldsymbol{MPA}(m) = \boldsymbol{MPB}(m) = \begin{bmatrix} \cos\frac{m\pi x}{b}\cos\frac{0\pi y}{h} & \cdots & \cos\frac{m\pi x}{b}\cos\frac{(N-1)\pi y}{h} \\ \vdots & \ddots & \vdots \\ \cos\frac{m\pi x}{b}\cos\frac{0\pi y}{h} & \cdots & \cos\frac{m\pi x}{b}\cos\frac{(N-1)\pi y}{h} \end{bmatrix}_{q\times N} \tag{2.60}$$

$$\boldsymbol{A}(m) = \begin{pmatrix} A_{m0} \\ A_{m1} \\ \cdot \\ \cdot \\ \cdot \\ A_{m(N-1)} \end{pmatrix} \quad \boldsymbol{B}(m) = \begin{pmatrix} B_{m0} \\ B_{m1} \\ \cdot \\ \cdot \\ \cdot \\ B_{m(N-1)} \end{pmatrix} \tag{2.61}$$

and m =0, 1, 2,……, M-1.

Let

$$\mathbf{P_1^+} = \begin{pmatrix} \boldsymbol{A}(0) \\ \boldsymbol{A}(1) \\ \vdots \\ \boldsymbol{A}(M-1) \end{pmatrix} \quad \mathbf{P_1^-} = \begin{pmatrix} \boldsymbol{B}(0) \\ \boldsymbol{B}(1) \\ \vdots \\ \boldsymbol{B}(M-1) \end{pmatrix} \tag{2.62}$$

Equation 2.59 can be re-written in a more compact vector form

$$\mathbf{p_1} = \mathbf{M_{11}} \begin{pmatrix} \mathbf{P_1^+} \\ \mathbf{P_1^-} \end{pmatrix} \tag{2.63}$$

Similarly, sound pressures at the outlet (where $z = 0$ is also locally set) is

$$\mathbf{p_2} = \mathbf{M_{21}} \begin{pmatrix} \mathbf{P_2^+} \\ \mathbf{P_2^-} \end{pmatrix} \tag{2.64}$$

The particle velocity corresponding to the sound pressure in Equation 2.57 is

$$v(x,y,z) = \sum_{m=0}^{\infty} \sum_{n=0}^{\infty} \frac{k_{z,m,n}}{\rho\omega} \cos\frac{m\pi x}{b} \cos\frac{n\pi y}{h} \left[A_{mn}\, \mathrm{e}^{-\mathrm{j}k_{z,m,n}z} - B_{mn}\mathrm{e}^{\mathrm{j}k_{z,m,n}z}\right] \tag{2.65}$$

Express the particle velocities of the q boundary elements at the inlet (where $z = 0$) in terms of the modal amplitudes at the inlet to get

$$\begin{pmatrix} v_{11} \\ v_{12} \\ \cdot \\ \cdot \\ \cdot \\ v_{1q} \end{pmatrix} = [\boldsymbol{MVA}(0), \boldsymbol{MVA}(1), \dots, \boldsymbol{MVA}(M-1), \boldsymbol{MVB}(0), \boldsymbol{MVB}(1), \dots, \boldsymbol{MVB}(M-1)] \begin{pmatrix} \boldsymbol{A}(0) \\ \boldsymbol{A}(1) \\ \vdots \\ \boldsymbol{A}(M-1) \\ \boldsymbol{B}(0) \\ \boldsymbol{B}(1) \\ \vdots \\ \boldsymbol{B}(M-1) \end{pmatrix} \tag{2.66}$$

where

$$\boldsymbol{MVA}(m) = -\boldsymbol{MVB}(m)$$

$$= \begin{bmatrix} \frac{k_{z,m,0}}{\rho\omega} \cos\frac{m\pi x}{b} \cos\frac{0\pi y}{h} & \cdots & \frac{k_{z,m,N-1}}{\rho\omega} \cos\frac{m\pi x}{b} \cos\frac{(N-1)\pi y}{h} \\ \vdots & \ddots & \vdots \\ \frac{k_{z,m,0}}{\rho\omega} \cos\frac{m\pi x}{b} \cos\frac{0\pi y}{h} & \cdots & \frac{k_{z,m,N-1}}{\rho\omega} \cos\frac{m\pi x}{b} \cos\frac{(N-1)\pi y}{h} \end{bmatrix}_{q\times N} \tag{2.67}$$

or in a more compact vector form

$$\mathbf{v_1} = \mathbf{M_{12}} \begin{pmatrix} \mathbf{P_1^+} \\ \mathbf{P_1^-} \end{pmatrix} \tag{2.68}$$

Similarly, particle velocities at the outlet is

$$\mathbf{v_2} = \mathbf{M_{22}} \begin{pmatrix} \mathbf{P_2^+} \\ \mathbf{P_2^-} \end{pmatrix} \tag{2.69}$$

The rest of the derivation is the same as Equations 2.22-2.28.

2.7.2 Rectangular Test Case

The rectangular test case is a square lined duct as shown in Figure 2.9. The lining material (flow resistivity=8,000 Rayl/m) on all four sides is 0.0508 m thick, and is covered by a 30% open perforated facing sheet.

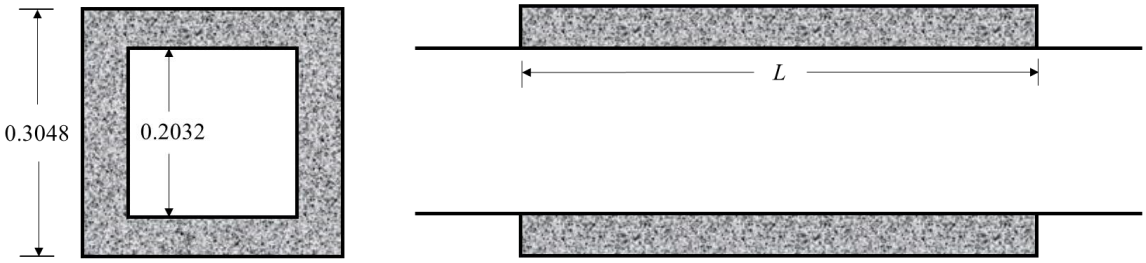

Figure 2.9 Square lined duct test case (Unit: m; *L* = 0.9144 m).

Table 2.4 Cut-on Frequencies at Inlet/Outlet of the Square Lined Duct.

Cut-on Frequency (Hz)	Mode (*m*, *n*)
1688	(1, 0), (0,1)
2387	(1, 1)
3376	(2, 0), (0,2)
3774	(2, 1), (1,2)
4774	(2, 2)
5064	(3, 0), (0,3)
5338	(3, 1), (1,3)
6086	(3, 2), (2,3)
6752	(4, 0), (0,4)
6960	(4, 1), (1,4)
7162	(3, 3)
7549	(4, 2), (2,4)
8440	(5, 0), (0,5)

Due to the symmetry of the design, only ¼ of the lined duct has to be modeled in the BEM. If the lining is modeled by the local impedance boundary condition (as opposed to the bulk-reacting modeling), a simple analytical solution for sound attenuation can be obtained by using the first-mode method proposed by Ingard (1994). Although sound attenuation along a lined duct is not really the TL, it can still be very close due to the simple uniform design. Table 2.4 lists all the cut-on frequencies at room temperature up to 8440 Hz. Since the 6th mode in each direction will not appear until 8440 Hz, $M = N = 5$ is sufficient to solve the problem up to 8000 Hz. The BEM mesh has 529 elements at the inlet, and 529 elements at the outlet. This generates a 1058x1058 impedance matrix at each frequency. Figure 2.10 compares the TL from BEM to the analytical solution for attenuation. Surprisingly, both solutions agree very well with each other. The reason for such a good agreement may be due to the fact that there is barely any reflection from a straight duct and at the same time the first mode probably dominates the attenuation behavior.

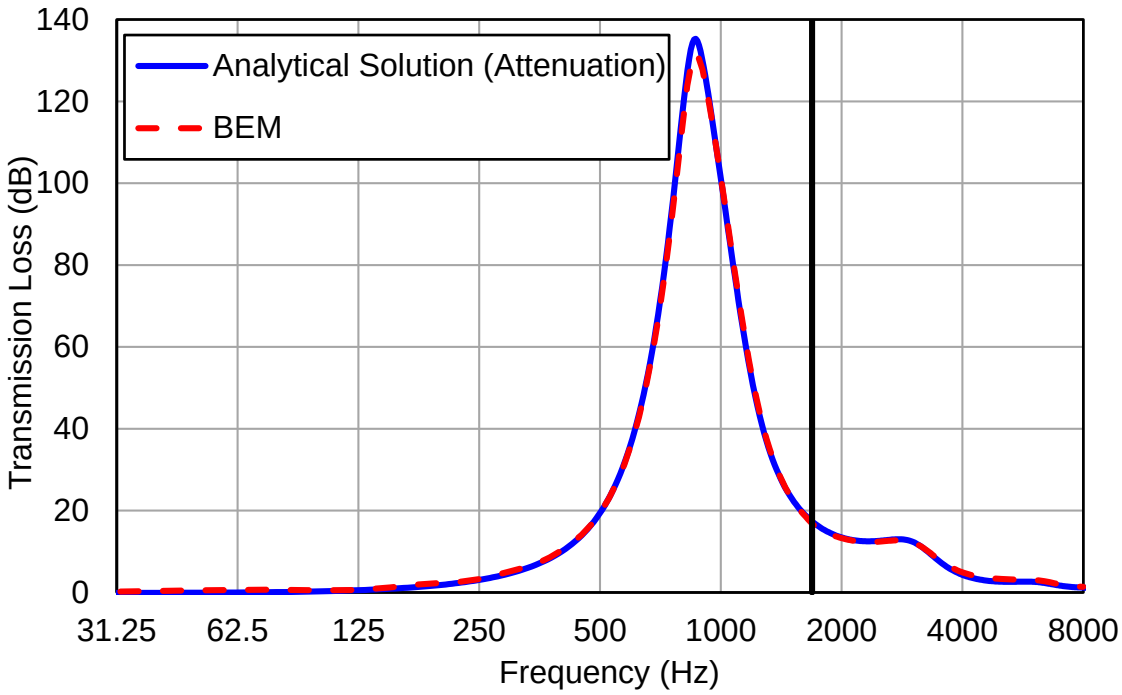

Figure 2.10 Comparison between the BEM (TL) and the analytical solution (attenuation) for the square lined duct.

2.8 Summary

In this chapter, it is demonstrated that the BEM impedance matrix can be converted into the scattering matrix for the axisymmetric configuration, non-axisymmetric circular and the rectangular inlet/outlet shapes based on the point collocation method. The BEM impedance matrix is a very useful BEM output if the solutions from multiple velocity boundary condition sets are solved simultaneously. Conversion of the BEM impedance to the scattering matrix enables the inclusion of higher-order modes in the TL computation for large silencers. The transformation from the BEM impedance matrix to the scattering matrix is validated by either an analytical solution or experimental data, directly or indirectly, for all three configurations.

Chapter 3 BEM ANALYSIS OF LARGE MULTI-INLET MULTI-OUTLET SILENCERS

3.1 Introduction

In Chapter 2, large silencers with a single inlet and a single outlet are analyzed by using the substructured BEM in conjunction with the proposed impedance-to-scattering matrix method. In applications, silencers with multiple inlets and multiple outlets are also quite common. For example, a three-port silencer, which can be one inlet with two outlets or two inlets with one outlet, are frequently used to split or merge exhaust gas streams.

The acoustic performance of multi-inlet and multi-outlet mufflers has been investigated by many researchers below the plane-wave cutoff frequency of the inlets and outlets. Selamet and Ji (2000) proposed a three-dimensional analytical approach to determine the TL of simple circular expansion chambers with a single inlet and two outlets. Similarly, Denia et al. (2003) used a mode-matching method for the acoustical attenuation analysis of elliptical expansion chambers with one inlet and two outlets. Wu et al. (2008) also studied the acoustic performance of a single-inlet/double-outlet cylindrical expansion-chamber based on the modal meshing approach originally proposed by Munjal (1987). Besides the analytical approaches, which are only applicable to very simple configurations, Jiang et al. (2005), Mimani and Munjal (2012) and Xin et al. (2014) used the numerical impedance matrix to derive the TL for small mufflers with multiple inlets and multiple outlets.

The existing literature on the TL analysis of multi-inlet/multi-outlet mufflers are all based on the assumption that only plane waves exist in the inlet and outlet ducts. Therefore, the existing methods for calculating the TL of multi-inlet and multi-outlet mufflers are only suited to small inlet and outlet cross sections where the plane-wave assumption is still valid. However, large multi-inlet/multi-outlet silencers are commonly used in the power generation industry. The plane-wave cutoff frequency of the inlet and outlet ducts can be less than a few hundred Hz, while the frequency range of interest normally goes up to 8000 Hz or higher.

In this chapter, the impedance-to-scattering matrix method is extended to the three-port silencers (Wang et al., 2016 and 2017) for simplicity and for illustration purposes. The method can also be extended to more general multi-inlet and multi-outlet silencers. To validate the proposed method, we compare the TL from the proposed BEM to the equivalent IL solution using AML (Automatically Matched Layer) available in the commercial FEM software, Virtual.Lab. The AML is a special implementation of the “Perfectly Matched Layer” (Berenger, 1994, Tam et al., 1998 and Bermúdez et al., 2007) boundary condition for non-reflective boundaries in FEM. It is well known that when the inlets and outlets are assumed anechoic, the IL is equivalent to the TL. In Virtual.Lab, the AML boundary condition can be easily applied at both the inlet and outlet end to calculate the IL (which is equivalent to the TL) if a single incident wave (loading) is applied to the inlet. However, at this point, the incident wave can be applied to only one inlet in Virtual.Lab. Therefore, the AML/FEM validation in this study is limited to large silencers with one inlet and two outlets only.

3.2 Lumped Impedance matrix method

Before the introduction of the proposed impedance-to-scattering method, Jiang et al's (2005) impedance matrix method for silencers with two inlets is reviewed first in this section.

Figure 3.1 Two-inlet and one-outlet silencer.

As shown in Figure 3.1, the impedance matrix is defined as

$$\begin{Bmatrix} p_1 \\ p_2 \\ p_3 \end{Bmatrix} = \begin{bmatrix} z_{11} & z_{12} & z_{13} \\ z_{21} & z_{22} & z_{23} \\ z_{31} & z_{32} & z_{33} \end{bmatrix} \begin{Bmatrix} v_1 \\ v_2 \\ v_3 \end{Bmatrix} \tag{3.1}$$

where subscripts 1,2 and 3 denote the first inlet, second inlet and outlet location respectively. Below the plane-wave cutoff frequency at the inlets and outlet, the sound pressures and particle velocities at each cross section are uniform. Above the cutoff frequency, the non-uniform sound pressure distribution over the inlets and the outlet is simply averaged out by Jiang et al. (2005). Therefore, a lumped 3X3 impedance matrix can always be obtained at each frequency. Because of this sound pressure averaging procedure, TL is only accurate below the plane-wave cutoff frequency of the inlets/outlet. Nonetheless, it can still provide an

approximate solution above the cutoff frequency, especially within just a few hundred Hz above the cutoff.

The sound pressure and particle velocity at any point inside the inlet duct can be expressed as

$$p = p_i + p_r \tag{3.2}$$

$$v = \frac{p_i - p_r}{\rho c} \tag{3.3}$$

where p_i and p_r are the incident and reflected wave components, respectively. ρ is the air density, and c is the speed of sound.

Since the anechoic termination is assumed for the TL computation, only the transmitted wave component exists inside the outlet duct.

After the substitution of the wave components into Equation 3.1, it then can be expressed as

$$\begin{Bmatrix} p_{1i} + p_{1r} \\ p_{2i} + p_{2r} \\ p_{3t} \end{Bmatrix} = \begin{bmatrix} \frac{z_{11}}{\rho c} & \frac{z_{11}}{\rho c} & \frac{z_{11}}{\rho c} \\ \frac{z_{11}}{\rho c} & \frac{z_{11}}{\rho c} & \frac{z_{11}}{\rho c} \\ \frac{z_{11}}{\rho c} & \frac{z_{11}}{\rho c} & \frac{z_{11}}{\rho c} \end{bmatrix} \begin{Bmatrix} p_{1i} - p_{1r} \\ p_{2i} - p_{2r} \\ p_{3t} \end{Bmatrix} \tag{3.4}$$

Adding $p_{1i} - p_{1r}$ to both sides of the first equation and $p_{2i} - p_{2r}$ to the second equation, yields

$$\begin{Bmatrix} 2p_{1i} \\ 2p_{2i} \\ p_{3t} \end{Bmatrix} = \begin{bmatrix} \frac{z_{11}}{\rho c} + 1 & \frac{z_{11}}{\rho c} & \frac{z_{11}}{\rho c} \\ \frac{z_{11}}{\rho c} & \frac{z_{11}}{\rho c} + 1 & \frac{z_{11}}{\rho c} \\ \frac{z_{11}}{\rho c} & \frac{z_{11}}{\rho c} & \frac{z_{11}}{\rho c} \end{bmatrix} \begin{Bmatrix} p_{1i} - p_{1r} \\ p_{2i} - p_{2r} \\ p_{3t} \end{Bmatrix} \tag{3.5}$$

A ratio of the incident sound pressure at the second inlet to the incident sound pressure at the first inlet has to be defined first for a silencer with two inlets. This ratio is in general a complex number. If the ratio is equal to one, the means the two incident waves have the same amplitude and are in phase. If the ratio is equal to negative one, the two incident waves are 180^o out of phase. In real applications, the ratio may be determined by measuring the amplitude and phase angle of sound pressure at the end of the two exhaust pipes, if an anechoic termination is assumed. A complex ratio β between the two incident sound pressures at the inlets is defined as

$$p_{i2} = \beta p_{i1} \tag{3.6}$$

For simplicity of notation, denote the above 3X3 matrix by **A** and its items by a_{ij}. Substituting the ratio β into Equation 3.5, and dividing both sides of all three equations by p_{3t}, Equation 3.5 can be re-arranged as

$$\begin{bmatrix} -2 & a_{11} & a_{12} \\ -2\beta & a_{21} & a_{22} \\ 0 & a_{31} & a_{32} \end{bmatrix} \begin{Bmatrix} \frac{p_{1i}}{p_{3t}} \\ \frac{p_{1i} - p_{1r}}{p_{3t}} \\ \frac{p_{2i} - p_{2r}}{p_{3t}} \end{Bmatrix} = \begin{Bmatrix} -a_{13} \\ -a_{23} \\ 1 - a_{33} \end{Bmatrix} \tag{3.7}$$

The unknown $\frac{p_{1i}}{p_{3t}}$ can be solved by

$$\frac{p_{1i}}{p_{3t}} = \frac{\begin{vmatrix} -a_{13} & a_{11} & a_{12} \\ -a_{23} & a_{21} & a_{22} \\ 1-a_{33} & a_{31} & a_{32} \end{vmatrix}}{\begin{vmatrix} -2 & a_{11} & a_{12} \\ -2\beta & a_{21} & a_{22} \\ 0 & a_{31} & a_{32} \end{vmatrix}} \tag{3.8}$$

With the $\frac{p_{1i}}{p_{3t}}$ available, TL can be obtained by Equation 3.9 as shown below:

$$TL = 10\log_{10}\frac{W_{1i}+W_{2i}}{W_{3t}} = 10\log_{10}\left|\frac{p_{1i}}{p_{3t}}\right| + 10\log_{10}\frac{S_1+|\beta|^2 S_2}{S_3} \tag{3.9}$$

where S_1, S_2, S_3 are cross-sectional areas of two inlets and the outlet, respectively.

3.3 Impedance-to-Scattering matrix method

In this section, the derivation of the impedance-to-scattering matrix method is demonstrated by using a two-inlet/one-outlet silencer. It can be found at the end of the derivation that the scattering matrix of a one-inlet/two-outlet silencer remains the same.

3.3.1 BEM impedance matrix

The BEM impedance matrix $\mathbf{Z}$ of a two-inlet/one-outlet silencer is defined by

$$\begin{pmatrix} p_{11} \\ p_{12} \\ \vdots \\ p_{1X} \\ \cdots\cdots \\ p_{21} \\ p_{22} \\ \vdots \\ p_{2Y} \\ \cdots\cdots \\ p_{31} \\ p_{32} \\ \vdots \\ p_{3Q} \end{pmatrix} = \begin{bmatrix} Z_{1,1} & \cdots & Z_{1,X+Y+Q} \\ \vdots & \ddots & \vdots \\ Z_{X+Y+Q,1} & \cdots & Z_{X+Y+Q,X+Y+Q} \end{bmatrix} \begin{pmatrix} v_{11} \\ v_{12} \\ \vdots \\ v_{1X} \\ \cdots\cdots \\ v_{21} \\ v_{22} \\ \vdots \\ v_{2Y} \\ \cdots\cdots \\ v_{31} \\ v_{32} \\ \vdots \\ v_{3Q} \end{pmatrix} \tag{3.10}$$

where p and v denote the sound pressure and particle velocity at the inlet and outlet. For p and v, the first subscript 1, 2 and 3 represent inlet 1, inlet 2 and outlet, respectively; the second subscript represents the boundary element numbering (X constant boundary elements at inlet 1, Y constant boundary elements at inlet 2, and Q constant boundary elements at the outlet). The impedance matrix can be obtained by "turning on" v =1 on each element at the two inlets and the outlet successively, one at a time. Although there are a total of $\mathrm{X}+\mathrm{Y}+\mathrm{Q}$ velocity boundary condition sets, they all share the same BEM coefficient matrix. Therefore, only one matrix inverse is needed at each frequency.

Equation (3.10) can re-written in a more compact vector form:

$$\begin{pmatrix} \mathbf{p_1} \\ \mathbf{p_2} \\ \mathbf{p_3} \end{pmatrix} = \begin{bmatrix} \mathbf{Z_{11}} & \mathbf{Z_{12}} & \mathbf{Z_{13}} \\ \mathbf{Z_{21}} & \mathbf{Z_{22}} & \mathbf{Z_{23}} \\ \mathbf{Z_{31}} & \mathbf{Z_{32}} & \mathbf{Z_{33}} \end{bmatrix} \begin{pmatrix} \mathbf{v_1} \\ \mathbf{v_2} \\ \mathbf{v_3} \end{pmatrix} \tag{3.11}$$

where 1, 2 and 3 denote the inlet 1, inlet 2 and the outlet, respectively, and the element numbering index is dropped. In Jiang et al. (2005), Equation 3.11 is lumped into Equation 3.1 after averaging out the non-uniform pressure distributions over the inlets and the outlet.

3.3.2 Scattering matrix

The scattering matrix **S** relates the modal amplitudes in the inlets and outlet ducts:

$$\begin{pmatrix} P_{30}^{+} \\ P_{31}^{+} \\ \vdots \\ P_{3(N-1)}^{+} \\ \cdots \\ P_{10}^{-} \\ P_{11}^{-} \\ \vdots \\ P_{1(N-1)}^{-} \\ \cdots \\ P_{20}^{-} \\ P_{21}^{-} \\ \vdots \\ P_{2(N-1)}^{-} \end{pmatrix} = \begin{bmatrix} S_{1,1} & \cdots & S_{1,3N} \\ \vdots & \ddots & \vdots \\ S_{3N,1} & \cdots & S_{3N,3N} \end{bmatrix} \begin{pmatrix} P_{10}^{+} \\ P_{11}^{+} \\ \vdots \\ P_{1(N-1)}^{+} \\ \cdots \\ P_{20}^{+} \\ P_{21}^{+} \\ \vdots \\ P_{2(N-1)}^{+} \\ \cdots \\ P_{30}^{-} \\ P_{31}^{-} \\ \vdots \\ P_{3(N-1)}^{-} \end{pmatrix} \tag{3.12}$$

where P denotes the wave amplitude of a particular mode. The superscript + on P represents the right-traveling wave and – the left-traveling wave; the first subscript 1, 2 and 3 represent inlet 1, inlet 2 and outlet, respectively. Assume that there are

N modes in each of the two inlet ducts and the outlet duct as well. The N modes may include evanescent modes, but normally one evanescent mode is enough if the inlet and outlet ducts have a certain length that can ensure the next evanescent mode has a negligible contribution when it travels to the inlets and outlet. Equation (3.12) can be re-written in a more compact vector form:

$$\begin{pmatrix} \mathbf{P_3^+} \\ \mathbf{P_1^-} \\ \mathbf{P_2^-} \end{pmatrix} = \begin{bmatrix} \mathbf{S_{11}} & \mathbf{S_{12}} & \mathbf{S_{13}} \\ \mathbf{S_{21}} & \mathbf{S_{22}} & \mathbf{S_{23}} \\ \mathbf{S_{31}} & \mathbf{S_{32}} & \mathbf{S_{33}} \end{bmatrix} \begin{pmatrix} \mathbf{P_1^+} \\ \mathbf{P_2^+} \\ \mathbf{P_3^-} \end{pmatrix} \tag{3.13}$$

3.3.3 Transformation from impedance matrix to scattering matrix

The modal expansion of sound pressure and particle velocity inside a cylindrical duct with a non-axisymmetric solution can be retrieved from Section 2.5.1.

For convenience, $z = 0$ is locally set at the inlet cross section. Therefore, the modal expansion of sound pressures of the X boundary elements at inlet 1 can be expressed in the matrix form

$$\begin{pmatrix} p_{11} \\ p_{12} \\ \cdot \\ \cdot \\ \cdot \\ p_{1\mathrm{X}} \end{pmatrix} = [\boldsymbol{MPA_{0n}}, \boldsymbol{MPA_{mn}^+}, \boldsymbol{MPA_{mn}^-}, \boldsymbol{MPB_{0n}}, \boldsymbol{MPB_{mn}^+}, \boldsymbol{MPB_{mn}^-}] \begin{pmatrix} \boldsymbol{A_{0n}} \\ \boldsymbol{A_{mn}^+} \\ \boldsymbol{A_{mn}^-} \\ \boldsymbol{B_{0n}} \\ \boldsymbol{B_{mn}^+} \\ \boldsymbol{B_{mn}^-} \end{pmatrix} \tag{3.14}$$

The detail of each item in Equation 3.14 can be found in Section 2.5.1.

Equation 3.14 can be re-written in a more compact vector form

$$\mathbf{p_1} = \mathbf{M_{11}} \begin{pmatrix} \mathbf{P_1^+} \\ \mathbf{P_1^-} \end{pmatrix} \tag{3.15}$$

Similarly, sound pressures at inlet 2 and the outlet (where $z = 0$ is also locally set) are

$$\mathbf{p_2} = \mathbf{M_{21}} \begin{pmatrix} \mathbf{P_2^+} \\ \mathbf{P_2^-} \end{pmatrix} \tag{3.16}$$

$$\mathbf{p_3} = \mathbf{M_{31}} \begin{pmatrix} \mathbf{P_3^+} \\ \mathbf{P_3^-} \end{pmatrix} \tag{3.17}$$

Express the particle velocities of the X boundary elements at inlet 1 (where $z = 0$) in terms of the modal amplitudes to get

$$\begin{pmatrix} v_{11} \\ v_{12} \\ . \\ . \\ . \\ v_{1q} \end{pmatrix} = [\boldsymbol{MVA_{0n}}, \boldsymbol{MVA_{mn}^+}, \boldsymbol{MVA_{mn}^-}, \boldsymbol{MVB_{0n}}, \boldsymbol{MVB_{mn}^+}, \boldsymbol{MVB_{mn}^-}] \begin{pmatrix} \boldsymbol{A_{0n}} \\ \boldsymbol{A_{mn}^+} \\ \boldsymbol{A_{mn}^-} \\ \boldsymbol{B_{0n}} \\ \boldsymbol{B_{mn}^+} \\ \boldsymbol{B_{mn}^-} \end{pmatrix} \tag{3.18}$$

The detail of each item in Equation 3.14 can be found in Section 2.5.1.

A more compact vector form of Equation 3.18 is

$$\mathbf{v_1} = \mathbf{M_{12}} \begin{pmatrix} \mathbf{P_1^+} \\ \mathbf{P_1^-} \end{pmatrix} \tag{3.19}$$

Similarly, particle velocities at inlet 2 and the outlet are

$$\mathbf{v_2} = \mathbf{M_{22}} \begin{pmatrix} \mathbf{P_2^+} \\ \mathbf{P_2^-} \end{pmatrix} \tag{3.20}$$

$$\mathbf{v_3} = \mathbf{M_{32}} \begin{pmatrix} \mathbf{P_3^+} \\ \mathbf{P_3^-} \end{pmatrix} \tag{3.21}$$

Substitute Equations 3.15, 3.16, 3.17, and 3.19, 3.20, 3.21 into Equation 3.11 to get

$$\mathbf{M_{11}} \begin{pmatrix} \mathbf{P_1^+} \\ \mathbf{P_1^-} \end{pmatrix} = \mathbf{Z_{11}M_{12}} \begin{pmatrix} \mathbf{P_1^+} \\ \mathbf{P_1^-} \end{pmatrix} + \mathbf{Z_{12}M_{22}} \begin{pmatrix} \mathbf{P_2^+} \\ \mathbf{P_2^-} \end{pmatrix} + \mathbf{Z_{13}M_{32}} \begin{pmatrix} \mathbf{P_3^+} \\ \mathbf{P_3^-} \end{pmatrix} \tag{3.22}$$

$$\mathbf{M_{21}} \begin{pmatrix} \mathbf{P_2^+} \\ \mathbf{P_2^-} \end{pmatrix} = \mathbf{Z_{21}M_{12}} \begin{pmatrix} \mathbf{P_1^+} \\ \mathbf{P_1^-} \end{pmatrix} + \mathbf{Z_{22}M_{22}} \begin{pmatrix} \mathbf{P_2^+} \\ \mathbf{P_2^-} \end{pmatrix} + \mathbf{Z_{32}M_{32}} \begin{pmatrix} \mathbf{P_3^+} \\ \mathbf{P_3^-} \end{pmatrix} \tag{3.23}$$

$$\mathbf{M_{31}} \begin{pmatrix} \mathbf{P_3^+} \\ \mathbf{P_3^-} \end{pmatrix} = \mathbf{Z_{31}M_{12}} \begin{pmatrix} \mathbf{P_1^+} \\ \mathbf{P_1^-} \end{pmatrix} + \mathbf{Z_{32}M_{22}} \begin{pmatrix} \mathbf{P_2^+} \\ \mathbf{P_2^-} \end{pmatrix} + \mathbf{Z_{33}M_{33}} \begin{pmatrix} \mathbf{P_3^+} \\ \mathbf{P_3^-} \end{pmatrix} \tag{3.24}$$

The above three equations are combined into a single matrix equation below:

$$\begin{bmatrix} \mathbf{M_{11} - Z_{11}M_{12}} \\ \mathbf{-Z_{21}M_{12}} \\ \mathbf{-Z_{31}M_{12}} \end{bmatrix} \begin{pmatrix} \mathbf{P_1^+} \\ \mathbf{P_1^-} \end{pmatrix} + \begin{bmatrix} \mathbf{-Z_{12}M_{22}} \\ \mathbf{M_{21} - Z_{22}M_{22}} \\ \mathbf{-Z_{32}M_{22}} \end{bmatrix} \begin{pmatrix} \mathbf{P_2^+} \\ \mathbf{P_2^-} \end{pmatrix} = \begin{bmatrix} \mathbf{Z_{13}M_{32}} \\ \mathbf{Z_{32}M_{32}} \\ \mathbf{-M_{31} + Z_{33}M_{33}} \end{bmatrix} \begin{pmatrix} \mathbf{P_3^+} \\ \mathbf{P_3^-} \end{pmatrix} \tag{3.25}$$

There is one more step before we can get to the scattering matrix. This is to move all known conditions to one side and all unknown conditions to the other. It should be pointed out that a well-posed boundary value problem should have a known condition at the inlet and another known condition at the outlet. For example, to find the TL, a certain incident wave ($\mathbf{P_1^+}$, $\mathbf{P_2^+}$) should be given at the two inlets, and the outlet is assumed anechoic ($\mathbf{P_3^- = 0}$). To split the matrix contributions to the incident and reflected waves in Equation 3.25, let

$$\begin{bmatrix} \mathbf{M_{11}} - \mathbf{Z_{11}M_{12}} \\ -\mathbf{Z_{21}M_{12}} \\ -\mathbf{Z_{31}M_{12}} \end{bmatrix} = [\mathbf{N_{11}} \quad \mathbf{N_{12}}] \tag{3.26}$$

$$\begin{bmatrix} -\mathbf{Z_{12}M_{22}} \\ \mathbf{M_{21}} - \mathbf{Z_{22}M_{22}} \\ -\mathbf{Z_{32}M_{22}} \end{bmatrix} = [\mathbf{N_{21}} \quad \mathbf{N_{22}}] \tag{3.27}$$

$$\begin{bmatrix} \mathbf{Z_{13}M_{32}} \\ \mathbf{Z_{32}M_{32}} \\ -\mathbf{M_{31}} + \mathbf{Z_{33}M_{33}} \end{bmatrix} = [\mathbf{N_{31}} \quad \mathbf{N_{32}}] \tag{3.28}$$

and re-arrange Equation 3.25 to obtain

$$[\mathbf{N_{31}} \quad -\mathbf{N_{12}} \quad -\mathbf{N_{22}}] \begin{pmatrix} \mathbf{P_3^+} \\ \mathbf{P_1^-} \\ \mathbf{P_2^-} \end{pmatrix} = [\mathbf{N_{11}} \quad \mathbf{N_{21}} \quad -\mathbf{N_{32}}] \begin{pmatrix} \mathbf{P_1^+} \\ \mathbf{P_2^+} \\ \mathbf{P_3^-} \end{pmatrix} \tag{3.29}$$

Equation 3.29 is now “well-posed” because it has both inlet and outlet components on each side. Since there are always more boundary elements than the number of propagating modes, a least-squares matrix inverse procedure can be performed on Equation 3.29 to get the scattering matrix **S**,

$$\begin{pmatrix} \mathbf{P_3^+} \\ \mathbf{P_1^-} \\ \mathbf{P_2^-} \end{pmatrix} = \begin{bmatrix} \mathbf{S_{11}} & \mathbf{S_{12}} & \mathbf{S_{13}} \\ \mathbf{S_{21}} & \mathbf{S_{22}} & \mathbf{S_{23}} \\ \mathbf{S_{31}} & \mathbf{S_{32}} & \mathbf{S_{33}} \end{bmatrix} \begin{pmatrix} \mathbf{P_1^+} \\ \mathbf{P_2^+} \\ \mathbf{P_3^-} \end{pmatrix} \tag{3.30}$$

For silencers with one inlet and two outlets, the above scattering matrix remains the same if 1 and 2 now represent the two outlets and 3 represents the inlet. The only thing that needs to modify is the input from (1,0,0..), (1,0,0..) and (0,0,0,…) to (0,0,0,…) , (0,0,0,…) and (1,0,0..).

3.4 Test Cases

The first two test cases compare the difference between the lumped impedance matrix method (Jiang et al. 2005) and the proposed impedance-to-scattering matrix method for silencers with two inlets and one outlet. To compute the TL of a two-inlet silencer, a complex ratio β between the two incident sound pressures at the inlets is required. In this section, we set $\beta = 1$.

The first test case is an expansion chamber with two inlets and one outlet as shown in Figure 3.2. The same test case was used in Jiang et al. (2005) up to 4000 Hz. The plane-wave cutoff frequency of a 0.04 m diameter tube is 5025 Hz at room temperature. Even though there are no higher-order modes in the frequency range of interest, *M* = 2 and *N* = 2 are still used to test the current formulation. Figure 3.3 shows the TL comparison between the proposed impedance-to-scattering matrix method and the lumped impedance matrix method. It is seen that the two methods produce identical results below the cutoff frequency as expected.

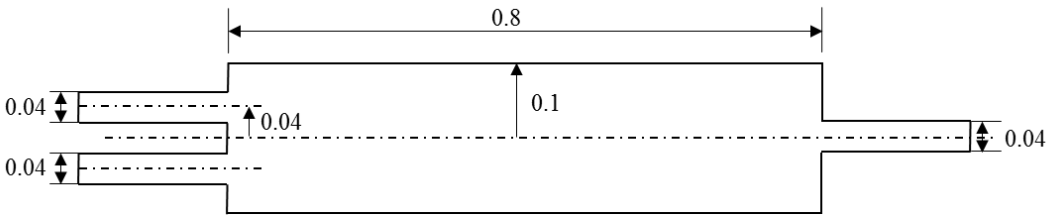

Figure 3.2 Simple expansion chamber with two inlets and one outlet (Unit: m).

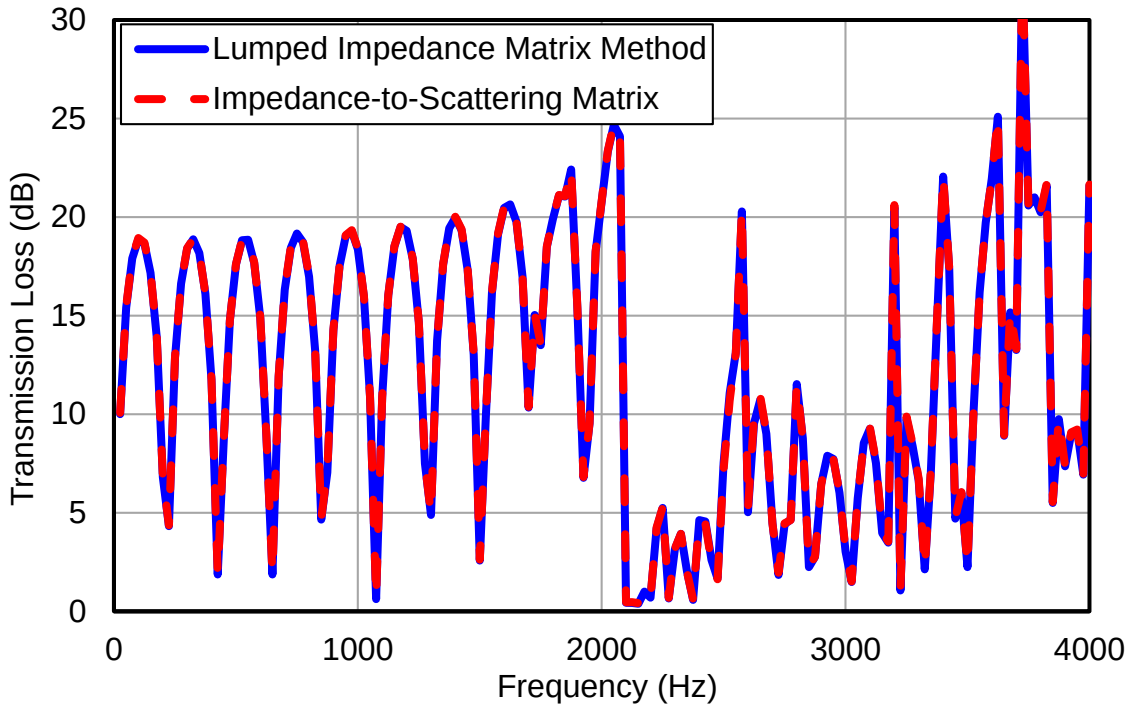

Figure 3.3 TL comparison between impedance-to-scattering matrix and lumped impedance matrix method.

The second test case is a round bar silencer with two inlets as shown in Figure 3.4. The absorptive bar is made of polyester (flow resistivity=16,000 Rayl/m) and is covered by a 30% open perforated facing sheet and two rigid end panels. Due to the size of the silencer, the substructuring technique is used to obtain the resultant impedance matrix before it is converted into the scattering matrix. The template substructure is 1/9 of substructure 2, and its impedance matrix can be repeatedly used 9 times in the impedance matrix synthesis procedure.

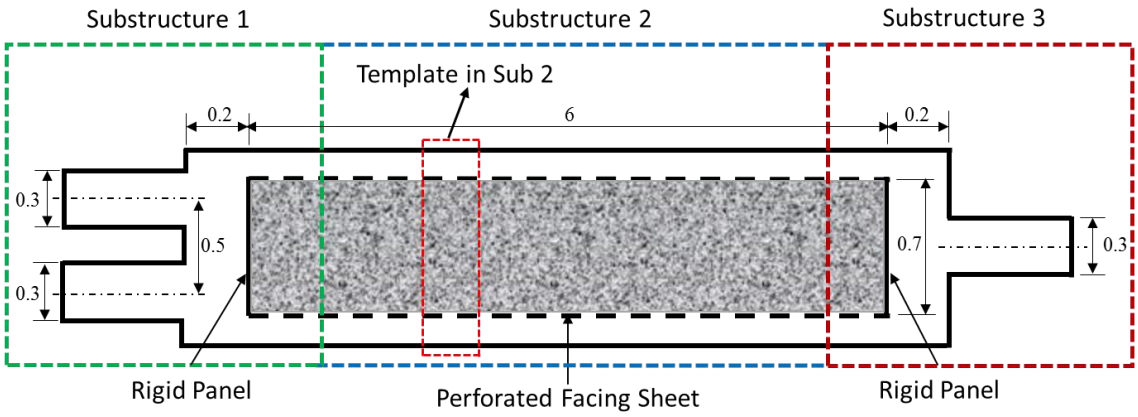

Figure 3.4 A two-inlet round bar silencer model with three substructures (Unit: m).

The cut-off frequency of the large outlet is 670 Hz at room temperature, and we run the test case up to 2500 Hz. To consider the higher-order modes, we select M = 7 and N = 3. Figure 3.5 shows the comparison between the impedance-to-scattering matrix method and the lumped impedance matrix method. The pressure averaging procedure works well below the plane-wave cutoff frequency of the inlets/outlet because the sound pressure distribution is still uniform at any cross section of the inlet/outlet ducts. Above the cutoff, sound pressure distribution over each cross section gradually becomes nonuniform as higher-order modes begin to emerge. This explains why both methods produce the same TL below the cutoff and the lumped impedance matrix result begins to diverge as the frequency goes higher.

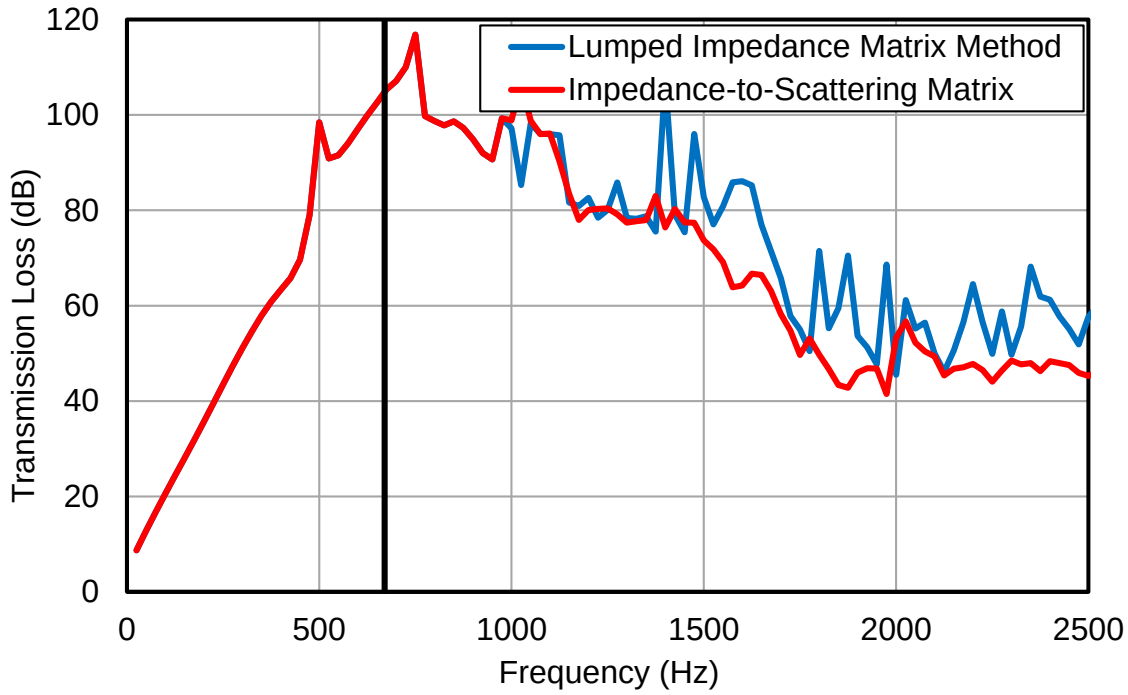

Figure 3.5 TL comparison between impedance-to-scattering matrix and lumped impedance matrix method.

At frequencies above the cutoff, the FEM/AML technique is used to validate the proposed impedance-to-scattering matrix method. At this point, since the incident source can only be applied to one inlet in Virtual.Lab, the following FEM/AML validation is limited to silencers with one inlet and two outlets. The third test case is a three-port expansion chamber as shown in Figure 3.6. The plane-wave cutoff frequency of a 0.08 m diameter tube is 2510 Hz at room temperature. To consider the higher-order modes, we select $M = 6$ and $N = 6$. Figure 3.7 compares the one-inlet/two-outlet expansion chamber between the impedance-to-scattering matrix method and the FEM/AML method. It is seen that both method compare very well with each other up to 8000 Hz.

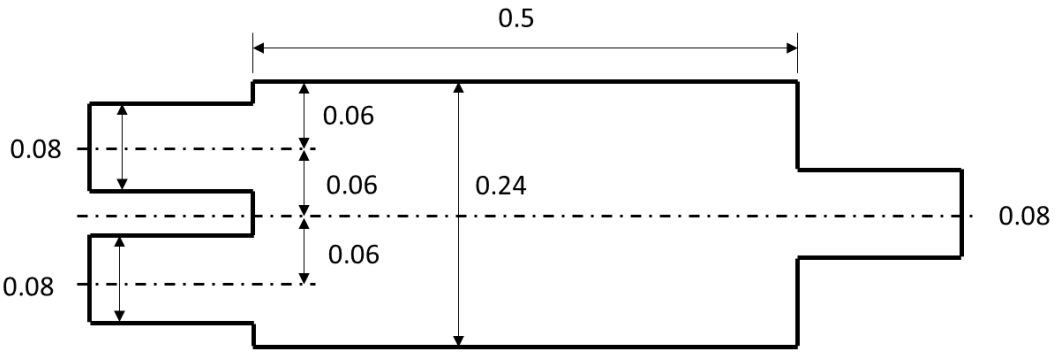

Figure 3.6 Three-port expansion chamber (Unit: m).

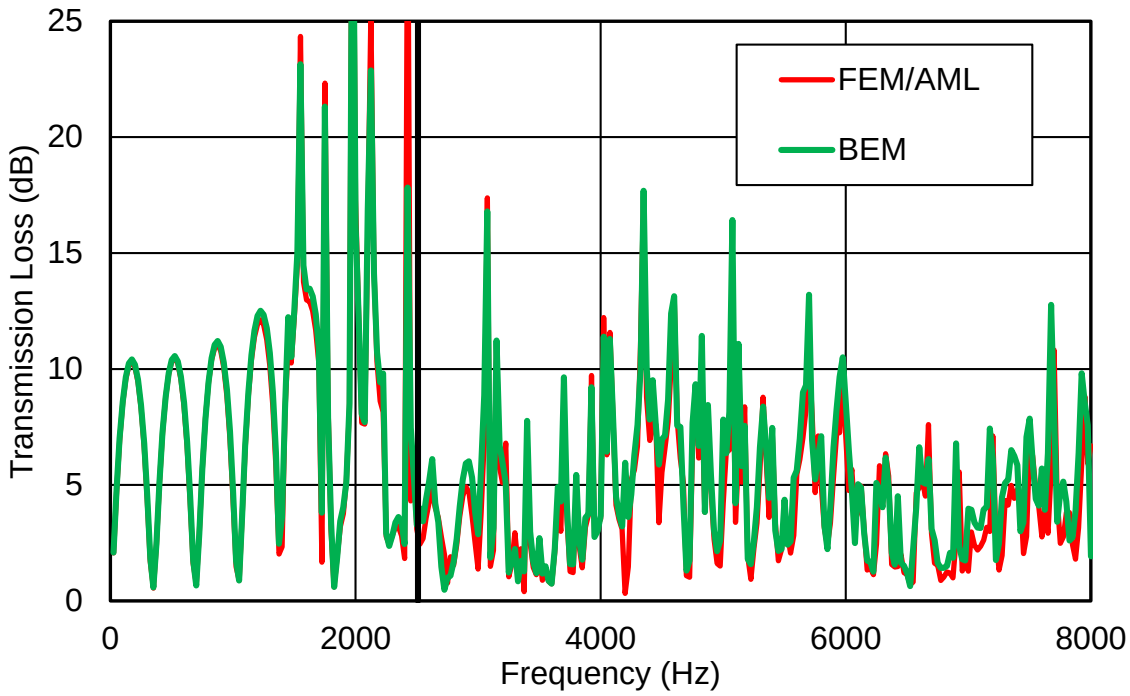

Figure 3.7 TL of the one-inlet/two-outlet expansion chamber comparison between FEM/AML and BEM.

The comparison between the one-inlet/two-outlet and the two-inlet/one-outlet expansion chamber is shown in Figure 3.8, and it is found that the TL is identical below the plane-wave cutoff frequency and starts to vary above the cutoff.

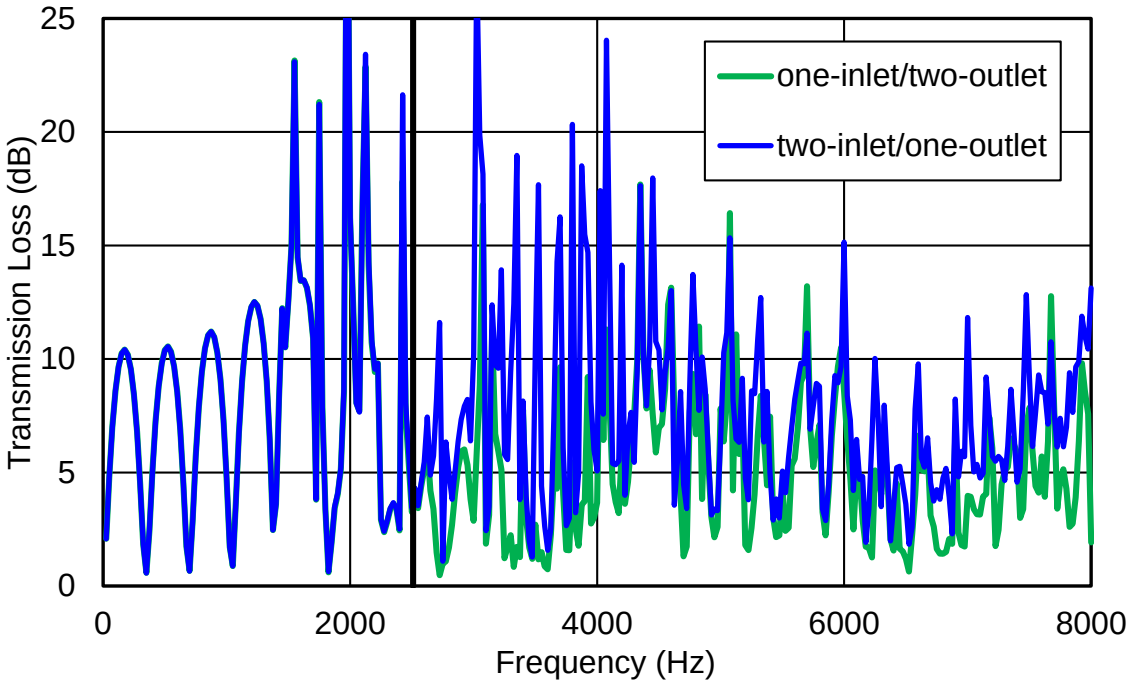

Figure 3.8 TL comparison between one-inlet/two-outlet and two-inlet/one-outlet expansion chamber.

The fourth test case is a three-port absorptive silencer as shown in Figure 3.9. The absorptive material is polyester (flow resistivity=16,000 Rayl/m, thickness = 0.05m) and is covered by a 30% open perforated facing sheet. Figure 3.10 compares the one-inlet/two-outlet expansion chamber comparison between the impedance-to-scattering matrix method and the FEM/AML method. It is seen that both method compare very well with each other up to 8000 Hz. The comparison between the one-inlet/two-outlet and the two-inlet/one-outlet arrangements is shown in Figure 3.11. It is seen that the two TL curves are identical below the plane-wave cutoff frequency. The difference between the two silencers is also minimal above the cutoff frequency.

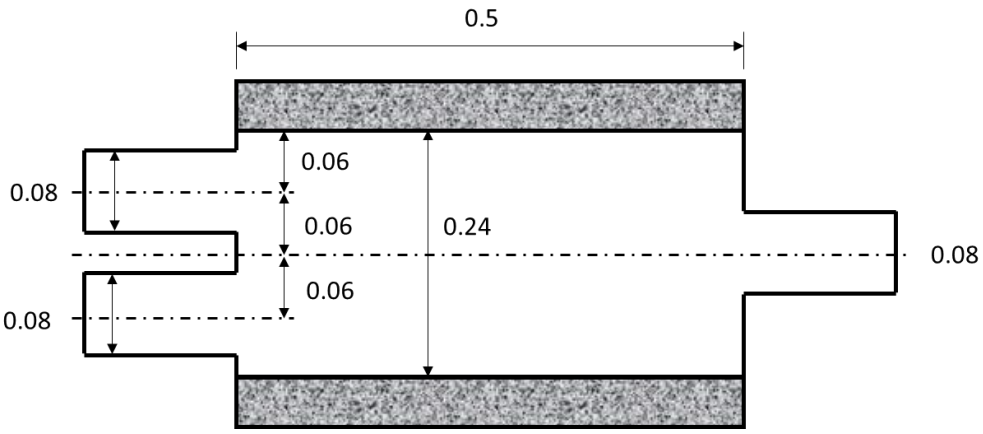

Figure 3.9 Three-port absorptive silencer (Unit: *m*).

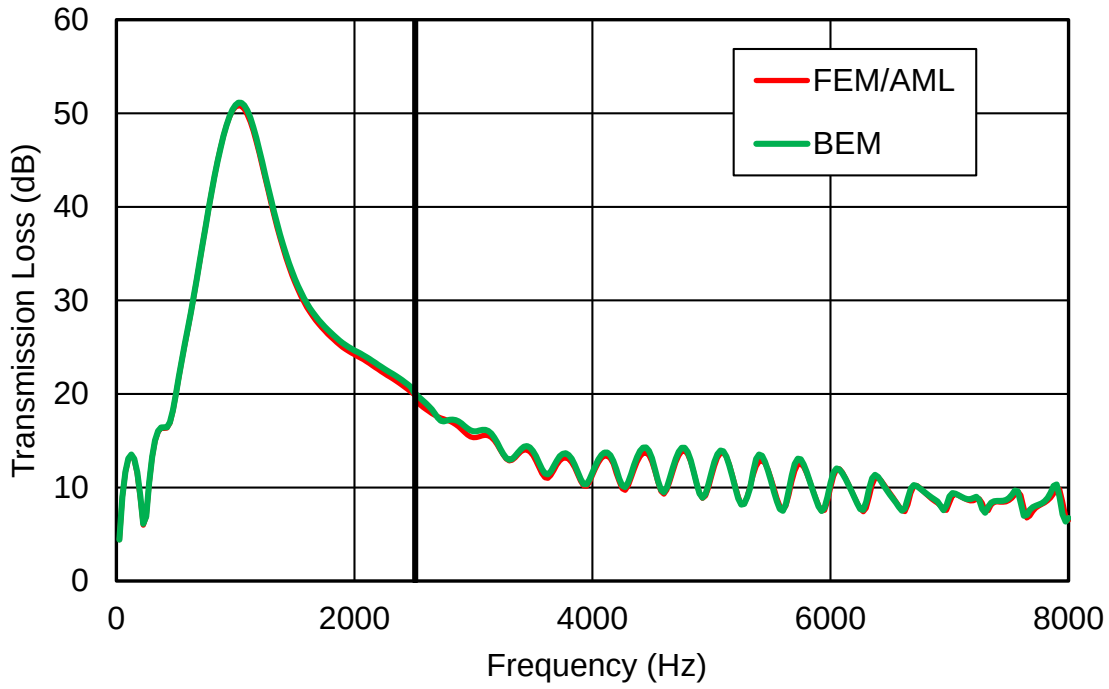

Figure 3.10 TL of the one-inlet/two-outlet absorptive silencer comparison between FEM/AML and BEM.

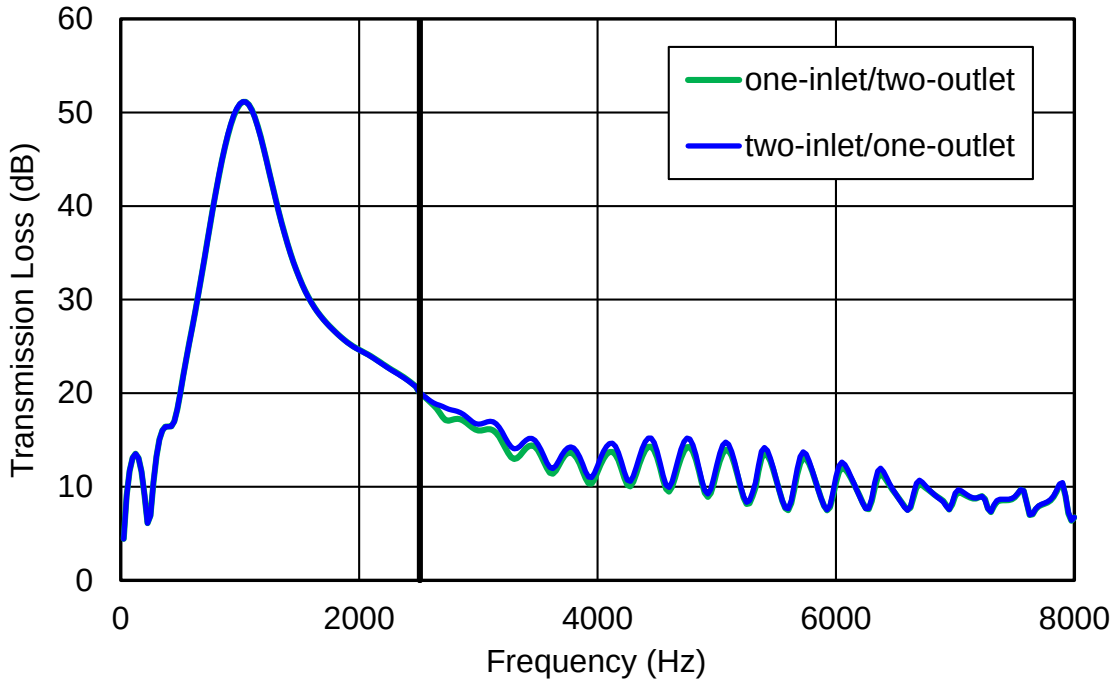

Figure 3.11 TL comparison between one-inlet/two-outlet and two-inlet/one-outlet absorptive silencer.

3.5 Summary

The impedance-to-scattering matrix method is extended to large multi-inlet and multi-outlet silencers. In this chapter, the two-inlet/one-outlet silencer is used to demonstrate the transformation from the impedance matrix to the scattering matrix.

Numerical results from the proposed impedance-to-scattering matrix method agree very well with the results from the lumped impedance matrix method below the plane-wave cutoff frequency. Above the cutoff, the lumped impedance matrix solution begins to diverge from the scattering matrix solution. Even though the pressure-averaging procedure to produce the lumped 3X3 impedance matrix has no theoretical basis above the plane-wave cutoff, the lumped impedance matrix method can still provide an approximate solution for comparison purposes.

The FEM/AML is used to validate the proposed impedance-to-scattering matrix method above the plane-wave cutoff frequency for silencers with the one inlet and two outlets. The one-inlet/two-outlet and the two-inlet/one-outlet silencers are also compared to each other. It is found that they have the identical TL below the plane-wave cutoff frequency, but begin to diverge slightly above the cutoff. Nonetheless, the difference is very small, especially for the absorptive silencer test case.

Chapter 4 INTEGRAL-BASED IMPEDANCE-TO-SCATTERING MARIX METHOD FOR LARGE SILENCER ANALYSIS

4.1 Introduction

In Chapter 2 and Chapter 3, a point collocation based impedance-to-scattering matrix method is proposed for large silencer analysis. In this method, modal expansion is used to express each sound pressure and particle velocity in terms of the duct modes at the centroid of each constant boundary element at the inlet and outlet. Substituting these point-wise modal expansions into the BEM impedance matrix relationship will result in the scattering matrix that relates the modes at the inlet and outlet. In the case of constant boundary elements, the centroid of each element is a natural choice, although the constant pressure and the constant velocity can apply to any point on the element. To avoid any uncertainties associated with where to collocate, an integral-based impedance-to-scattering matrix method based on the reciprocal identity method is developed in this chapter.

Zhou et al. (2016) proposed a numerical technique based on the reciprocal identity integral to determine the TL of large silencers at all frequencies. The reciprocal identity is an integral equation that couples two different sound fields on the same silencer. The first sound field used in the reciprocal identity coupling is an analytical solution with a single incident plane wave at the inlet and an anechoic termination at the outlet. This analytical solution represents an ideal condition under which the TL is defined. The second sound field used in the reciprocal identity coupling is the BEM solution associated with a random boundary condition

set. Each reciprocal identity that couples the two sound fields, one analytical and the other BEM associated with a random boundary condition set, forms one linearly independent equation. Depending on how many modes can propagate to the inlet and outlet at a given frequency, a minimum number of BEM solutions are needed for the reciprocal identity coupling. The BEM impedance matrix can naturally provide more than enough such solutions since each column of the impedance matrix represents a BEM solution corresponding to a unique boundary condition set. A least-squares procedure is then used to solve for the unknown modal amplitudes.

The proposed integral-based impedance-to-scattering matrix method is a direct extension of the reciprocal identity method by Zhou et al (2016). It should be noted that Zhou et al's reciprocal identity method was meant to calculate the TL only. In contrast, not only can the proposed extension calculate the TL, but it can also produce the scattering matrix of the silencer, which can bring additional benefits in other applications. One potential benefit is to combine subsystems in series or parallel connection by using the scattering matrix synthesis. Although combining subsystems in series or parallel connection can also be achieved by using the BEM impedance matrix synthesis (Lou et al. 2003), the scattering matrix is a more desirable matrix because it does not depend on any BEM mesh. In other words, a BEM impedance matrix is always associated with a particular BEM mesh, while the scattering matrix is a system property of the silencer itself. The details of the scattering matrix synthesis will be presented in Chapter 5. Additionally, the

proposed integral-based method can provide a comparison and validation tool for the collocation-based method presented in Chapter 2.

4.2 Reciprocal identity

In a homogeneous acoustic domain without mean flow, sound propagation in the frequency domain is governed by the Helmholtz equation. Different sets of boundary conditions may be applied to the boundary. With each different set of boundary conditions, the sound field is expected to be different. Let p_{A} and p_{B} represent two different sound pressure solutions corresponding to two distinct boundary condition sets, A and B, respectively. Both sound pressures, p_{A} and p_{B} satisfy the Helmholtz equation,

$$\nabla^2 p_{\mathrm{A}} + k^2 p_{\mathrm{A}} = 0 \tag{4.1}$$

$$\nabla^2 p_{\mathrm{B}} + k^2 p_{\mathrm{B}} = 0 \tag{4.2}$$

where *k* is the wavenumber. The Green's second identity is then applied to relate these two different sound fields,

$$\int_{\Omega} (p_{\mathrm{A}} \nabla^2 p_{\mathrm{B}} - p_{\mathrm{B}} \nabla^2 p_{\mathrm{A}}) \, \mathrm{dV} = \int_{\partial\Omega} \left(p_{\mathrm{A}} \frac{\partial p_{\mathrm{B}}}{\partial n} - p_{\mathrm{B}} \frac{\partial p_{\mathrm{A}}}{\partial n} \right) \mathrm{dS} \tag{4.3}$$

where n is the outward normal direction, Ω the homogeneous acoustic domain free of any thin or perforated bodies, and $\partial\Omega$ the boundary surface. Substituting Equation 4.1 and 4.2 into the above identity yields

$$\int_{\partial\Omega}\left(p_{\mathrm{A}}\frac{\partial p_{\mathrm{B}}}{\partial n}-p_{\mathrm{B}}\frac{\partial p_{\mathrm{A}}}{\partial n}\right)\,\mathrm{dS}=0 \tag{4.4}$$

Since the right-hand side of Equation 4.4 is zero, we may take the liberty of flipping the outward normal to the inward direction in Equation 4.4 so that it is consistent with most acoustic BEM software. In linear acoustics, the momentum equation relates the normal derivative of sound pressure to the normal particle velocity by

$$\frac{\partial p}{\partial n}=-j\rho\omega v \tag{4.5}$$

where ω is the angular frequency and v is the particle velocity in the normal direction. Equation 4.4 becomes

$$\int_{\partial\Omega}(p_{\mathrm{A}}v_{\mathrm{B}}-p_{\mathrm{B}}v_{\mathrm{A}})\,\mathrm{dS}=0 \tag{4.6}$$

where v_{A} and v_{B} are the particle velocities in the normal direction. Equation 4.6 is the classical reciprocal identity. This is actually the starting point of most BEM formulations when A represents the free-space Green's functions, and B represents the physical problem at hand. The boundary surface $\partial\Omega$ in the classical reciprocal identity, Equation 4.6, is still the entire external boundary enclosing the homogeneous acoustic domain free of any thin bodies, perforated tubes, or bulk-reacting materials. It has been proved (Zhou et al, 2013) that Equation 4.6 can be reduced to the inlet and outlet surfaces only, regardless of any complex internals inside the silencer and the chamber of silencer. In other words,

$$\int_{S_1+S_2} (p_A v_B - p_B v_A)\, dS = 0 \tag{4.7}$$

where S_1 is the inlet surface, and S_2 is the outlet surface.

4.3 A reciprocal identity method for TL computation

The reciprocal identity method proposed by Zhou et al. (2016) is briefly reviewed in this section. For demonstration purposes, only the axisymmetric configuration is presented here.

The modal expansion of sound pressure at the inlet and outlet ducts of an axisymmetric silencer is

$$p(r) = \sum_{n=0}^{N-1} \left(p_n^+ e^{-jk_{z,n}z} + p_n^- e^{+jk_{z,n}z}\right) J_0\left(k_{r,n}r\right) \tag{4.8}$$

where the subscripts z and r denote the axial and radial directions, respectively, J_0 is the Bessel function of the first kind of order zero, and the superscripts $+$ and $-$ represent the incident and reflected waves, respectively. Although the series expansion goes to infinity in Equation 4.8, there will only be a finite number of propagating modes in each frequency range. In practice, at least one evanescent mode beyond the highest propagating mode should be included in case the frequency is close to the next propagating mode.

Recall that sound field A represents the analytical solution with an anechoic termination. For simplicity, the incident wave in the TL calculation is a single plane wave without any higher-order modes. On the other hand, the reflected wave may

include higher-order modes due to reflection from the silencer. At the inlet cross section (where $z = 0$ is locally set), the sound pressure can be written as

$$p_{A1}(r) = \sum_{n=0}^{N-1} (p_{A1n}^{+} + p_{A1n}^{-}) J_0\left(k_{r,n} r\right) \tag{4.9}$$

in which the subscripts 1 and *n* represent the waves in the inlet duct, and the order of modes, respectively. Since the incident wave in our TL computation is a single plane wave, we set p_{A10}^{+}=1, and all other $p_{A1n}^{+} = 0$ for *n* > 0. The corresponding particle velocity is

$$v_{A1}(r) = \frac{1}{\rho\omega} \sum_{n=0}^{N-1} k_{z,n} (p_{A1n}^{+} - p_{A1n}^{-}) J_0\left(k_{r,n} r\right) \tag{4.10}$$

Because of the anechoic termination assumption, the sound pressure at the outlet cross section (where $z = 0$ is also locally set) is

$$p_{A2}(r) = \sum_{n=0}^{N-1} p_{A2n}^{+} J_0\left(k_{r,n} r\right) \tag{4.11}$$

in which the subscript 2 represents the outlet. The corresponding particle velocity in the inward normal direction is

$$v_{A2}(r) = -\frac{1}{\rho\omega} \sum_{n=0}^{N-1} k_{z,n} p_{Aon}^{+} J_0(k_{r,n} r) \tag{4.12}$$

The axial wavenumber k_{zn} and the radial wavenumber k_{rn} are related by

$$k_{z,n}^2 = k^2 - k_{r,n}^2 \tag{4.13}$$

where n are the eigenvalues that must satisfy the rigid-wall boundary condition

$$J_0'(k_{r,n}a) = 0 \tag{4.14}$$

in which J_0' is the derivative of J_0, and a is the radius of the inlet/outlet duct.

There are 3*N* wave amplitudes in the analytical expansion, p_{A1n}^+, p_{A1n}^-, p_{A2n}^+, where *n* = 0, 1, 2, …, *N*-1. If a unit incident plane wave is assumed for the TL computation, $p_{A10}^+ = 1$ and all other $p_{A1n}^+ = 0$, then the remaining 2*N* wave amplitudes become the unknowns that can be solved by applying the reciprocal identity at least 2*N* times, each time with a BEM solution corresponding to a random boundary condition set. The BEM impedance matrix in Equation 2.1 can provide up to $q + l$ sets of such solutions, where q and l are the number of boundary elements at the inlet and the outlet, respectively. The total number of boundary elements at the inlet and outlet, $q + l$, is normally greater than 2*N*. This leads to the following $(q + l) \times 2N$ overdetermined system of equations

$$\mathbf{Ax} = \mathbf{B} \tag{4.15}$$

where $\mathbf{A} = [a_{jh}]$ $(j = 1, 2, \ldots, q + l; h = 1, 2, \ldots, 2N)$ is the system matrix, $\mathbf{x}=[p_{A10}^-, p_{A11}^-, \ldots, p_{A1(N-1)}^-, p_{A20}^+, p_{A21}^+, \ldots, p_{A2(N-1)}^+]^{\mathrm{T}}$ is the unknown vector of modal amplitudes, and $\mathbf{B} = [b_j]^{\mathrm{T}}$ is the right-hand side vector. The explicit expressions for a_{jh} and b_j are

$$a_{jh} = \int_{S_1} \left(v_{B1j} + \frac{k_{z,(h-1)}}{\rho\omega} p_{B1j} \right) J_0\left(k_{r,(h-1)} r\right) \mathrm{d}S \qquad (h = 1 \text{ to } N) \tag{4.16}$$

$$a_{jh} = \int_{S_2} \left(v_{B2j} - \frac{k_{z,(h-N-1)}}{\rho\omega} p_{B2j} \right) J_0\left(k_{r,(h-N-1)} r\right) \mathrm{d}S \quad (h = N+1 \text{ to } 2N) \tag{4.17}$$

$$b_j = -\int_{S_1} \left(v_{B1j} - \frac{p_{B1j}}{\rho c} \right) \mathrm{d}S \tag{4.18}$$

where the subscript *B* denotes the sound field *B*, 1 the inlet, 2 the outlet, *j* the *j*-th boundary condition set, and h the *h*-th unknown modal amplitude. For each boundary condition set, most of the velocities are zero except a unit velocity on a particular element, and the pressures are taken straight from the *j*-th column of the BEM impedance matrix. After the 2*N* unknown modal amplitudes are solved from Equation 4.15 by a least-square procedure, the transmitted sound power in the outlet duct can be evaluated. The incident sound power in the inlet duct is simply based on a unit plane wave. The TL can be obtained by the Equation 2.11.

4.4 Integral-based impedance-to-scattering matrix method

The modal expansion of sound pressure at any point *i* in the inlet/outlet duct is

$$p_i = \sum_{n=0}^{N-1} \Phi_n^i \left[P_n^+ \, \mathrm{e}^{-\mathrm{j}k_{z,n}z} + P_n^- \mathrm{e}^{\mathrm{j}k_{z,n}z} \right] \tag{4.19}$$

where P_n^+ and P_n^- are the modal amplitudes corresponding to the acoustic waves of order *n* travelling in the positive and negative *z* directions, respectively, k_z represents the wavenumber in the axial direction, Φ_n^i denotes the eigenfunction

value at the point *i*. For a circular or rectangular inlet/outlet, the eigenfunctions can be obtained analytically.

The particle velocity expression corresponding to the sound pressure in Equation 4.19 is

$$v_i = \frac{1}{\rho\omega}\sum_{n=0}^{N-1} k_{z,n}\Phi_n^i\left[P_n^+ \, \mathrm{e}^{-\mathrm{j}k_{z,n}z} - P_n^- \mathrm{e}^{\mathrm{j}k_{z,n}z}\right] \tag{4.20}$$

Let sound field A be the analytical modal expansion described above. For convenience, $z = 0$ is locally set at the inlet/outlet cross section. Let sound field B represent the BEM solution associated with an arbitrary boundary condition set prescribed at the inlet and outlet. Therefore, Equation 4.4 at the inlet surface can be expressed as

$$\int_{\mathrm{S}_1} (p_\mathrm{A} v_\mathrm{B} - p_\mathrm{B} v_\mathrm{A})\,\mathrm{dS} = \int_{\mathrm{S}_1} \sum_{n=0}^{N-1} \Phi_n^A \left(P_{1n}^+ \left(v_{Bj} - \frac{k_{z,n}}{\rho\omega} p_{Bj} \right) + P_{1n}^- \left(v_{Bj} + \frac{k_{z,n}}{\rho\omega} p_{Bj} \right) \right) \mathrm{dS} = 0 \tag{4.21}$$

where *j* denotes the *j*-th boundary condition, 1 the inlet. The BEM impedance matrix in Equation 2.1 can provide up to $q + l$ sets of boundary condition, where *q* and *l* are the number of boundary elements at the inlet and the outlet, respectively. For each boundary condition set, most of the velocities are zero except a unit velocity on a particular element, and the pressures are taken straight from the *j*-th column of the impedance matrix. The $q + l$ sets of Equation 4.21 can be represented in the matrix form below:

$$\begin{bmatrix} \int_{S_1}\left(v_{B1}-\frac{k_{z,0}}{\rho\omega}p_{B1}\right)\Phi_0^1 \mathrm{dS} & \cdots & \int_{S_1}\left(v_{B1}-\frac{k_{z,N-1}}{\rho\omega}p_{B1}\right)\Phi_{N-1}^1 \mathrm{dS} \\ \vdots & \ddots & \vdots \\ \int_{S_1}\left(v_{B(q+l)}-\frac{k_{z,0}}{\rho\omega}p_{B(q+l)}\right)\Phi_0^{q+l} \mathrm{dS} & \cdots & \int_{S_1}\left(v_{B(q+l)}-\frac{k_{z,0}}{\rho\omega}p_{B(q+l)}\right)\Phi_{N-1}^{q+l} \mathrm{dS} \end{bmatrix}$$

$$\begin{bmatrix} \int_{S_1}\left(v_{B1}+\frac{k_{z,0}}{\rho\omega}p_{B1}\right)\Phi_0^1 \mathrm{dS} & \cdots & \int_{S_1}\left(v_{B1}+\frac{k_{z,N-1}}{\rho\omega}p_{B1}\right)\Phi_{N-1}^1 \mathrm{dS} \\ \vdots & \ddots & \vdots \\ \int_{S_1}\left(v_{B(q+l)}+\frac{k_{z,0}}{\rho\omega}p_{B(q+l)}\right)\Phi_0^{q+l} \mathrm{dS} & \cdots & \int_{S_1}\left(v_{B(q+l)}+\frac{k_{z,0}}{\rho\omega}p_{B(q+l)}\right)\Phi_{N-1}^{q+l} \mathrm{dS} \end{bmatrix} \begin{pmatrix} P_{10}^+ \\ P_{11}^+ \\ \vdots \\ P_{1(N-1)}^+ \\ P_{10}^- \\ P_{11}^- \\ \vdots \\ P_{1(N-1)}^- \end{pmatrix} = \begin{pmatrix} 0 \\ \vdots \\ 0 \end{pmatrix} \tag{4.22}$$

Equation 4.22 can be re-written in a more compact vector form

$$\mathbf{A}\begin{pmatrix} \mathbf{P_1^+} \\ \mathbf{P_1^-} \end{pmatrix} = (\mathbf{0}) \tag{4.23}$$

where **A** is the “modal coefficients matrix” at the inlet cross section.

Similarly, at the outlet surface, we have

$$\mathbf{B}\begin{pmatrix} \mathbf{P_2^+} \\ \mathbf{P_2^-} \end{pmatrix} = (\mathbf{0}) \tag{4.24}$$

Equation 4.23 and 4.24 can be combined as

$$\mathbf{A}\begin{pmatrix} \mathbf{P_1^+} \\ \mathbf{P_1^-} \end{pmatrix} + \mathbf{B}\begin{pmatrix} \mathbf{P_2^+} \\ \mathbf{P_2^-} \end{pmatrix} = (\mathbf{0}) \tag{4.25}$$

After the rearrangement of Equation 4.25 and a least-squares matrix inverse performance, the scattering matrix **S** can be obtained thereafter.

4.5 Test Cases

The first test case is an axisymmetric round bar silencer shown in Figure 4.1, which is also used for the validation of the point collocation based impedance-to-scattering matrix method in Chapter 2. Figure 4.1 compares both the collocation-based and integral-based impedance-to-scattering matrix methods using N = 17 to the analytical solution. It is seen that the two different impedance-to-scattering matrix methods produce identical results, and compare very well with the analytical solution up to the frequency for which the analytical solution is valid. However, from Table 4.1, it is noticed the MATLAB computation time is much less in the collocation-based method than in the integral-based method. Figure 4.2 compares the solution of each method when N = 30 is selected. We can see that adding more evanescent modes barely changes the TL curve and solutions of the two methods are almost identical.

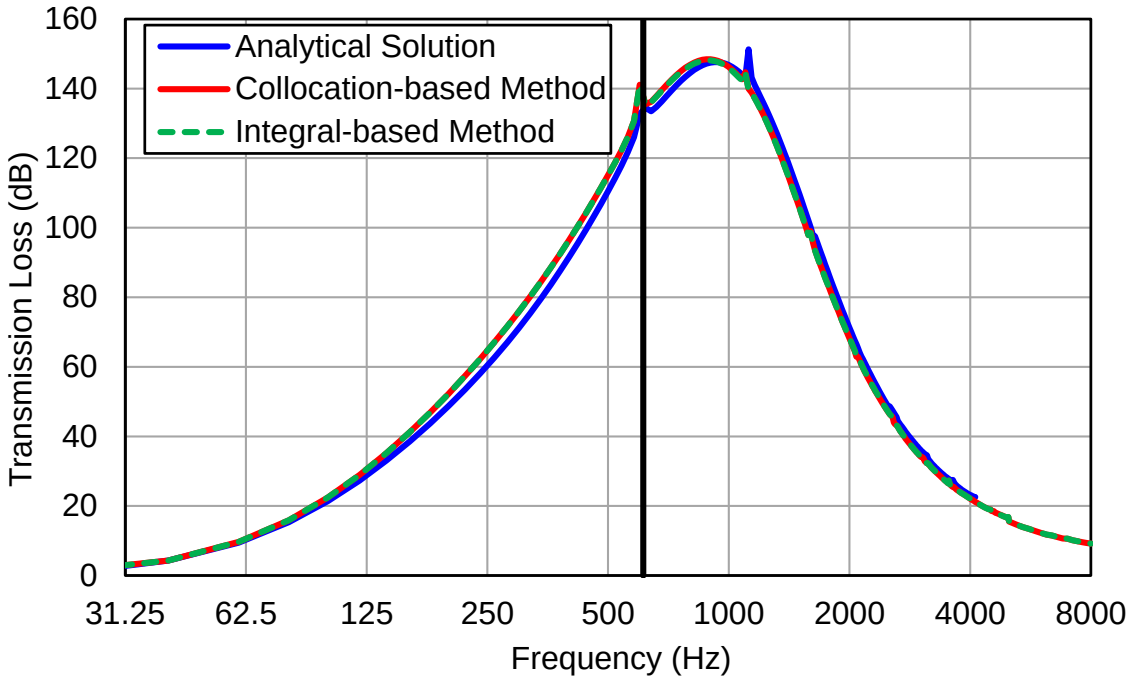

Figure 4.1 TL of the round bar silencer (*N*=17).

Table 4.1 Computational time per frequency comparison.

Method	Time (s)
Collocation-based	1.45
Integral-based	29.73

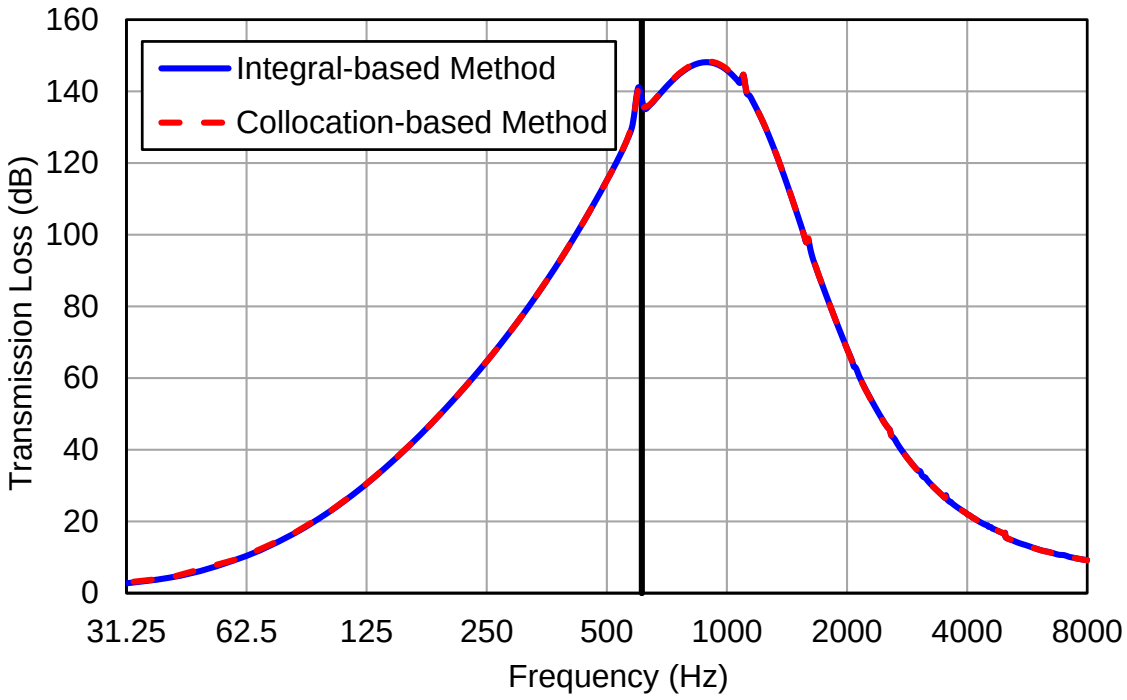

Figure 4.2 TL of the round bar silencer (*N*=30).

The second test case is a tuned dissipative large silencer as shown in Figure 4.3. The lining is made of polyester (flow resistivity=16,000 Rayl/m) and is covered by 30% open perforated facing sheets.

The substructured BEM is an ideal tool to obtain the resultant impedance matrix for this type of silencers. The pine-tree silencer is divided into three substructures as shown in Figure 4.4. For substructure 2, only a small template is modeled, and the impedance matrix of the template can be repeatedly used 5 times to obtain the impedance matrix of the middle section. In this silencer model, the BEM mesh has 13254 constant elements at the inlet and another group of 13254 elements at the outlet. This results in a 26508×26508 impedance matrix for each frequency. There are 692 propagating modes within 8000 Hz. Therefore, *N*=700 is selected to include all propagating modes up to 8000 Hz and some evanescent modes. It can

be seen that both methods produce an identical TL shown in Figure 4.5. Because there is more integral computation involved in this test case than the previous one, the difference of computation time between the two methods is more noticeable.

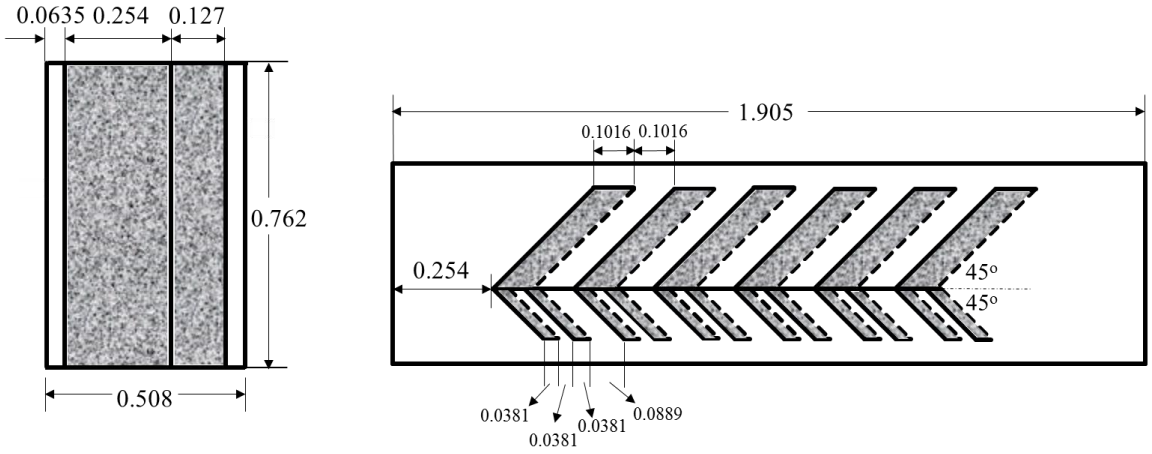

Figure 4.3 Dimensions of a tuned dissipative large silencer.

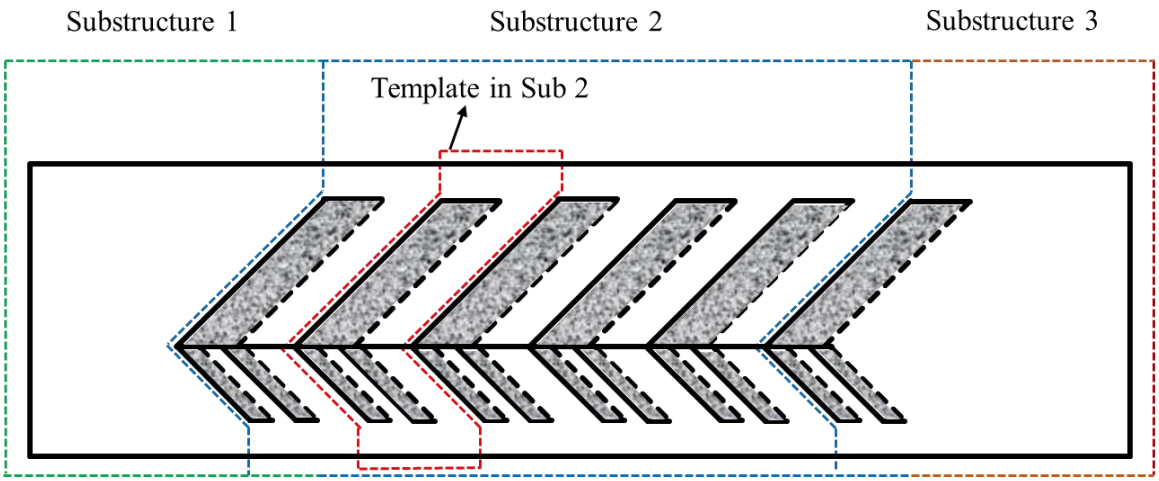

Figure 4.4 A tuned dissipative silencer model with three substructures.

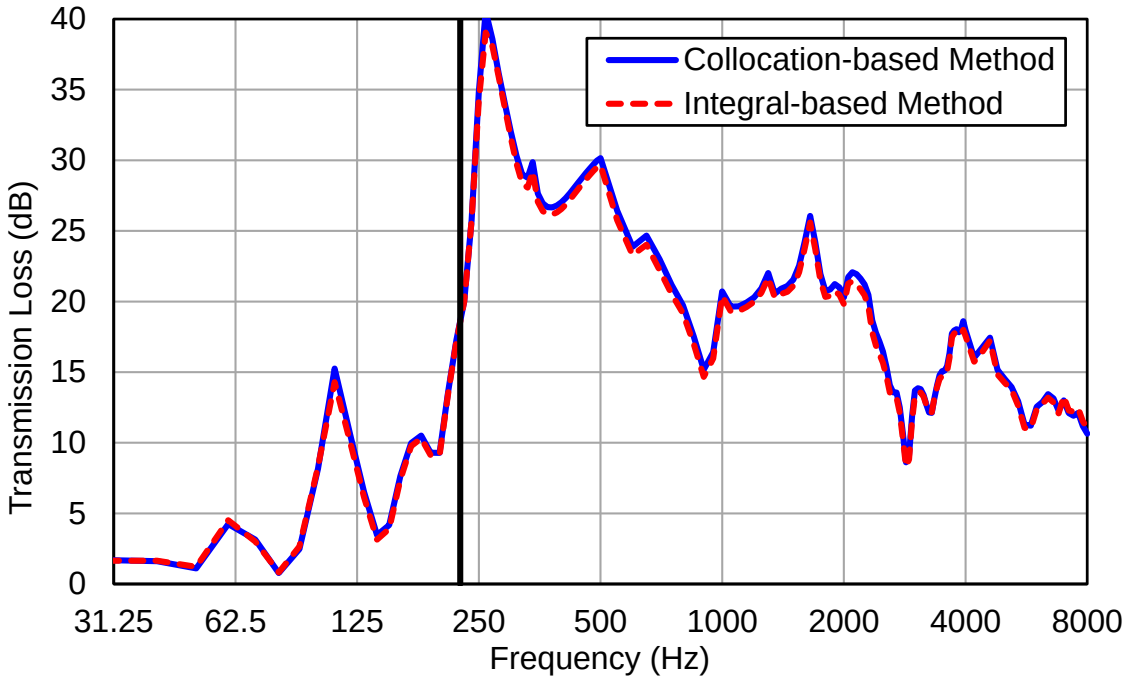

Figure 4.5 TL of the tuned dissipative silencer.

4.6 Summary

The reciprocal identity method can be used to convert the BEM impedance matrix to the scattering matrix for large silencer analysis. Since the reciprocal identity is an integral equation, the integral-based impedance-to-scattering matrix method can potential smooth out any irregularities associated with the selection of collocation points.

Two test cases, one axisymmetric round bar silencer and the other rectangular tuned dissipative silencer, are used to compare the difference of two impedance-to-scattering methods. Although the collocation-based method always has the uncertainty associated with the “optimal” collocation locations, the two test cases show that the accuracy and the stability are about the same for both methods. Because of the additional numerical integration involved in the integral-based

method, the computation time is much longer than the collocation-based method. Nonetheless, the integral-based method still can provide a comparison and validation tool for the collocation-based method, in case the silencer geometry becomes more complicated.

Chapter 5 ADVANCED BEM ANALYSIS FOR LARGE BAR SILENCERS

5.1 Introduction

Bar silencers are commonly used among all types of dissipative silencers in the power generation industry. The idea of bar silencers was first proposed by Nilsson and Söderqvist (1983), and they claimed that an array of square or round bars made of sound absorbing materials have certain advantages over a similarly configured splitter silencer. They explained the better performance of bar silencers by attributing to three major effects: (1) a ‘‘constriction effect’’, in which at low frequencies, the sound field within the silencer induces cylindrical waves within the bars, and has to travel through gradually decreasing cylindrical areas; (2) a ‘‘diagonal effect’’, in which with bars, waves enter the absorbing material via the corners, and the acoustically effective thickness of the material then becomes 20% greater than in a splitter-type silencer with the same baffle width; (3) a ‘‘slot effect’’, in which the bar geometry results in shorter distances between sound-absorbing surfaces and a greater area of sound-absorbing material exposed to the sound field (Cummings and Astey, 1996).

Cummings and Astey (1996) conducted an FEM analysis of sound attenuation in bar silencers, consisting of rectangular prisms of sound-absorbing material placed in a rectangular lattice arrangement within a rigid-walled duct. The numerically predicted results were compared to the experimental data. Comparison was also made between the acoustic performance of bar silencers and the equivalent splitter silencers, and the authors found that bar silencers tend to have better attenuation characteristics at low frequencies. Kirby et al. (2012) investigated the

performance difference of different silencer designs for gas turbine exhaust systems by using a hybrid 2-D FEM method. The performance of bar silencers was observed to be very dependent on the type of material chosen and the flow resistivity of the material.

On the BEM side, the reciprocal identity method (Zhou et al. 2016) and the proposed impedance-to-scattering matrix method (Wang and Wu, 2016) are also ideally suited to the TL analysis of bar silencers. Both methods express sound pressure and the corresponding particle velocity in the inlet and outlet ducts in terms of the analytical mode shapes. For circular and rectangular inlet/outlet cross sections, the analytical mode shapes can be found easily. However, for more complicated inlet/outlet configurations, the mode shapes have to be obtained numerically.

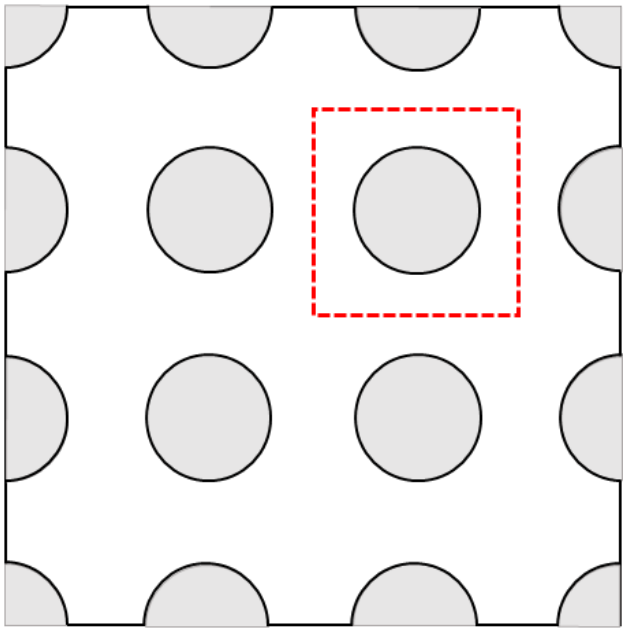

Figure 5.1 A rectangular unit isolated from an aligned lattice arrangement of round bars.

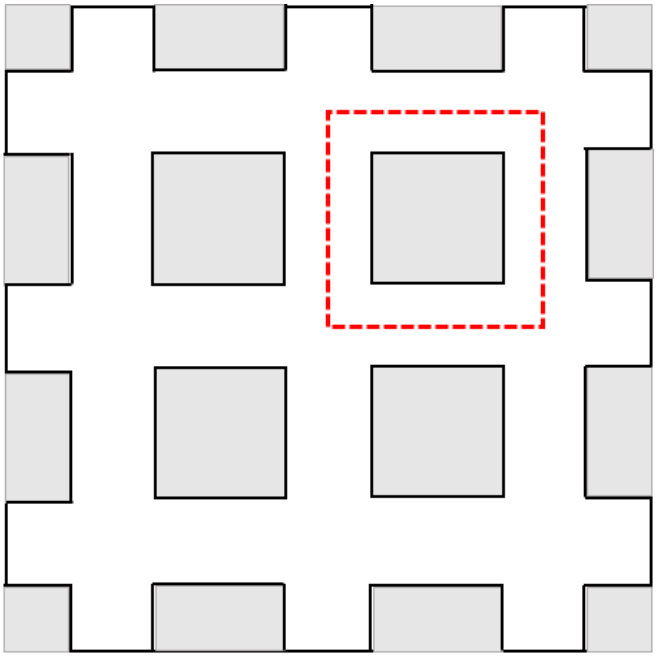

Figure 5.2 A rectangular unit isolated from an aligned lattice arrangement of square bars.

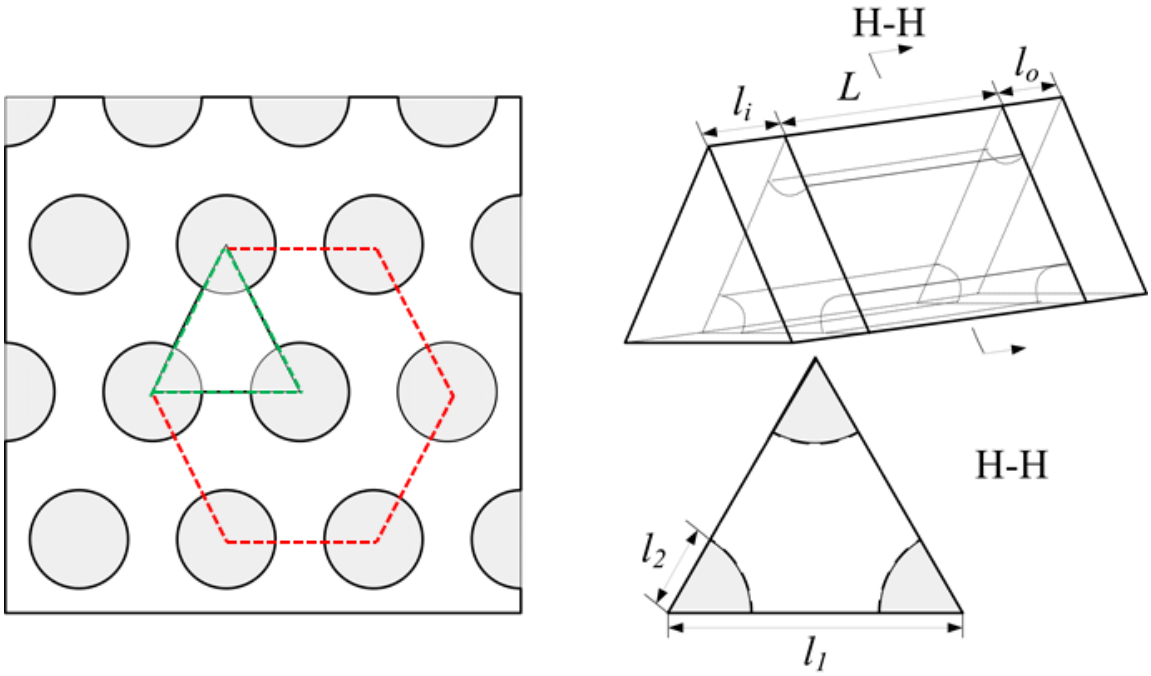

Figure 5.3 A triangular unit isolated from a shifted lattice arrangement of round bars.

Figures 5.1-5.3 demonstrate three typical lattice arrangements of bar silencers (Yang et al., 2017). Due to symmetry, only a small module is isolated from the lattice for analysis purposes. As shown in Figures 5.1 and 5.2, the isolated module is a rectangular duct with either a round or a rectangular bar inside, and the housing is assumed rigid due to symmetry. Figure 5.3 shows a shifted lattice arrangement of round bars and an isolated hexagon module. Due to rotational symmetry, the hexagon module can eventually be reduced to a triangular module. The mode shapes of a triangular module may be difficult to find analytically, but can be obtained numerically by using the 2-D FEM.

In the first part of this chapter, the impedance-to-scattering matrix method is extended to irregular inlet and outlet configurations where the mode shapes have to be determined by the 2-D FEM. Following the study of the impedance-to-scattering method using the numerical FEM modes, Redheffer's star product (Redheffer,1962) is introduced to combine the scattering matrices of subsystems into the resultant scattering matrix of the whole system. As mentioned in Chapter 4, even though the BEM impedance matrix may also be used to combine subsystems, the scattering matrix is a more desirable format due to its mesh-independent property.

In industry, one-third octave or octave band is a more preferable output format. Measurements of IL and NR for large silencers are normally performed in one-third or octave bands, but TL must be first determined in narrow bands because the TL computation requires additional post-processing of the measured or computed sound pressure data. Therefore, the conversion from the narrow-band TL to one-

third or octave band is needed in order to compare to the measured IL or NR. However, there has been no standard procedure for determining the TL in one-third or octave bands using measured data or simulation.

In the last part of this chapter, three different methods for determining TL are compared in one-third or octave bands. They are (1) the wave decomposition method, (2) the equivalent IL method, and (3) the direct conversion method, respectively. All three methods assume a constant-amplitude incident sound wave in the inlet duct at all frequencies. While the first two methods still rely on the plane-wave assumption in the inlet and outlet ducts, the direct conversion method can be used for large silencers at higher frequencies when higher-order cross modes propagate along with the plane waves in the inlet and outlet ducts.

5.2 Impedance-to-Scattering matrix method with 2-D FEM modes

In Chapter 2 to Chapter 4, the BEM impedance matrix is converted into the scattering matrix by introducing the modal expansion to sound pressure and particle velocity at a rectangular or circular inlet/outlet in terms of the corresponding analytical modes. In this section, the 2-D FEM is first applied to extract the numerical mode shapes of a general inlet/outlet cross section, which may not be rectangular or circular, before the modal expansion is introduced. Figure 5.4 shows a flow chart (from EABE paper) that demonstrates the procedure.

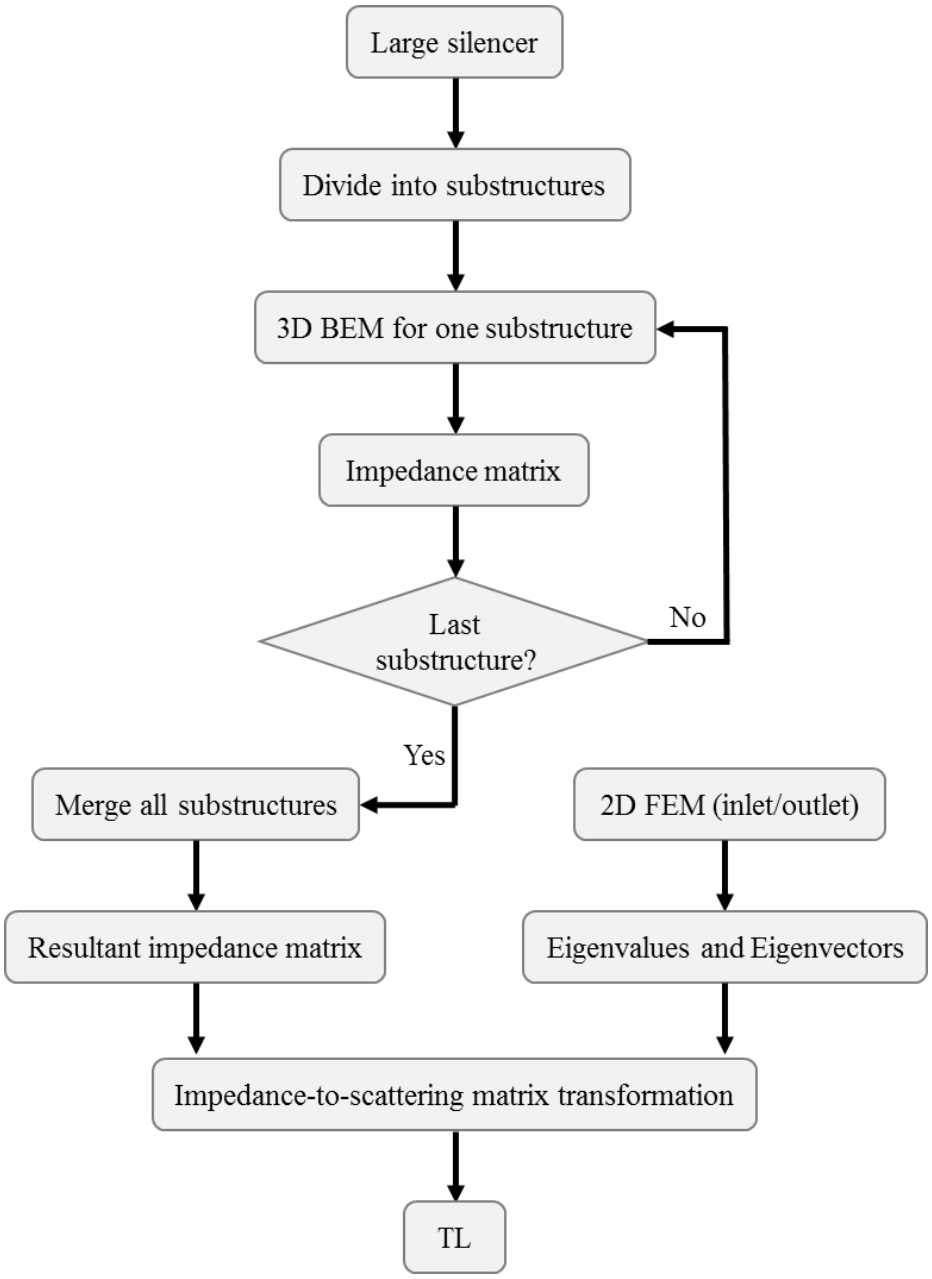

Figure 5.4 Flowchart of impedance-to-scattering matrix method with 2-D FEM modes computation procedure.

The modal expansion of sound pressure at the point i in the inlet/outlet duct is

$$p_i = \sum_{n=0}^{N-1} \Phi_n^i \left[P_n^+ \, \mathrm{e}^{-\mathrm{j}k_{z,n}z} + P_n^- \mathrm{e}^{\mathrm{j}k_{z,n}z} \right] \tag{5.1}$$

where P_n^+ and P_n^- are the modal amplitudes corresponding to the acoustic waves of order *n* travelling in the positive and negative *z* directions, respectively, k_z represents the wavenumber in the axial direction, Φ_n^i denotes the eigenfunction value at the point *i*. For a circular or rectangular inlet and outlet, the eigenfunctions can be obtained analytically. For irregular shapes, the eigenfunctions have to be obtained numerically.

The particle velocity expression at the point i in the inlet/outlet duct corresponding to the sound pressure in Equation 5.1 is

$$v_i = \frac{1}{\rho\omega} \sum_{n=0}^{N-1} k_{z,n} \Phi_n^i \left[P_n^+ \, \mathrm{e}^{-\mathrm{j}k_{z,n}z} - P_n^- \mathrm{e}^{\mathrm{j}k_{z,n}z} \right] \tag{5.2}$$

5.2.1 Eigenfunction extraction using 2D FEM

The governing differential equation for the transversal sound pressure in a 2-D cross section at the inlet and outlet (where $z = 0$ is locally set) is,

$$\nabla_{xy}{}^2 p_{xy} + k_{xy}^2 p_{\mathrm{xy}} = 0 \tag{5.3}$$

where p_{xy} is the transversal sound pressure, and k_{xy} is the transversal wavenumber.

The axial wavenumber k_z and the transversal wavenumber k_{xy} are related by

$$k_{xy}^2 + k_z^2 = 0 \tag{5.4}$$

The transversal sound pressure at any point i is expressed in terms of the shape functions by using FEM (Fang and Ji, 2013),

$$p_{xy,i} = \mathbf{N}^{\mathrm{T}}\mathbf{p} \tag{5.5}$$

where the matrix $\mathbf{N}$ consists of the column vectors of the global shape functions, and $\mathbf{p}$ is the column vector of the nodal values of transversal sound pressure.

After applying the Galerkin procedure, Equation 5.3 can be expressed as

$$\int_S \{N\}\left(\nabla_{xy}{}^2 p_{xy} + k_{xy}^2 p_{\mathrm{xy}}\right) \mathrm{d}S = \{0\} \tag{5.6}$$

After integration by parts, Equation 5.6 becomes

$$\int_L \{N\}\frac{\partial p_{xy}}{\partial n}\,\mathrm{d}L - \int_S \{\nabla N\}\cdot\nabla p_{xy}\,\mathrm{d}S + k_{xy}^2\int_S \{N\}p_{xy}\mathrm{d}S = \{0\} \tag{5.7}$$

where L is the boundary of the cross section S.

Substituting Equation 5.5 into Equation 5.7 produces

$$\int_L \{N\}\frac{\partial p_{xy}}{\partial n}\,\mathrm{d}L - \int_S \{\nabla N\}\{\nabla N\}^{\mathrm{T}}\,\mathrm{d}S\{p\} + k_{xy}^2\int_S \{N\}\{N\}^{\mathrm{T}}\mathrm{d}S\{p\} = \{0\} \tag{5.8}$$

Applying the rigid-wall boundary condition to Equation 5.8 yields the following eigen-equation,

$$\left(\mathbf{K} - k_{xy}^2\mathbf{M}\right)\mathbf{p} = \mathbf{0} \tag{5.9}$$

where $\mathbf{K}$ and $\mathbf{M}$ are the stiffness matrix and mass matrix, respectively. They are

$$\mathbf{K} = \sum \int_{S_e} (\nabla \mathbf{N})_e (\nabla \mathbf{N})_e^{\mathrm{T}} \, \mathrm{d}S_e \tag{5.10}$$

$$\mathbf{M} = \sum \int_{S_e} (\mathbf{N})_e (\mathbf{N})_e^{\mathrm{T}} \, \mathrm{d}S_e \tag{5.11}$$

where the subscript e denotes the element.

If the number of nodes is n, n eigenvalues k_{xy} $(1 \leq i \leq n)$ and the associated eigenvectors $(\mathbf{\Phi})_i$ with length of n may be obtained by solving Equation 5.9.

With the numerical modes at the inlet and outlet available, the impedance matrix can be converted to the scattering matrix by using either the collocation-based or the integral-based method as illustrated in previous chapters.

5.2.2 Test cases

The first test case is a rectangular bar silencer as shown in Figure 5.5. This test case was first reported by Kirby et al. (Kirby et al., 2014) using the hybrid analytical and 2D FEM method based on the point-collocation method. The dimensions of the silencer is shown in Figure 5.6 with $d_x = 0.28\,m$, $d_y = 0.21\,m$, $e_x = 0.06\,m$, $e_y = 0.045\,m$, and $L = 0.9\,m$. The flow resistivity for the sound absorbing material is 19307 *rayls/m*. The porosity of the perforated facing sheet is 27%, hole diameter $d_h = 0.003\,m$, and wall thickness $t_w = 0.0016\,m$. All values of the parameters are

the same as the test case studied by Kirby et al. (Kirby et al., 2014). Even though the inlet/outlet is rectangular, numerical modes are still calculated by FEM and used for the impedance-to-scattering matrix method to validate the proposed procedure. Figure 5.7 compares the BEM result from the impedance-to-scattering matrix using the 2D FEM to the numerical solution by Kirby et al., along with the insertion loss (IL) measurement data from the reference (Kirby et al., 2014). In practice, IL is easier to measure on-site, but it is not the same as the more theoretical TL. Nonetheless, it does provide a reference for comparison purposes. For large dissipative silencers, the trend of IL should be close to the trend of TL. As shown in Figure 5.7, it is seen that both numerical TL predictions are higher than the IL measurement but the proposed method compares fairly well with Kirby et al.'s point collocation method for TL up to 8000 Hz. The minor discrepancies could be due to the FEM interpolation of the modes at the centroid of each element.

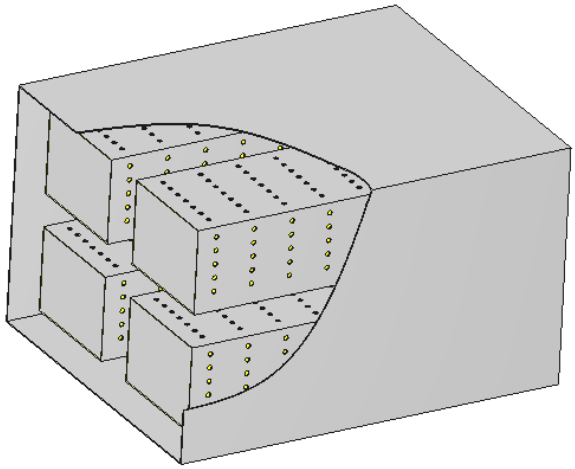

Figure 5.5 3D sketch of the rectangular bar silencer.

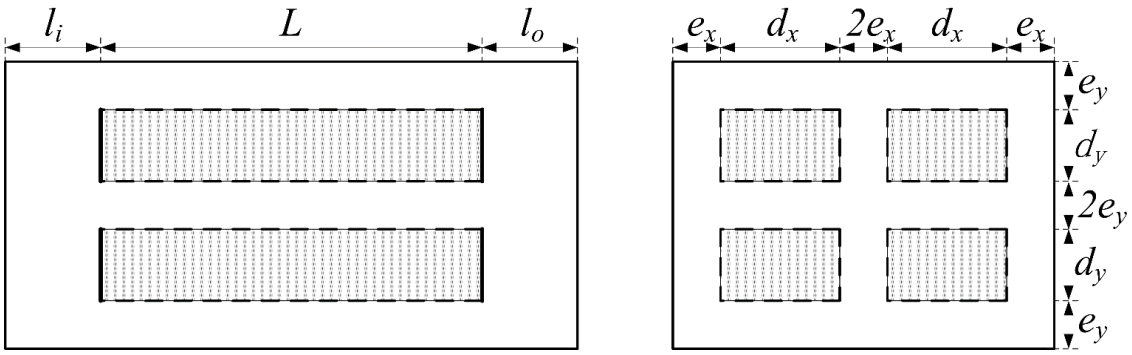

Figure 5.6 Dimensions of the rectangular bar silencer.

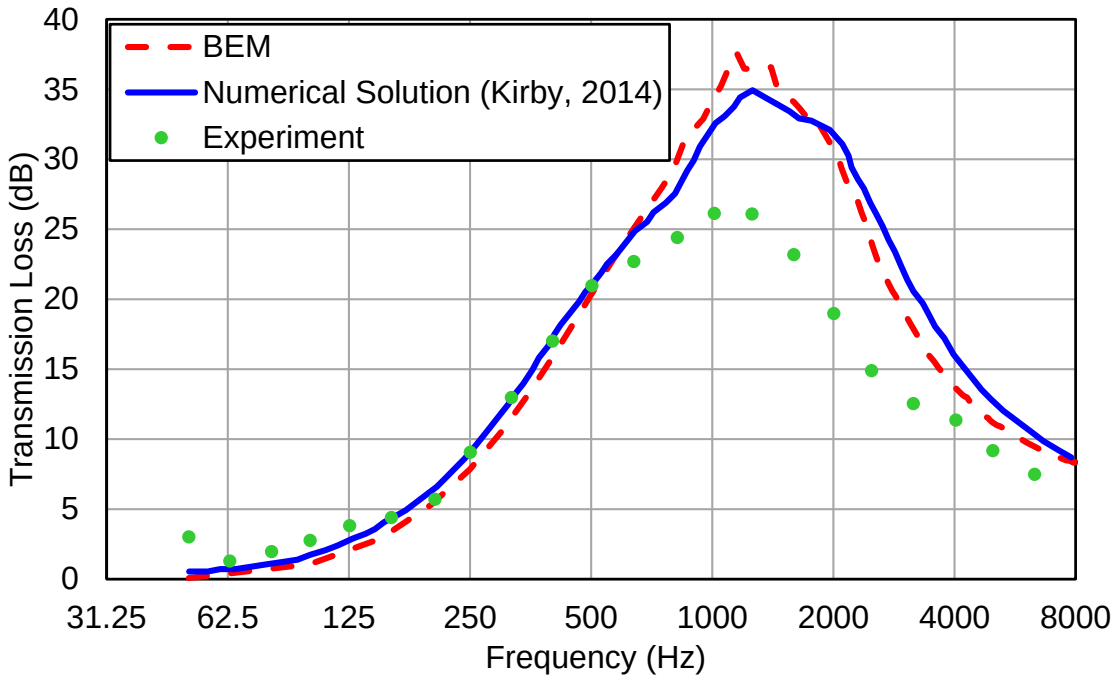

Figure 5.7 TL comparison of the rectangular bar silencer.

The second test case is a triangular module isolated from a shifted lattice arrangement of round bars shown in Figure 5.3. With reference to Figure 5.8, $L = 2\ m$, $l_1 = 0.4\ m$, and $l_2 = 0.1\ m$.

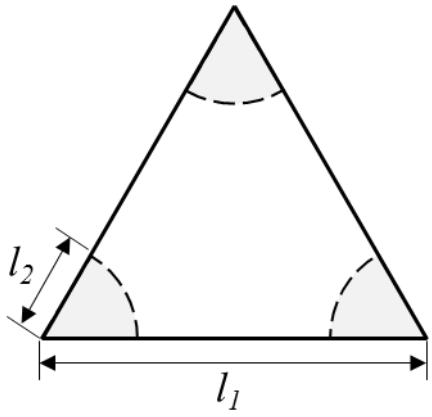

Figure 5.8 Cross section of a triangular module isolated from a shifted lattice arrangement of round bars.

Table 5.1 Three study cases of the triangle module.

Case number	Flow resistivity (*rayls/m*)	Porosity
1	16000	0.30
2	16000	0.08
3	1800	0.30

As shown in Table 5.1, case study for different flow resistivity and porosity combinations are developed and the respective TL results are compared in Figure 5.9. Increasing the porosity of the perforated facing sheet may improve the acoustic attenuation performance at higher frequencies; however, this may be at the expense of a small reduction of TL at lower frequencies. It should be noticed that at very high frequencies, the effect of flow resistivity is very little.

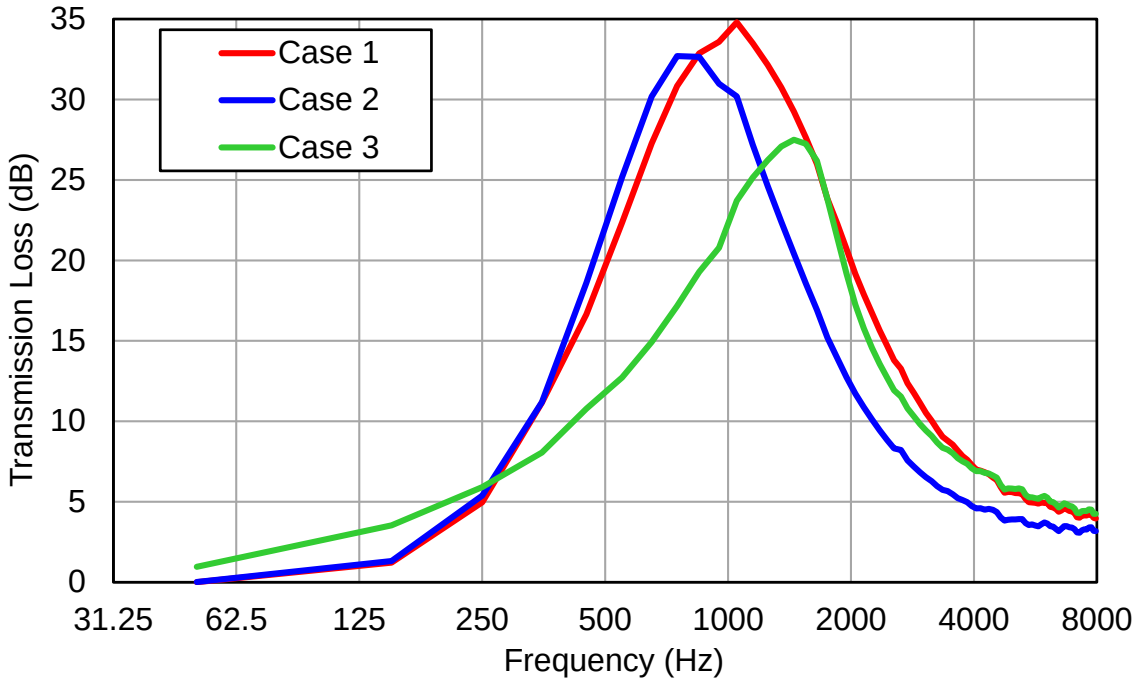

Figure 5.9 TL comparison of three study cases of the triangle module.

The last test case is a comparison between the triangular module and the square module to demonstrate the advantage of the shifted lattice arrangement shown in Figure 5.3 over the aligned lattice arrangement shown in Figure 5.1. Figure 5.10 shows the dimensions of the two different bar silencer designs with $l_1 = 0.4\ m$, and $l_2 = 0.1\ m$. The round bar is made of polyester with flow resistivity *R*=16000 *rayls/m*, and is covered by a 30% open perforated facing sheet.

The TL comparison of the two designs is shown in Figure 5.11, and it is seen that triangular module has better performance over 1000 Hz. This is because the shifted lattice (triangular module) is a more compact design than the aligned lattice (square module).

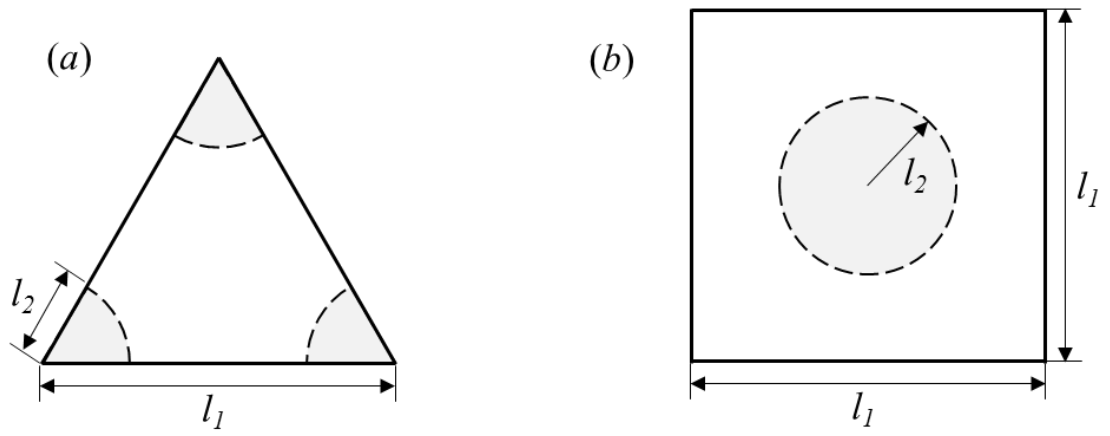

Figure 5.10 Dimensions of the two different designs: (*a*) Triangular module; (*b*) Square module.

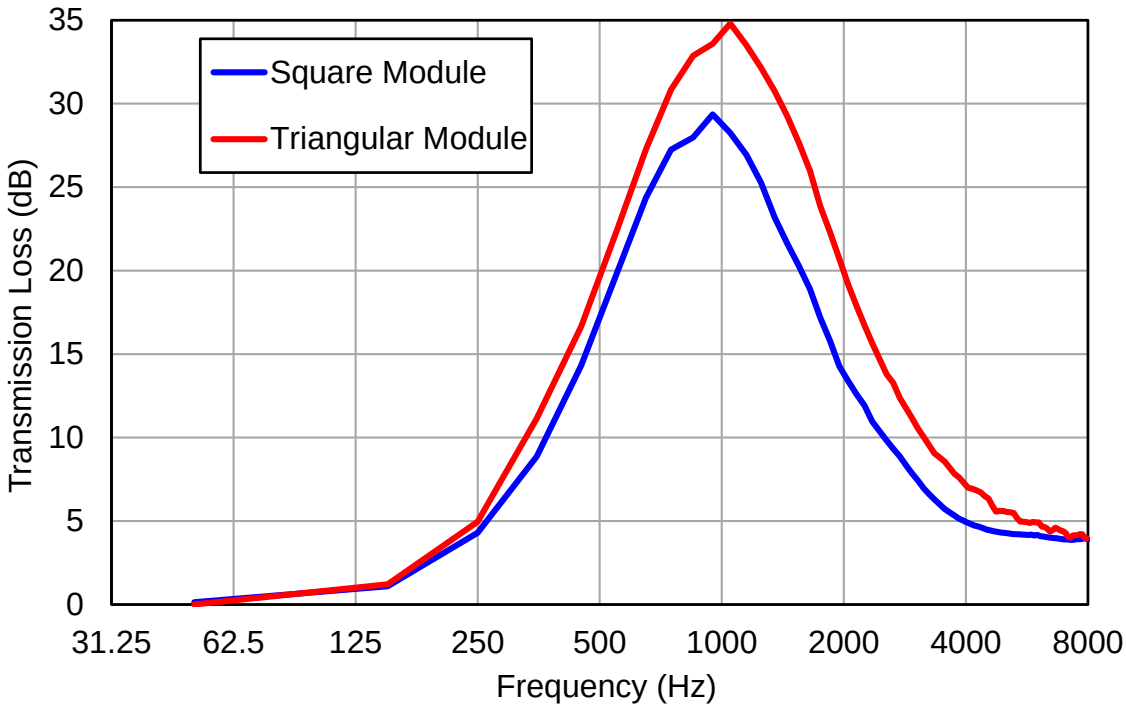

Figure 5.11 TL comparison between the triangular and square modules.

5.3 Scattering Matrix Synthesis

The impedance matrix synthesis has been used to combine subsystems in series connection before (Lou et al., 2003, Park et al., 2009, and Yang and Ji, 2016). One disadvantage of using the impedance matrix synthesis is that it always requires a piece of BEM mesh at the inlet and outlet to go with the impedance matrix. On the other hand, the scattering matrix is a system property and is mesh independent, making it a more desirable format than the BEM impedance matrix.

5.3.1 Redheffer's star product

By using the Redheffer's star product (Redheffer, 1962), the scattering matrices from two subsystems can be combined into a single scattering matrix.

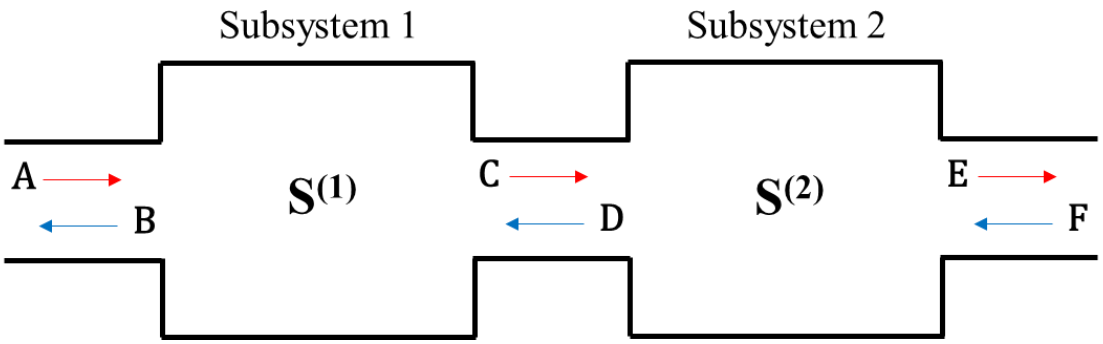

Figure 5.12 Two subsystems combination using the scattering matrix synthesis approach.

The scattering matrix of each subsystem can be written as

$$\begin{pmatrix} \mathbf{C} \\ \mathbf{B} \end{pmatrix} = \mathbf{S}^{(1)} \begin{pmatrix} \mathbf{A} \\ \mathbf{D} \end{pmatrix} = \begin{bmatrix} \mathbf{S}_{11}^{(1)} & \mathbf{S}_{12}^{(1)} \\ \mathbf{S}_{21}^{(1)} & \mathbf{S}_{22}^{(1)} \end{bmatrix} \begin{pmatrix} \mathbf{A} \\ \mathbf{D} \end{pmatrix} \quad \begin{pmatrix} \mathbf{E} \\ \mathbf{D} \end{pmatrix} = \mathbf{S}^{(2)} \begin{pmatrix} \mathbf{C} \\ \mathbf{F} \end{pmatrix} = \begin{bmatrix} \mathbf{S}_{11}^{(2)} & \mathbf{S}_{12}^{(2)} \\ \mathbf{S}_{21}^{(2)} & \mathbf{S}_{22}^{(2)} \end{bmatrix} \begin{pmatrix} \mathbf{C} \\ \mathbf{F} \end{pmatrix} \tag{5.12}$$

and the combined scattering matrix as

$$\begin{pmatrix}\mathbf{E}\\ \mathbf{B}\end{pmatrix} = \mathbf{S}\begin{pmatrix}\mathbf{A}\\ \mathbf{D}\end{pmatrix} = \mathbf{S}^{(1)} \otimes \mathbf{S}^{(2)} = \begin{bmatrix}\mathbf{S_{11}} & \mathbf{S_{12}}\\ \mathbf{S_{21}} & \mathbf{S_{22}}\end{bmatrix}\begin{pmatrix}\mathbf{A}\\ \mathbf{D}\end{pmatrix} \tag{5.13}$$

where

$$\mathbf{S_{11}} = \mathbf{S_{11}^{(2)}}\left[\mathbf{I} - \mathbf{S_{12}^{(1)}S_{21}^{(2)}}\right]^{-1}\mathbf{S_{11}^{(1)}} \tag{5.14}$$

$$\mathbf{S_{12}} = \mathbf{S_{12}^{(2)}} + \mathbf{S_{11}^{(2)}}\left[\mathbf{I} - \mathbf{S_{12}^{(1)}S_{21}^{(2)}}\right]^{-1}\mathbf{S_{12}^{(1)}S_{22}^{(2)}} \tag{5.15}$$

$$\mathbf{S_{21}} = \mathbf{S_{21}^{(1)}} + \mathbf{S_{22}^{(1)}}\left[\mathbf{I} - \mathbf{S_{21}^{(2)}S_{12}^{(1)}}\right]^{-1}\mathbf{S_{21}^{(2)}S_{11}^{(1)}} \tag{5.16}$$

$$\mathbf{S_{22}} = \mathbf{S_{22}^{(1)}}\left[\mathbf{I} - \mathbf{S_{21}^{(2)}S_{12}^{(1)}}\right]^{-1}\mathbf{S_{22}^{(2)}} \tag{5.17}$$

By following the rule above, the scattering matrices of n subsystems in series connection can be combined to form a single resultant scattering matrix for the entire system for TL computation or further study.

5.3.2 Test cases

The first test case is a two-subsystem bar silencer as shown in Figure 5.13. The purpose of this test case is to validate the scattering matrix synthesis by comparing to the impedance matrix synthesis. The impedance matrix of each subsystem can be obtained by following the same BEM substructuring procedure shown in Figure 2.1, and the mesh size of each subsystem is the same as the test case used in Section 2.4.2. The more traditional way to combine two subsystems is to use the impedance matrix synthesis. However, instead of combining the impedance matrices of the two subsystems, we convert each subsystem impedance matrix to

a corresponding subsystem scattering matrix first, and then the Redheffer's star product is used to obtain the resultant scattering matrix for the whole system. The TL can be obtained from the resultant scattering matrix afterwards. Since the combined length (6 m) of the two bars is the same as the length of the single bar design reported in Section 2.4.2, the TL of this two-bar design is also compared to the TL of the original one-bar design to study any potential benefits of sudden area change in the middle of the silencer. It is seen from Figure 5.14 that the two synthesis methods produce identical results, and the two-bar design also provides additional attenuation above the cutoff frequency due to the sudden area change.

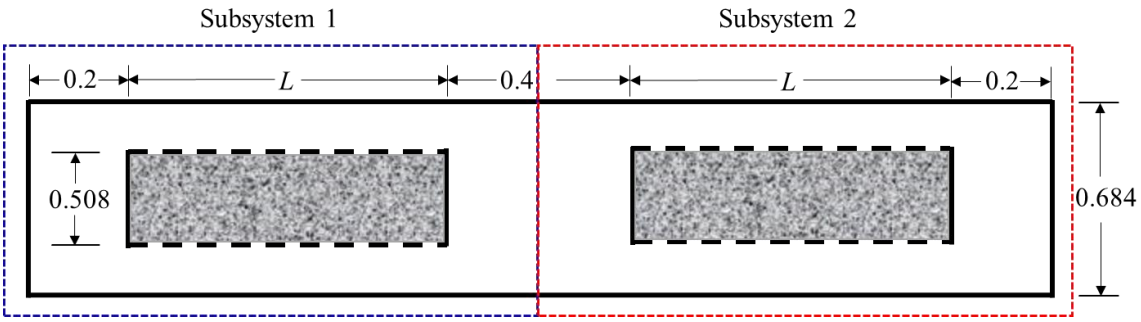

Figure 5.13 A two-subsystem bar silencer (L = 3 m).

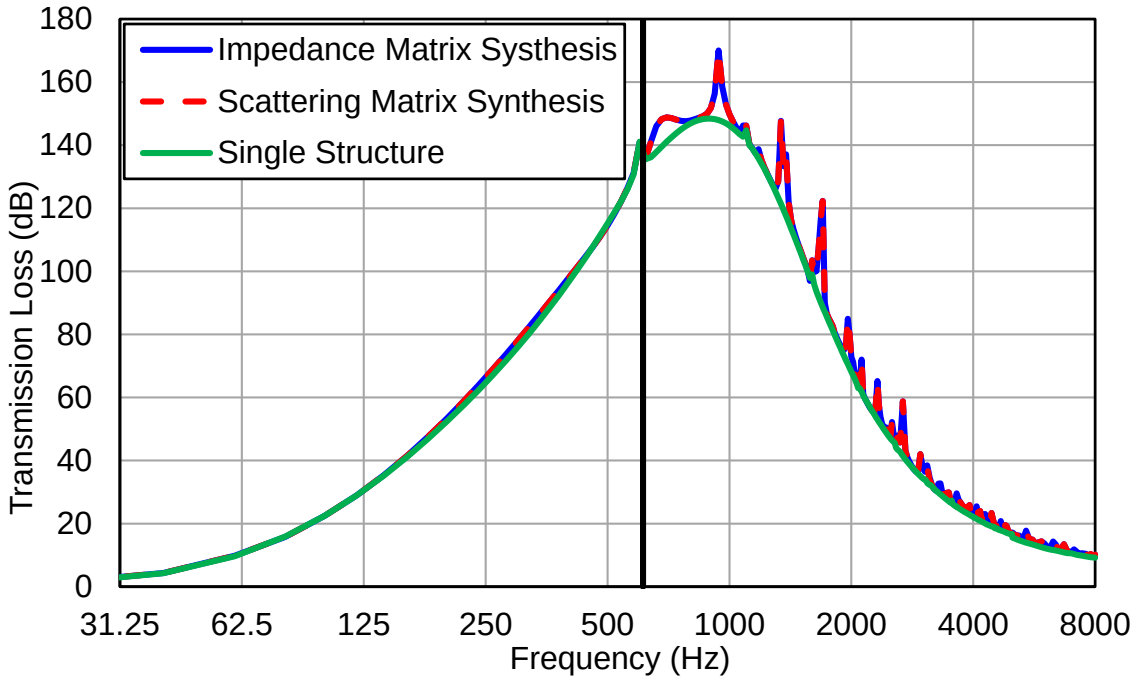

Figure 5.14 TL of the two subsystems bar silencer.

It should be noted that the impedance matrix must be always associated with a particular BEM mesh due to its element-based nature. However, the scattering matrix is a system property that does not rely on any mesh. To confirm the mesh independent property of the scattering matrix, we alter the mesh size of the two subsystems to ensure that they don't have the same mesh. The first subsystem has 690 constant elements at the inlet and another group of 690 elements at the outlet. The second subsystem has 740 constant elements at the inlet and another group of 740 elements at the outlet. In the traditional impedance matrix synthesis, the two BEM impedance matrices are not compatible and, therefore, cannot be combined at all. However, this is not an issue for the scattering matrix synthesis as long as both scattering matrices have the same number of modes. In this test

case, we select 17 modes in both subsystems. From Figure 5.15, it can be verified that the scattering matrix synthesis is mesh independent.

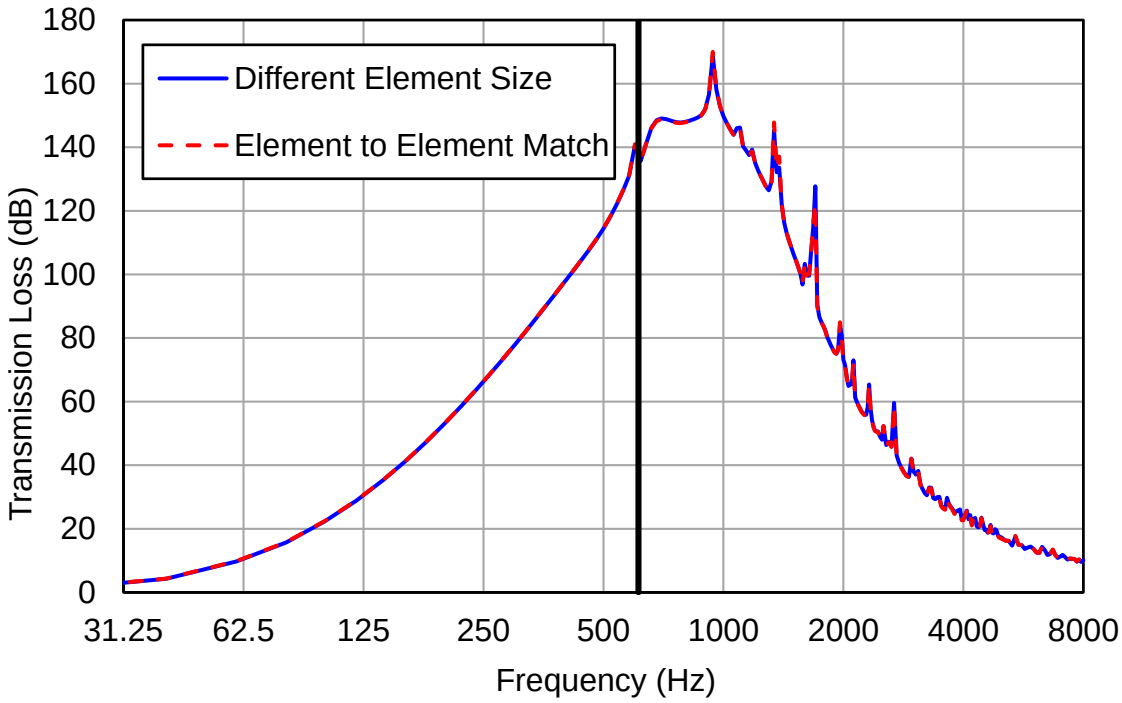

Figure 5.15 Comparison between the element-to-element match and the different element size combination.

In Chapter 2, a so-called "transfer scattering matrix" was introduced to combine subsystems in series connection. The transfer scattering matrix is shown below again:

$$\begin{pmatrix} \mathbf{P_1^+} \\ \mathbf{P_1^-} \end{pmatrix} = \begin{bmatrix} \mathbf{S_{11}^*} & \mathbf{S_{12}^*} \\ \mathbf{S_{21}^*} & \mathbf{S_{22}^*} \end{bmatrix} \begin{pmatrix} \mathbf{P_2^+} \\ \mathbf{P_2^-} \end{pmatrix} \tag{5.18}$$

Due to its direct inlet-to-outlet relationship, the resultant transfer impedance matrix of a cascaded system can be obtained by simply multiplying the subsystem transfer impedances together. In other words,

$$\boldsymbol{S}^{*} = \boldsymbol{S}_{\boldsymbol{1}}^{*} * \boldsymbol{S}_{\boldsymbol{2}}^{*} * \ldots * \boldsymbol{S}_{\boldsymbol{n}}^{*} \tag{5.19}$$

This method was used to validate the TL of a small non-axisymmetric silencer in Chapter 2. However, by applying this method to the current test case, it is surprising to find that the transfer scattering matrix method is only valid at low frequencies, as shown in Figure 5.16. From Figure 5.16, it is seen that as the frequency gets close to the cutoff frequency, the transfer scattering matrix method becomes unstable. One possible explanation is that the transfer scattering matrix is ill-conditioned when a large number of higher-order modes are used. Table 5.2 shows the condition number comparison of the scattering matrix versus the transfer scattering matrix of a subsystem at 420 Hz, at which the TL starts to diverge. It is found that the condition number of the transfer scattering matrix is several orders higher than that of the scattering matrix, especially when more higher-order modes are included.

Table 5.2 Condition number comparison at 420 Hz.

Number of Modes / Matrix Type	$N = 1$	$N = 17$
Scattering Matrix	1.02	62.82
Transfer Scattering Matrix	1.43×10^{5}	4.45×10^{20}

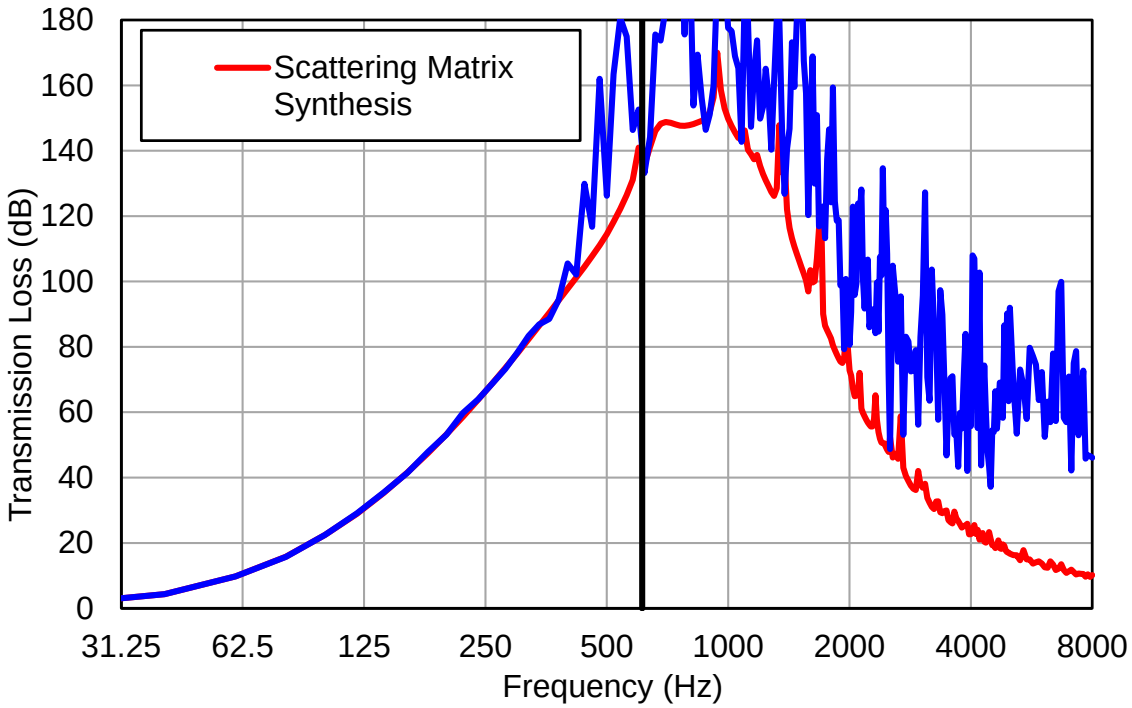

Figure 5.16 Comparison between the scattering matrix and transfer scattering matrix synthesis (*N* =17).

5.4 Large silencer transmission loss in octave band

5.4.1 Octave and one-third octave band

Each octave band filter has a fixed center frequency and is twice as wide as the one before it, as shown in Figure 5.17. In other words, the bands are related by the following relationship

$$\frac{f_u}{f_l} = 2 \tag{5.20}$$

where f_u and f_l are the upper limit and lower limit frequency of the band, respectively.

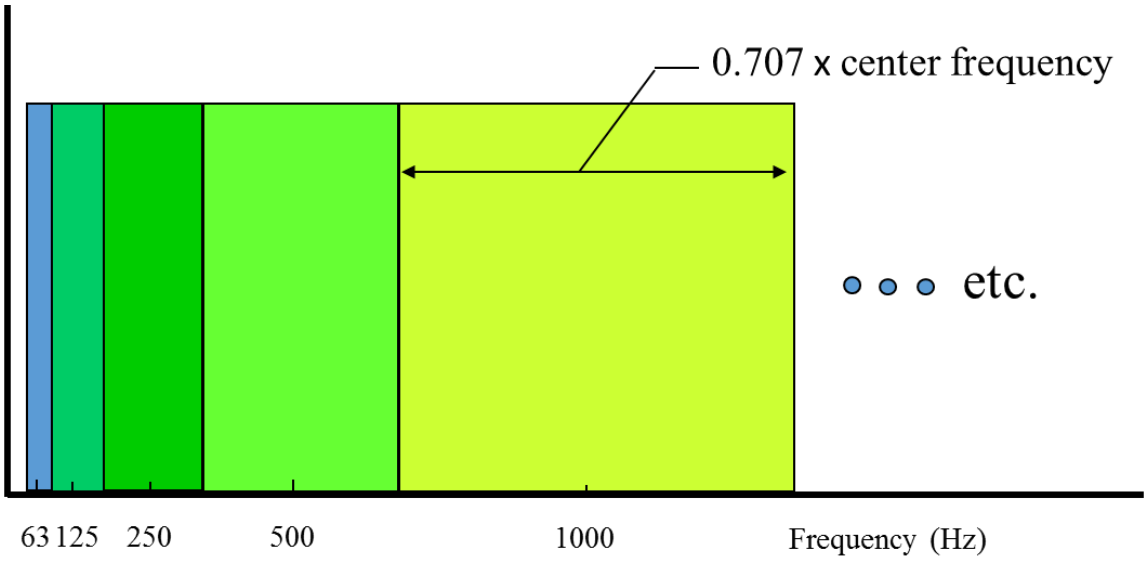

Figure 5.17 Octave band filters.

Each octave band filter may be divided into three one-third octave band filters for greater frequency resolution. The standard center, lower and upper limit frequencies for octave and one-third octave bands below 2900 Hz are shown in Table 5.3.

Table 5.3 Octave and One-Third Octave Bands Comparison

(Beranek and Vér, 2006).

Octave			One-Third Octave		
Lower Band Limit	Center	Upper Band Limit	Lower Band Limit	Center	Upper Band Limit
11	16	22	14.1	16	17.8
			17.8	20	22.4
			22.4	25	28.2
22	31.5	44	28.2	31.5	35.5
			35.5	40	44.7
			44.7	50	56.2
44	63	88	56.2	63	70.8
			70.8	80	89.1
			89.1	100	112
88	125	177	112	125	141
			141	160	178
			178	200	224
177	250	355	224	250	282
			282	315	355
			355	400	447
355	500	710	447	500	562
			562	630	708
			708	800	891
710	1,000	1,420	891	1,000	1,122
			1,122	1,250	1,413
			1,413	1,600	1,778
1,420	2,000	2,840	1,778	2,000	2,239
			2,239	2,500	2,818

To convert the narrow bands to octave bands (octave bands or one-third octave bands), it is necessary to calculate the overall sound level in each band filter. Since the sound level scales are logarithmic, they cannot be combined algebraically. Instead, the energy addition theorem is applied to combine the narrow-band sound power levels in each band filter to obtain the overall sound power level for a given

band. This is essentially the numerical integration of sound power over each band divided by the bandwidth. In other words, the end result is the average sound power in each band. In practice, only a simple summation or integration procedure of the sound power is performed without doing the average if the same frequency increment is used at every measurement point.

5.4.2 Methods for determination of silencer transmission loss in octave band

In this section, three different methods are presented to convert the narrow-band TL into octave or one-third octave bands. All three methods are based on the assumption of a constant amplitude incident wave across the frequency range. In reality, however, the incident sound power may be different at each frequency.

Wave decomposition method

W_i and W_t obtained by the method illustrated in section 1.1.3 in narrow bands are integrated (or simply summed) over each band to get the TL in octave bands:

$$TL = 10\log_{10}\left(\frac{W_i}{W_t}\right) \tag{5.21}$$

Equivalent Insertion Loss Method

This method assumes that the four-pole matrix of the silencer as shown in Equation 1.4, has been either measured or calculated in narrow bands. However, it should be noted that the four-pole matrix does not exist above the plane-wave cutoff of the inlet and outlet ducts. The narrow-band TL can be calculated by Equation 1.6 in terms of the four-pole parameters.

Figure 5.18(a) shows the basic components of a typical duct silencing system and 5.17(b) shows the corresponding circuit analog of the acoustical system. In 5.17(b), Z_S is the source impedance, Z_T is the termination impedance, p_1 and u_1 are the sound pressure and particle velocity at inlet, and p_2 and u_2 are the sound pressure and particle velocity at outlet, respectively. Relations among these quantities are shown in Equation 5.22, 5.23 and 5.24,

$$p_s = p_1 + Z_S u_1 \tag{5.22}$$

$$\begin{Bmatrix} p_1 \\ u_1 \end{Bmatrix} = \begin{bmatrix} T_{11} & T_{12} \\ T_{21} & T_{22} \end{bmatrix} \begin{Bmatrix} p_1 \\ u_1 \end{Bmatrix} \tag{5.23}$$

$$p_2 = Z_T u_2 \tag{5.24}$$

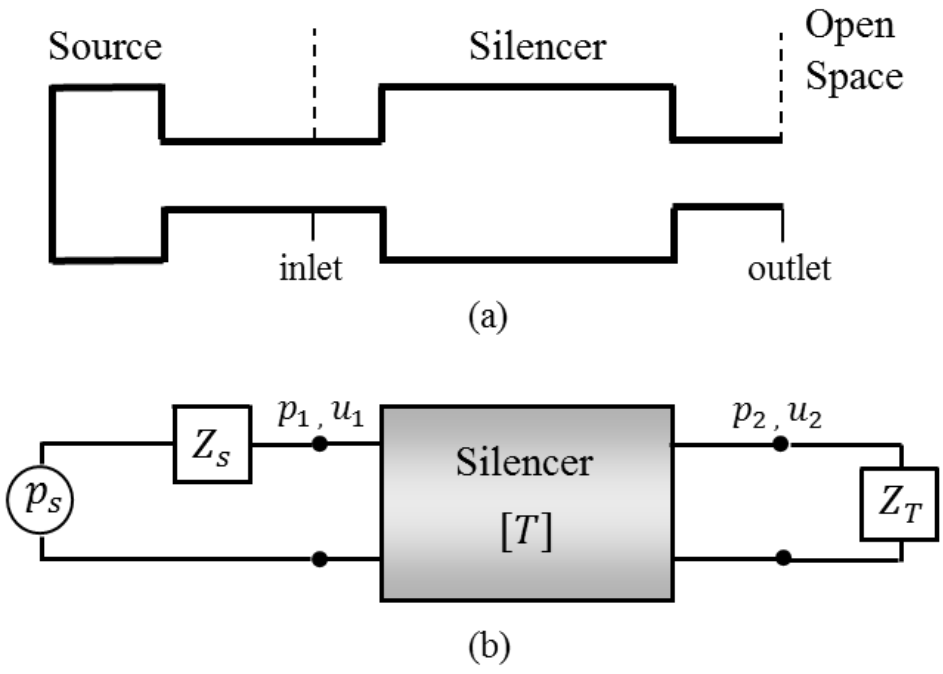

Figure 5.18 (a) Typical duct silencing system; (b) Electric analog.

p_o can also be expressed in terms of $[T]$, Z_S, Z_T and p_s by solving the equations above,

$$p_o = \frac{Z_T p_s}{(Z_T T_{11} + T_{12} + Z_S Z_T T_{21} + Z_S T_{22})} \tag{5.25}$$

Thus, insertion loss (IL) can be calculated by

$$IL = 20\log_{10}\left|\frac{Z_T T_{11} + T_{12} + Z_S Z_T T_{21} + Z_S T_{22}}{(Z_T D_{11} + D_{12} + Z_S Z_T D_{21} + Z_S D_{22})}\right| \tag{5.26}$$

where $[D]$ is the four-pole matrix of the straight replacement pipe. It is noted that when the source and termination are anechoic, Equation 5.26 can be reduced to Equation 1.6. In other words, the IL is the same as TL if both the source and termination are anechoic.

To compute the TL in octave bands, the sound pressures at the outlets of the two cases shown in Figure 5.19 are computed. Since both the source and termination are anechoic, the computed IL is the same as the TL.

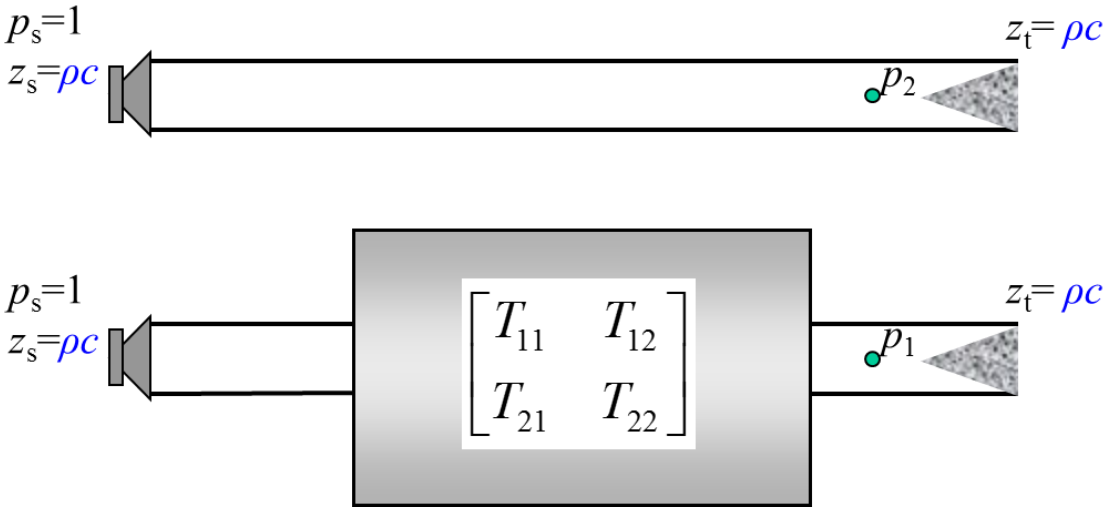

Figure 5.19 Two pseudo cases.

According to Equation 5.25, if the source and termination are both anechoic, the sound pressures p_1 and p_2 at the termination of the straight pipe and the silencer, respectively, can be calculated separately by using the following equations:

$$p_1 = \frac{p_s}{\left(T_{11} + \frac{T_{12}}{\rho c} + T_{21}\rho c + T_{22}\right)} \tag{5.27}$$

$$p_2 = \frac{p_s}{\left(D_{11} + \frac{D_{12}}{\rho c} + D_{21}\rho c + D_{22}\right)} \tag{5.28}$$

Assume p_s is constant across the frequency range, and then convert p_1 and p_2 to octave-band sound pressure levels SPL_1 and SPL_2, respectively. It can be proved that a constant p_s with an anechoic source is equivalent to a constant incident wave. Then, the equivalent TL can be calculated by

$$TL = IL = SPL_2 - SPL_1 \tag{5.29}$$

Direct Conversion Method

If the narrow-band TL is available already, the direct conversion method can be easily applied by following the simple steps below:

1: Set the incident sound power W_i =1 in Equation 5.21 at all frequencies.

2: Calculate the corresponding transmitted sound power W_t at each frequency from the narrow-band TL.

3: Convert both W_i and W_t into octave bands by doing simple integration (or summation).

4: Calculate the TL from the octave-band W_i and W_t.

5.4.3 Test cases

The first test case is the simple expansion shown in Figure 5.20. One-third octave band TL curves using the three different methods presented in this section are compared to the narrow-band TL in Figure 5.21. The frequency stepping used in the narrow-band calculation is 10 Hz. It is seen from Figure 5.21 that all three methods produce the identical TL and that is why only one red curve is displayed. Below the plane-wave cutoff frequency at the inlet and outlet, all three methods are all valid to convert the narrow band TL into the one-third octave or octave band.

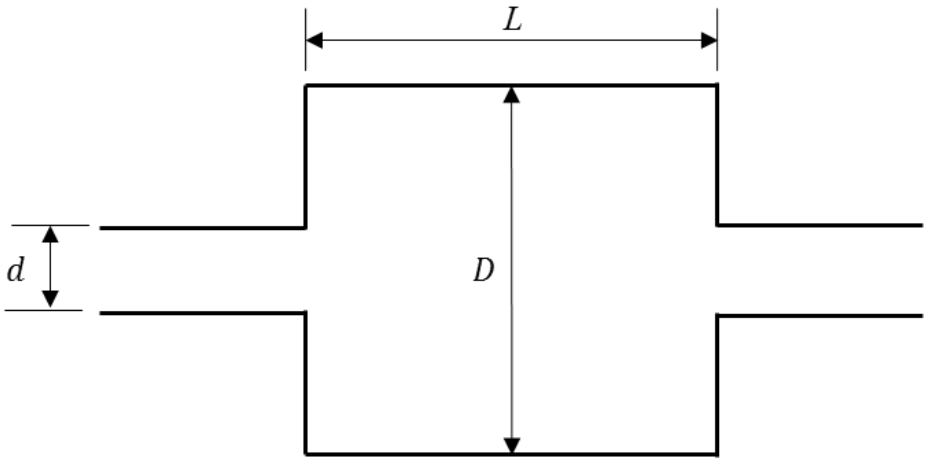

Figure 5.20 Simple expansion chamber.

(L=200 mm, d=35 mm, D =150 mm).

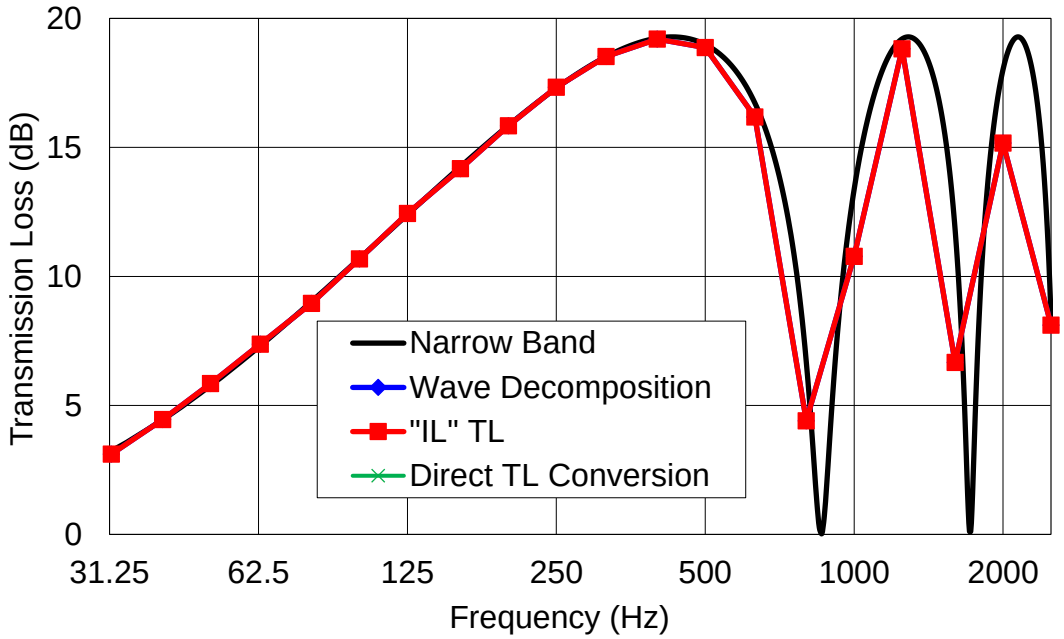

Figure 5.21 Transmission loss comparison of simple expansion chamber.

The second test case is a large round bar silencer shown in Figure 2.1. The narrow-band TL can be obtained by applying the proposed impedance-to-scattering method.

Due to the large cross section of the silencer, the plane-wave assumption is not valid anymore at the inlet and outlet. Therefore, only the direct conversion method can be used to convert the narrow-band TL into octave bands. Figure 5.22 shows the comparison between the narrow-band TL, the 1/3-octave band TL, and the octave-band TL. It can be seen that the one-third octave band TL curve is close to the narrow band TL for the highly absorptive silencer, and the peak value of the octave band TL is decreased.

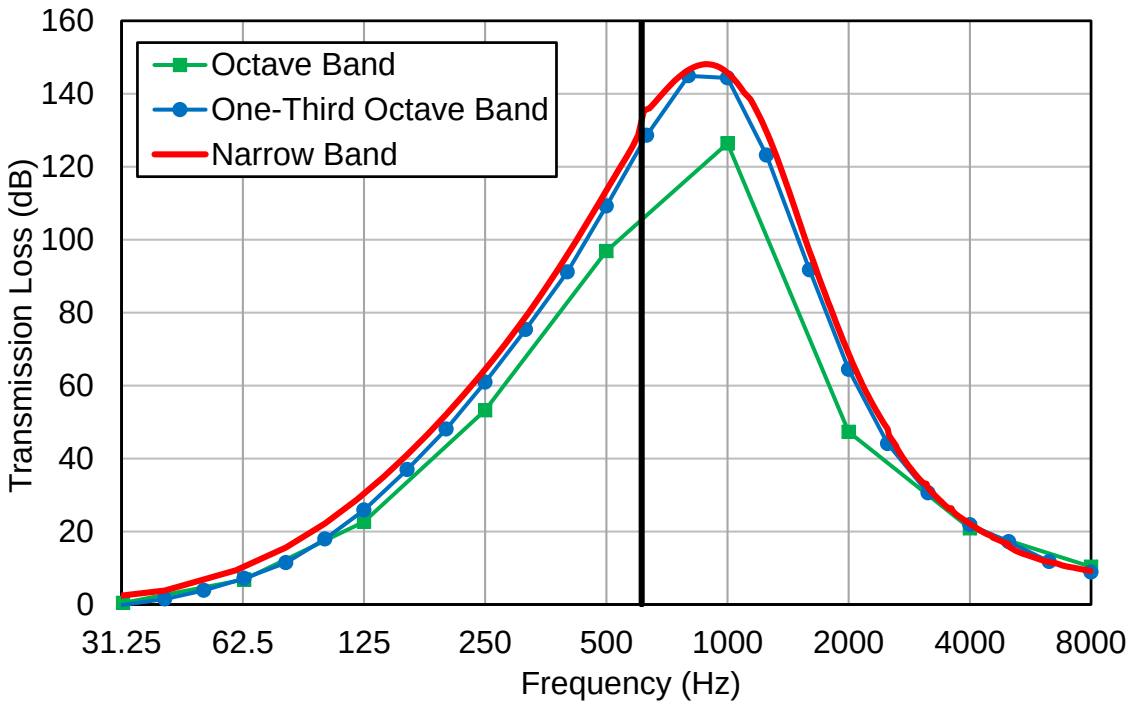

Figure 5.22 Transmission loss of the round bar silencer.

5.5 Summary

In order to study the acoustic attenuation of large silencers with irregular inlet and outlet configurations, the cross-sectional modes at the inlet and outlet are extracted by the 2-D FEM first. The proposed method is first validated by the numerical solution by Kirby et al. (2014) on a rectangular bar silencer test case. A triangular unit isolated from a shifted lattice arrangement of round bars is modeled later to study its performance advantages over the aligned lattice design. It is found that increasing the porosity of the perforated facing sheet may improve the acoustic attenuation performance at higher frequencies but this may be at the expense of a small reduction of TL at lower frequencies and the effect of flow resistivity is very little at very high frequencies. Because of the more compact design of shifted lattice (triangular module) than the aligned lattice (square module), it is seen that triangular module has better attenuation over 1000 Hz.

Bar silencers usually consist of several subsystems as shown in Figure 5.13. The scattering matrix synthesis using the Redheffer's star product is developed in this chapter. Since the scattering matrix is mesh-independent, the scattering matrix synthesis does not require a BEM mesh to be attached to it. Additionally, it takes much less memory space to store the scattering matrix than impedance matrix. Compared to the so-called transfer scattering matrix method, the scattering matrix synthesis is more stable above the plane-wave cutoff frequency.

Finally, three methods for converting the narrow-band TL to one-third octave or octave band are developed. There has been no existing standard procedure for determining the TL in one-third or octave bands using measured data or

simulation. All three methods are valid for the TL conversion below the plane-wave cutoff frequency at the inlet and outlet, and the direct conversion method can still be used above the cutoff frequency.

Chapter 6 SEMI-ANALYTICAL AND BEM SOLUTIONS OF LARGE TUNED DISSIPATIVE SILENCERS

6.1 Introduction

The noise spectrum at the gas turbine exhaust is contributed by not only the broadband noise but also tonal components due to the rotor stator interaction, combustion instabilities (Kudernatsch, 2000) and the fan exhaust. Noise with tonal components is always found to be more annoying than the broadband noise at the same overall level without a tone. However, typical large dissipative silencers such as parallel-baffle silencers, bar silencers and lined ducts are only good at reducing broadband noise since they don't have any reactive components.

To attenuate the broadband noise while suppressing tonal noise, tuned dissipative silencers are commonly used. Tuned dissipative silencers consist of baffles containing cavities which can be designed or tuned for optimum acoustical performance at selected frequencies (Bell, 1993). Figure 6.1 shows a typical tuned dissipative silencer, which is sometimes called "pine-tree silencer" because of its configuration. As shown in Figure 6.1, absorbing material is attached to one side of each inclined shape of a cavity, to increase the bandwidth of spectral attenuation near the target frequencies. As a result, tuned dissipative silencers can accommodate normal fluctuations in operating temperature. These types of silencers are particularly effective for attenuating tonal fan noise at the blade pass frequency and its harmonics. Additionally, thanks to the inclined angle of each cavity with respect to the flow direction, these silencers are usually used in exhaust

flows with heavy dust load since dust deposits on the branches of the trees will slide down naturally (Mechel, 2002).

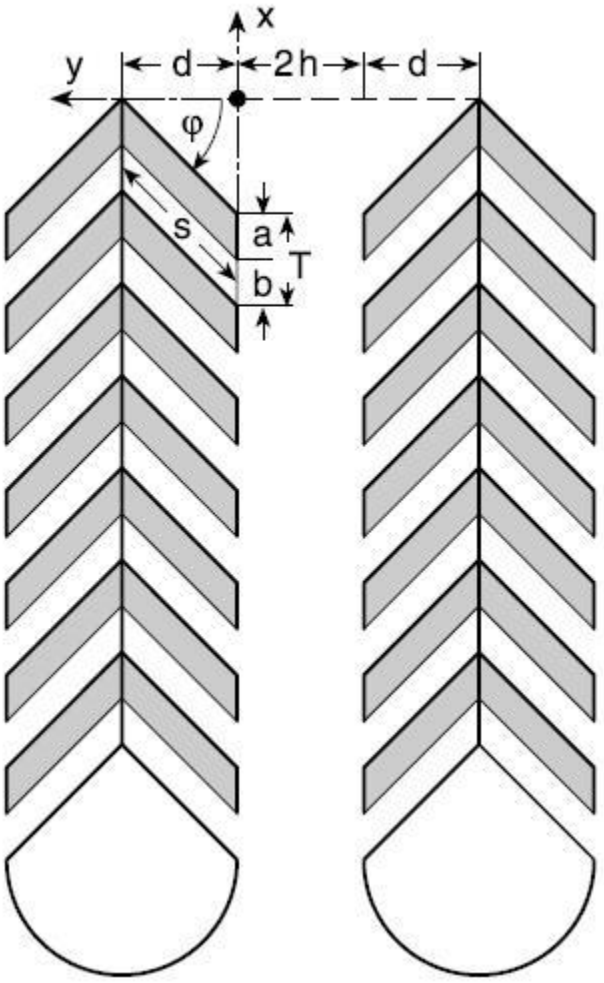

Figure 6.1 A pine-tree silencer (Mechel, 2002).

To the author's knowledge, there has been no work directly related to the TL analysis of pine-tree silencers. Mechel (1998, 2002) provided approximate design formulas, but they are not applicable for low frequencies below 70 Hz. Even though pine-tree silencers have not been thoroughly investigated, the acoustic attenuation performance of lined resonators and array resonators have been studied and improved by many researchers. Selemet et al. (2005) developed a two-

dimensional closed-form analytical solution to investigate the acoustic performance of a concentric circular Helmholtz resonator lined with fibrous material. The fibrous material in the cavity has been found to lower the resonance frequency and the peak transmission loss. The resonance frequency shifts to lower frequencies and the overall transmission loss decreases relative to the empty chamber with increasing flow resistivity. For low frequencies below the resonance, the transmission loss with thicker absorbent is slightly higher, whereas this behavior is reversed on the other side of resonance. Howard and Craig (Howard and Craig, 2014) conducted tests on three orifice geometries of side-branches on an adaptive quarter-wave tube to determine which was the least compromised by the high-speed exhaust gas passing over the side-branch. The side-branch geometries tested were a sharp edge, a backward inclined branch, and a bell mouth. The experimental results showed that the side-branch with a bell-mouth geometry resulted in the greatest noise reduction by an adaptive quarter-wave tube. Wang and Mak (2012) presented a theoretical study of a duct loaded with identical side-branch resonators based on the Bloch wave theory (Kittel, 1986) and the transfer matrix method to investigate wave propagation in the duct. A duct with several identical resonators exhibits a unique attenuation characteristic caused by structural periodicity, and may, if carefully designed, provide a much broader noise attenuation bands compared to a single resonator. Seo and Kim (2005) tested serial and parallel arrangements of resonators to obtain broader impedance mismatch characteristics in broadband. It was found out that the serial arrangement mainly increases the peak of TL at the resonance frequency and the

parallel arrangement logarithmically increases the peak of TL and expands the bandwidth. Coulon et al. (2016) used a 2D FEM model coupled to a global MATLAB optimization solver to optimize three or more Helmholtz resonator arrays. Among different types of constructions, arrays made of concentric resonators with transversal openings offer the most efficient and flexible design to optimize distance between openings.

In this chapter, a two-dimensional first-mode semi-analytical solution is presented to quickly evaluate the performance of pine-tree silencers below the plane-wave cut-off frequency. The proposed method can provide a quick assessment of the acoustic attenuation performance of large tuned dissipative silencers during the initial design stage. Additionally, the semi-analytical method can also provide a low-frequency benchmark solution for the 3D BEM, which is not limited to the plane-wave cut-off frequency when used in conjunction with the impedance-to-scattering matrix method.

6.2 Semi-analytical solution of large tuned dissipative silencers

The objective of this section is to present a two-dimensional first-model semi-analytical solution for the TL analysis of tuned dissipative silencers below the plane-wave cutoff frequency. To study the problem using a semi-analytical method, the tuned dissipative silencer is divided into 4 sections as shown in Figure 6.3. The four-pole transfer matrices of section 2 and section 3 can be determined by the proposed two-dimensional first-mode analytical solution. For section 1 and 4, it may be difficult to derive the analytical solution because of the irregular shapes. Therefore, the impedance matrix is calculated by BEM. Although BEM is

still used, it is applied to two small sections only. The four-pole transfer matrices in sections 2 and 3 can be easily converted to two corresponding impedance matrices. After that, the impedance matrix synthesis technique is performed to form the resultant impedance matrix of the whole model. The TL of the test case can then be obtained after converting the resultant impedance matrix back to the four-pole transfer matrix. This semi-analytical solution has a combination of both an analytical approach and a numerical approach (BEM). The analytical approach is applied to the core part of the silencer design (the pine tree), while the BEM is only applied to the inlet and outlet transition ducts.

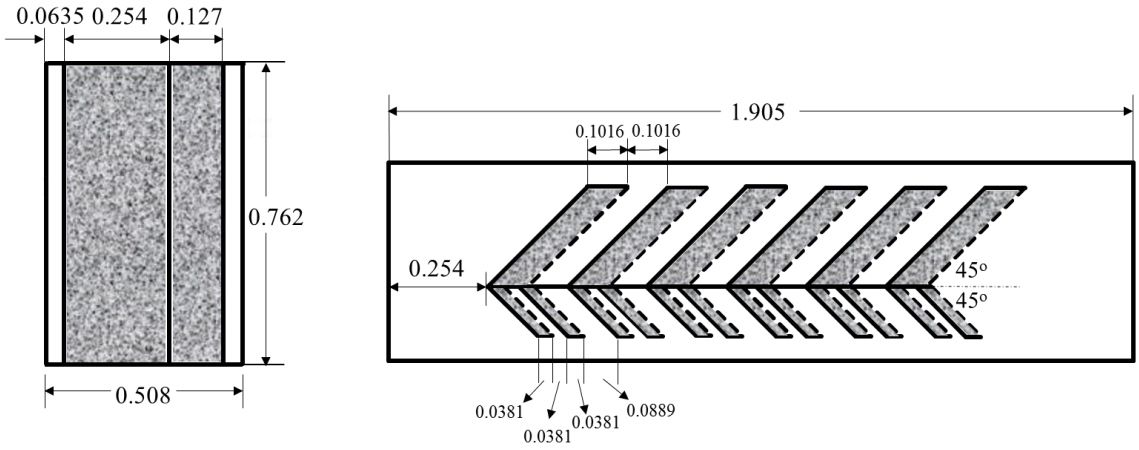

Figure 6.2 A tuned dissipative silencer test case (Unit: m).

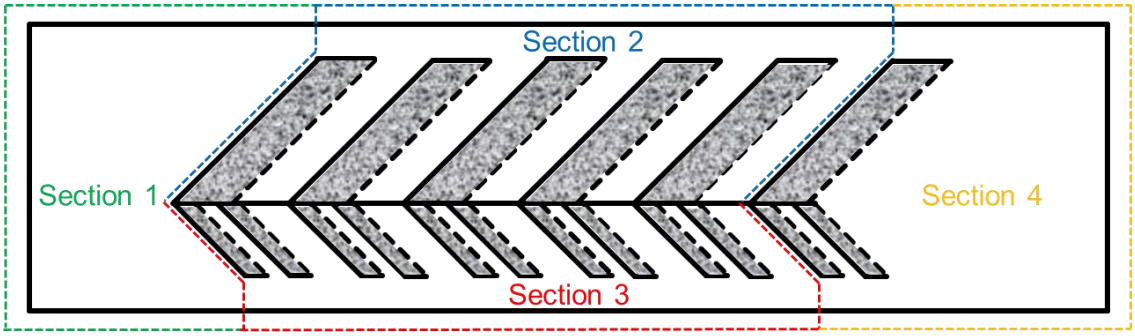

Figure 6.3 Four sections of the divided tuned dissipative silencer test case.

6.2.1 Transfer matrix determination of lined resonator

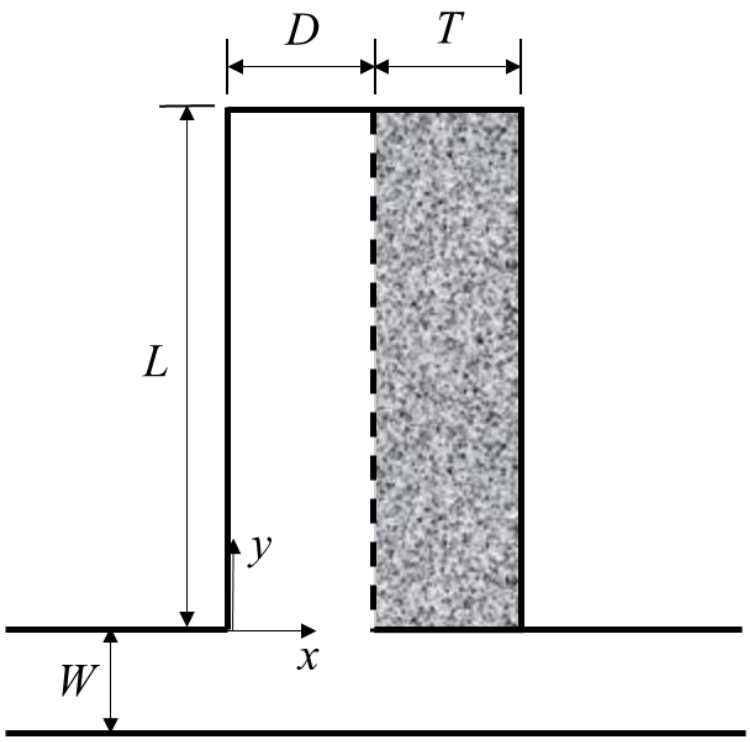

Figure 6.4 A lined resonator.

As shown in Figure 6.4, inside the main duct of a lined resonator, the sound pressure can be expressed in terms of the first mode by

$$p_{(x,y)} = (Ae^{-jk_x x} + Be^{jk_x x})(Ce^{-jk_y y} + De^{jk_y y}) \tag{6.1}$$

where *A*, *B*, *C*, and *D* are undetermined coefficients. The wavenumber in the x direction, k_x, and the wavenumber in y direction, k_y, are related by

$$k_x^2 + k_y^2 = k^2 \tag{6.2}$$

Apply the rigid boundary conditions at $x = 0$ and $y = L$, in other words, $\frac{\partial p}{\partial x} = 0$ at $x = 0$, and $\frac{\partial p}{\partial y} = 0$ at $y = L$, to get

$$A = B \tag{6.3}$$

$$D = Ce^{-2jk_yL} \tag{6.4}$$

Substitute Equations 6.3 and 6.4 into Equation 6.1, and lump *A* and *B* with *C* to redefine a new undetermined coefficient *C*. The general expression of sound pressure becomes

$$p_{(x,y)} = C\cos(k_x x)\,(e^{-jk_y y} + e^{jk_y(y-2L)}) \tag{6.5}$$

The expression for the particle velocity in the x direction corresponding to Equation 6.5 is

$$u_x = \frac{j}{\rho\omega}\frac{\partial p}{\partial x} = C\frac{j}{\rho\omega}(-k_x\sin(k_x x))\,(e^{-jk_y y} + e^{jk_y(y-2L)}) \tag{6.6}$$

The local impedance at $x = D$ is defined as

$$Z_m = \frac{p}{u_x} = j\rho\omega\frac{\cos(k_x D)}{k_x\sin(k_x D)} \tag{6.7}$$

To determine the local impedance of the porous material in the rectangular duct, the transfer matrix of the porous material in the rectangular duct is obtained first,

$$\begin{pmatrix} p_1 \\ u_1 \end{pmatrix} = \begin{bmatrix} \cos(\hat{k}d) & i\hat{\rho}\hat{c}\sin(\hat{k}d) \\ \frac{i}{\hat{\rho}\hat{c}}\sin(\hat{k}d) & \cos(\hat{k}d) \end{bmatrix} \begin{pmatrix} p_2 \\ u_2 \end{pmatrix} \tag{6.8}$$

where d is the thickness of the material, $\hat{k}$ is the complex wavenumber of the material, $\hat{\rho}\hat{c}$ is the characteristic impedance of the material.

Because of the rigid-wall boundary condition, $u_2 = 0$, the local impedance is

$$Z_m = \frac{p_1}{u_1} = -i\hat{\rho}\hat{c}\cot(\hat{k}d) \tag{6.9}$$

In this case , $Z_m = -i\hat{\rho}\hat{c}\cot(\hat{k}T)$.

Substituting the expression of Z_m into Equation 6.7 produces

$$j\rho\omega\frac{\cos(k_x D)}{k_x \sin(k_x D)} + j\hat{\rho}\hat{c}\cot(\hat{k}T) = 0 \tag{6.10}$$

Equation 6.10 is the characteristic equation and the wavenumber in x direction k_x can be obtained by solving the nonlinear equation numerically.

The wavenumber in y direction, k_y, can be obtained from Equation 6.2 thereafter.

Therefore, the local impedance at the opening of the side branch ($y = 0$) can be expressed as

$$Z = \frac{p}{u_y} = \frac{-j\rho\omega\cot(k_y L)}{k_y} \tag{6.11}$$

With the local impedance at the opening of the side branch available, the transfer matrix of the lined resonator is

$$[T] = \begin{bmatrix} 1 & 0 \\ S_b/_Z & 1 \end{bmatrix} \tag{6.12}$$

where S_b is the cross section area of the opening of the side branch.

The TL of the lined resonator can be calculated by

$$TL = 20 \log_{10} \left(\frac{1}{2} \left| T_{11} + \frac{T_{12}}{\rho c} + \rho c T_{21} + T_{22} \right| \right) \tag{6.13}$$

6.2.2 Impedance matrix synthesis

Section 2 and 3 in Figure 6.2 both contain a series of lined resonators. Between any two neighboring line resonators, there is also a short straight duct that connects the two lined resonators. The four-pole transfer matrix of each lined resonator can be obtained by Eq. (6.12), and the four-pole transfer matrix of the connecting short straight duct can be easily obtained by the plane-wave theory. The resultant transfer matrices of the sections 2 and 3 in Figure 6.2 can be obtained by simply multiplying the corresponding four-pole transfer matrices together. Each of the two resultant four-pole transfer matrices is then converted to a corresponding impedance matrix by

$$[Z] = \begin{bmatrix} \frac{T_{11}}{T_{21}} & T_{12} - \frac{T_{11}T_{22}}{T_{21}} \\ \frac{1}{T_{21}} & -\frac{T_{22}}{T_{21}} \end{bmatrix} \tag{6.14}$$

where $[Z]$ is impedance matrix, and T_{11}, T_{12}, T_{21} and T_{22} are four poles of the transfer matrix.

The BEM is then applied to produce the impedance matrices of sections 1 and 4 in Figure 6.3. The impedance matrix of each section can be expressed as

$$\begin{Bmatrix} p_1 \\ p_2 \\ p_3 \end{Bmatrix} = \begin{bmatrix} Z_{11}^1 & Z_{12}^1 & Z_{13}^1 \\ Z_{21}^1 & Z_{22}^1 & Z_{22}^1 \\ Z_{31}^1 & Z_{32}^1 & Z_{33}^1 \end{bmatrix} \begin{Bmatrix} u_1 \\ u_2 \\ u_3 \end{Bmatrix} \tag{6.15}$$

$$\begin{Bmatrix} p_2 \\ p_4 \end{Bmatrix} = \begin{bmatrix} Z_{11}^2 & Z_{12}^2 \\ Z_{21}^2 & Z_{22}^2 \end{bmatrix} \begin{Bmatrix} u_2 \\ u_4 \end{Bmatrix} \tag{6.16}$$

$$\begin{Bmatrix} p_3 \\ p_5 \end{Bmatrix} = \begin{bmatrix} Z_{11}^3 & Z_{12}^3 \\ Z_{21}^3 & Z_{22}^3 \end{bmatrix} \begin{Bmatrix} u_3 \\ u_5 \end{Bmatrix} \tag{6.17}$$

$$\begin{Bmatrix} p_4 \\ p_5 \\ p_6 \end{Bmatrix} = \begin{bmatrix} Z_{11}^4 & Z_{12}^4 & Z_{13}^4 \\ Z_{21}^4 & Z_{22}^4 & Z_{22}^4 \\ Z_{31}^4 & Z_{32}^4 & Z_{33}^4 \end{bmatrix} \begin{Bmatrix} u_4 \\ u_5 \\ u_6 \end{Bmatrix} \tag{6.18}$$

After some manipulations of Equations 6.15 to 6.18, u_2, u_3, u_4 and u_5 can be expressed in terms of u_1 and u_6:

$$\begin{bmatrix} Z_{22}^1 - Z_{11}^2 & Z_{23}^1 & -Z_{12}^2 & 0 \\ Z_{32}^1 & Z_{33}^1 - Z_{11}^3 & 0 & -Z_{12}^3 \\ -Z_{21}^2 & 0 & Z_{11}^4 - Z_{22}^2 & Z_{12}^4 \\ 0 & -Z_{21}^3 & Z_{21}^4 & Z_{22}^4 - Z_{22}^3 \end{bmatrix} \begin{Bmatrix} u_2 \\ u_3 \\ u_4 \\ u_5 \end{Bmatrix} = \begin{bmatrix} -Z_{21}^1 & 0 \\ -Z_{31}^1 & 0 \\ 0 & -Z_{13}^4 \\ 0 & -Z_{23}^4 \end{bmatrix} \begin{Bmatrix} u_1 \\ u_6 \end{Bmatrix} \tag{6.19}$$

Matrix inverse is then performed on Equation 6.19 to produce

$$\begin{Bmatrix} u_2 \\ u_3 \\ u_4 \\ u_5 \end{Bmatrix} = \begin{bmatrix} A & B \\ C & D \\ E & F \\ G & H \end{bmatrix} \begin{Bmatrix} u_1 \\ u_6 \end{Bmatrix} \tag{6.20}$$

Sound pressure p_1 and p_6 can be expressed in terms of u_1 and u_6 by

$$\begin{Bmatrix} p_1 \\ p_6 \end{Bmatrix} = \begin{bmatrix} Z_{11}^1 + Z_{12}^1 A + Z_{13}^1 C & Z_{12}^1 B + Z_{13}^1 D \\ Z_{31}^4 E + Z_{32}^4 G & Z_{33}^4 + Z_{31}^4 F + Z_{32}^4 H \end{bmatrix} \begin{Bmatrix} u_1 \\ u_6 \end{Bmatrix} \tag{6.21}$$

Similar to Equation 6.14, the resultant impedance matrix of the full model can be converted back to the corresponding transfer matrix by

$$[T] = \begin{bmatrix} \frac{Z_{11}}{Z_{21}} & Z_{12} - \frac{Z_{11}Z_{22}}{Z_{21}} \\ \frac{1}{Z_{21}} & -\frac{Z_{22}}{Z_{21}} \end{bmatrix} \tag{6.22}$$

Finally, the TL of the tuned dissipative silencer can be obtained by Equation 6.13.

6.2.3 Validation of the semi-analytical solution

The 2D analytical solution for the TL of an isolated lined resonator should be validated first before we can move on to a full tuned dissipative silencer. The first test case is shown in Figure 6.4 with $L = 10\sqrt{2}$", $T = D = 4$", $W = 2.5$" and the depth (for 3D BEM comparison purposes) of the resonator is 2". The porous material has a flow resistivity *R*=16000 $rayls/m$, and is covered by a 30% open perforated facing sheet. It can be seen in Figure 6.5 that the 2D analytical solution matches very well with the 3D BEM solution. The computed natural frequency of this lined resonator is around 165 Hz. The theoretical natural frequency of the resonator without any lining is 240 Hz. Therefore, the natural frequency is shifted to the lower frequency with porous material attached to one side, and the 2D analytical solution is able to catch the natural frequency accurately.

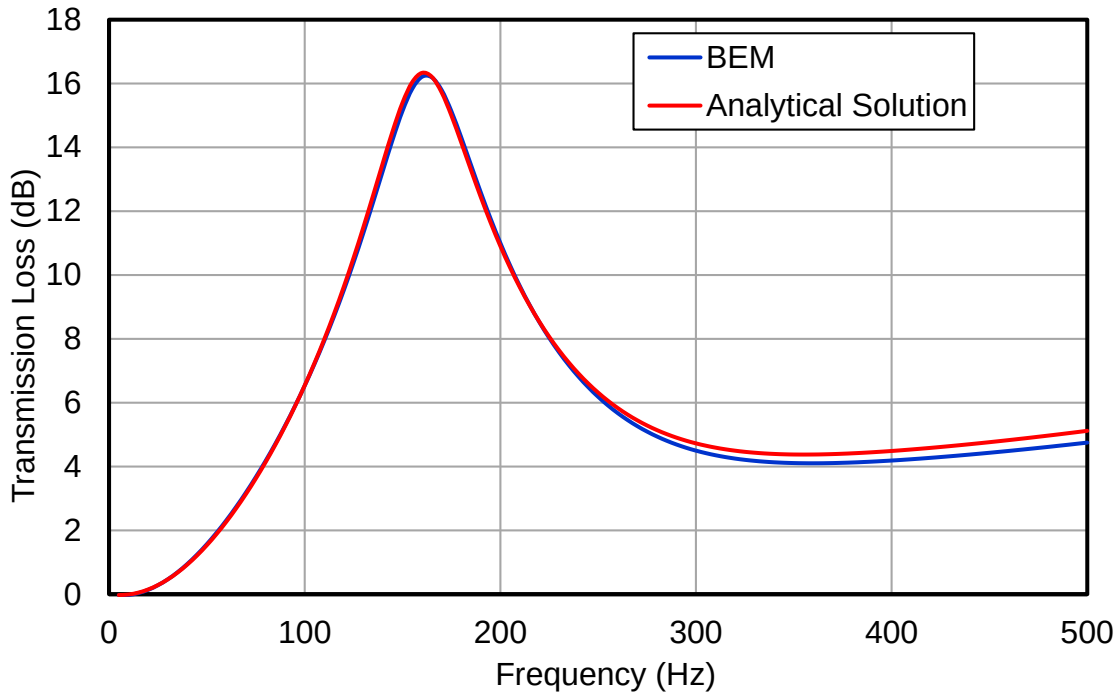

Figure 6.5 TL comparison between the BEM and analytical solution.

The second test case is also a lined resonator but the side branch is inclined with 45 degree as shown in Figure 6.6, in which $L = 10"$, $T = D = 4"$, $W = 2.5"$ and the depth (for 3D BEM) of the resonator is $2"$. The porous material has a flow resistivity *R*=16000 $rayls/m$, and is covered by a 30% open perforated facing sheet.

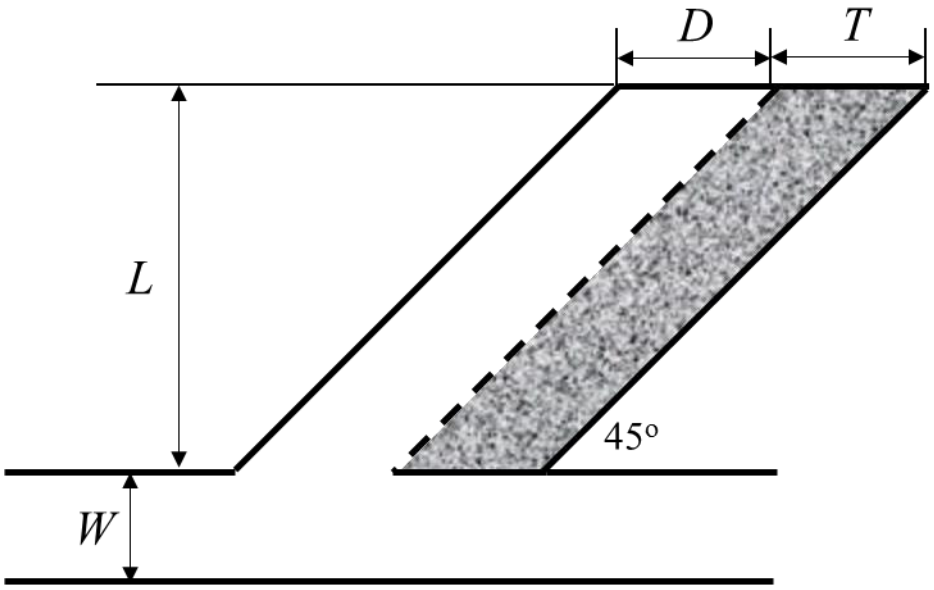

Figure 6.6 A lined resonator inclined with 45 degree.

Since the derivation of the analytical solution is based on a vertical side branch, in order to apply the analytical solution to an inclined side branch, the width of the air channel of the side branch D has to be adjusted to $D * \sin\theta$, where θ is the incline angle of the side branch. Figure 6.7 shows the comparison between the BEM and analytical solution for the inclined test case. The two solutions compare fairly well with each other.

Figure 6.8 compares the inclined lined resonator to the vertical lined resonator, and it can be seen that the natural frequency of the inclined lined resonator is shifted to a lower frequency, and the peak value is slightly lower than the vertical lined resonator.

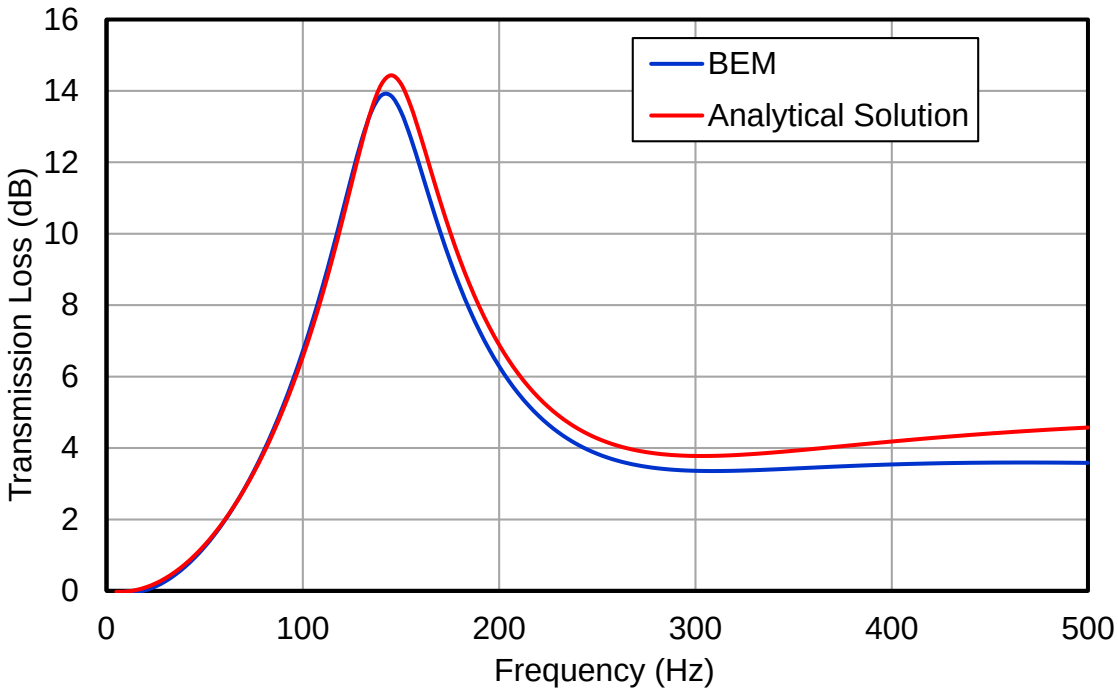

Figure 6.7 TL comparison between the BEM and analytical solution.

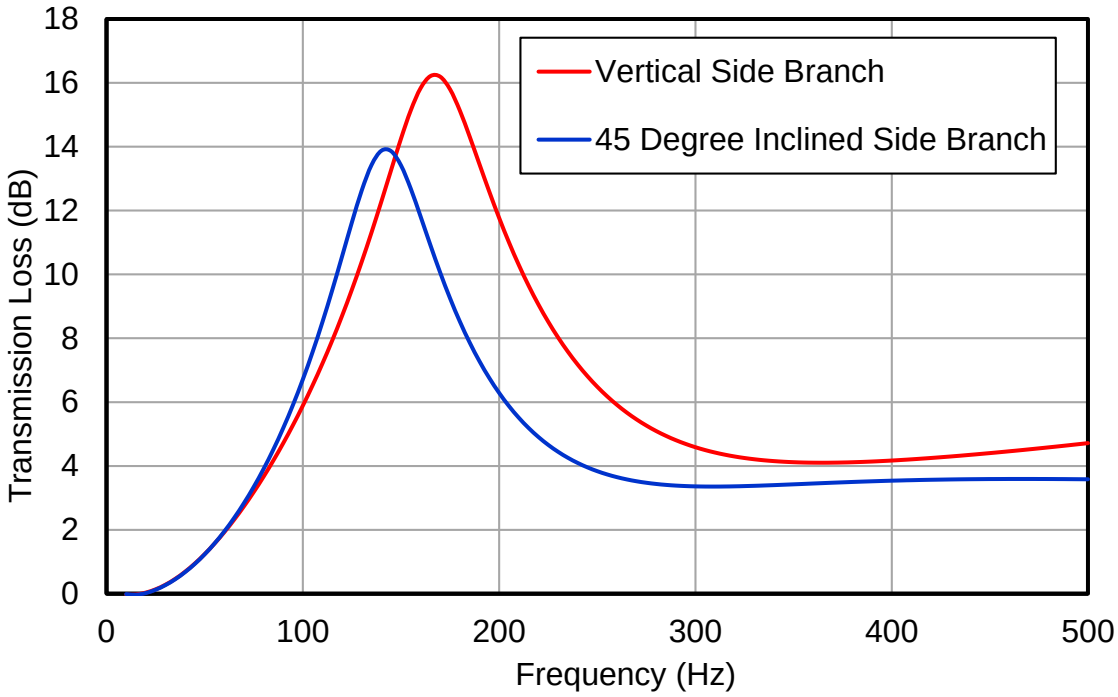

Figure 6.8 TL comparison between the vertical and 45 degree inclined side branch.

After the validation of a single lined resonator in the previous two test cases, the third test case is an inclined resonator array shown in Figure 6.9, which is used to validate the multiplication of the analytical transfer matrices. Each of five inclined resonator has the same dimensions as in the second test case. The 2D analytical solution compares very well with the 3D BEM solution, as shown in Figure 6.10.

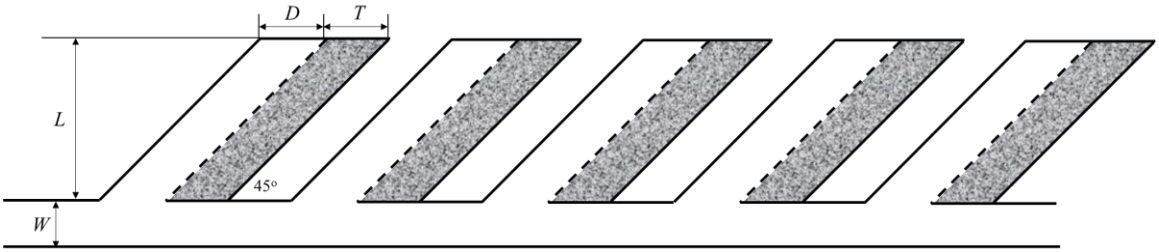

Figure 6.9 An inclined resonator array.

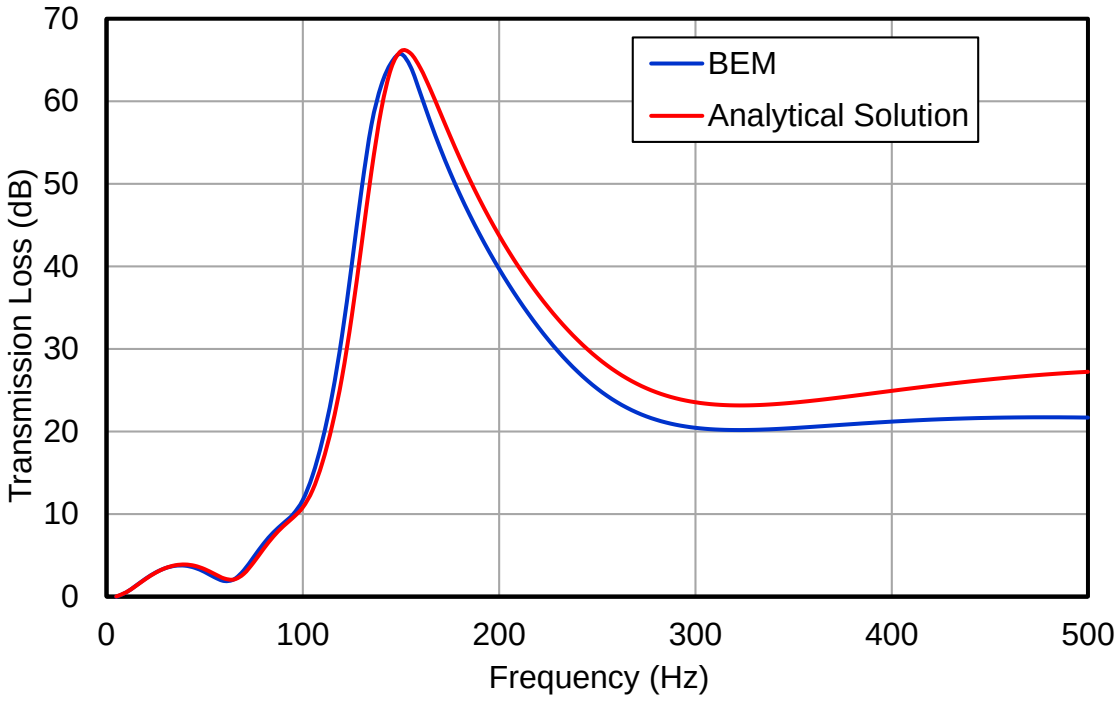

Figure 6.10 TL comparison between the BEM and analytical solution.

In the first three test cases, we have validated the 2D first-mode analytical solution for either a single lined resonator or an array of lined resonators in series connection. Therefore, the transfer matrices of section 2 and section 3 shown in Figure 6.3 can be obtained by the proposed 2D analytical method with confidence. The two transfer matrices are then converted to the corresponding impedance matrices in order to connect to the inlet (section 1) and outlet (section 4). The BEM is used to obtain the impedance matrices of section 1 and section 4. By performing the impedance matrix synthesis, the resultant impedance matrix of the full model can be obtained. The TL of the dissipative silencer can be computed if the resultant impedance matrix is converted back to the four-pole transfer matrix.

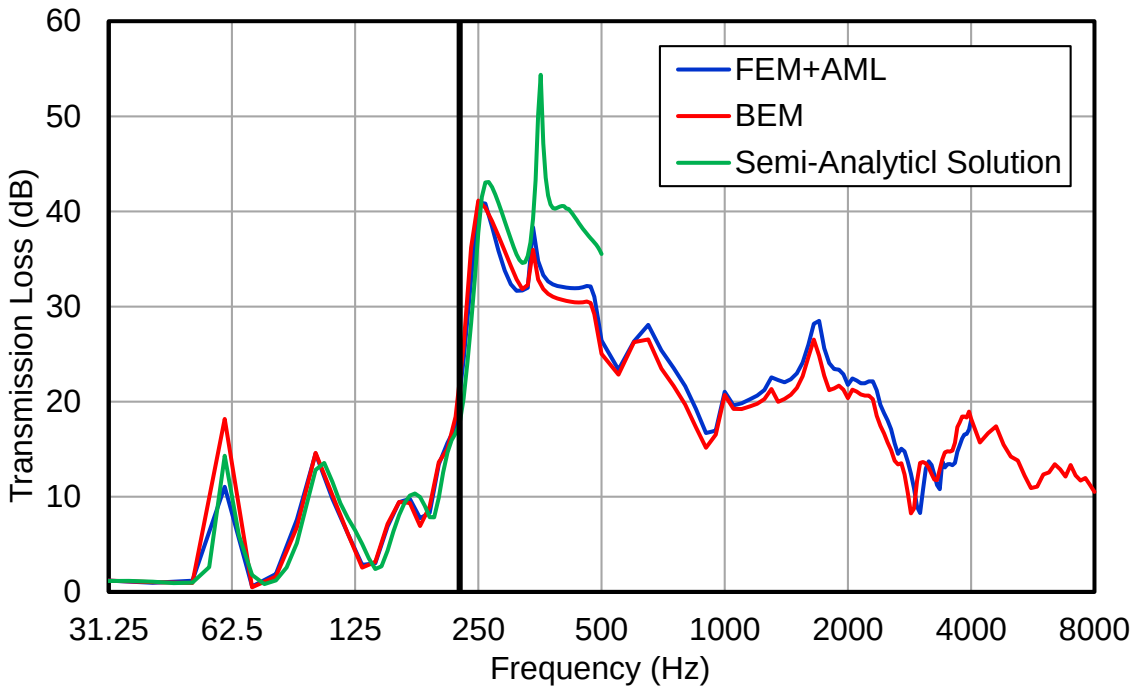

Figure 6.11 TL comparison among the FEM+AML, BEM and analytical solution.

The dimensions of the tuned dissipative silencer test case are shown in Figure 6.2, and the porous material has a flow resistivity R=16000 $rayls/m$, and is covered by

a 30% open perforated facing sheet. Figure 6.11 compares three different TL solutions of the tuned dissipative silencer: BEM, FEM+AML (Virtual.Lab) and proposed semi-analytical solution. It should be noted that the FEM+AML solution requires more computer memory at high frequencies than the BEM because it does not have the substructuring capability. Therefore, the FEM+AML analysis stops at 4000 Hz. Also, the 2D semi-analytical solution is only theoretically valid up to the plane-wave cut-off frequency. Nonetheless, all three methods agree very well with each other below the plane-wave cutoff frequency, which is 225 Hz. Above the cutoff frequency, the FEM+AML solution generally matches the BEM solution up to 4000 Hz. It is also found that the 2D semi-analytical method can still provide a decent approximate solution slightly above the theoretical cut-off frequency.

6.3 BEM analysis of large tuned dissipative silencers

In this section, the tuned dissipative silencer shown in Figure 6.2 is fully investigated to better understand the acoustic attenuation performance.

6.3.1 Difference between locally reacting and bulk reacting modelling of sound absorbing material

In BEM or FEM, the sound absorbing material can be modelled by two different approaches: locally reacting or bulk-reacting. In the locally reacting case, the normal surface impedance is derived as a boundary condition. In the bulk-reacting case, bulk properties (complex density and complex speed of sound) are used to describe the sound absorbing material (Crocker, 2007). The bulk-reacting

properties can be measured by the two-cavity method (Utsuno et al., 1990) or the two-source method (Tao et al., 2003). Therefore, locally reacting modelling does not consider the axial wave propagation occurred in the sound absorbing material, while the bulk reacting modelling method includes three-dimensional wave propagation (Bies et al., 1991).

Figure 6.12 shows the TL comparison between the locally reacting and bulk reacting modelling of sound absorbing material for the tuned dissipative silencer test case. It can be seen that the two methods have some minor disagreements at low frequencies but they do generally match each other quite well above 1000 Hz. Since the locally reacting BEM model is easier to create and is slightly more computationally efficient, all remaining test cases in this chapter will be modeled by the locally reacting approach.

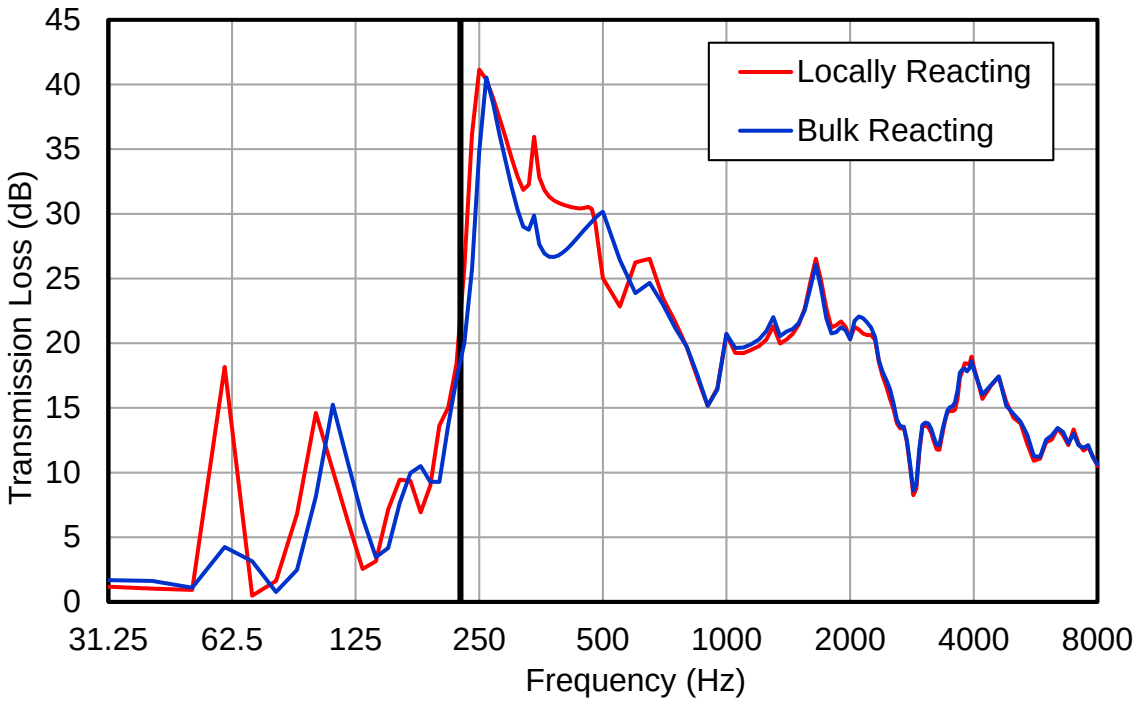

Figure 6.12 TL comparison between the locally reacting and bulk reacting modelling of sound absorbing material.

6.3.2 Effect of the sound absorbing material

Cavities inside of the tuned dissipative silencer are designed or tuned for optimum acoustical performance at selected target frequencies, and the sound absorbing material attached to one side of each cavity can increase the bandwidth of spectral attenuation around the target frequencies while providing the broadband attenuation at high frequencies. As shown in Figure 6.13, with the help of the sound absorbing material, TL is much higher between 200 to 2000 Hz. It should also be noted that the natural frequencies will shift lower with the sound absorbing material attached. Therefore, the 2D semi-analytical method may be used as a quick design tool to fine tune the peak frequencies.

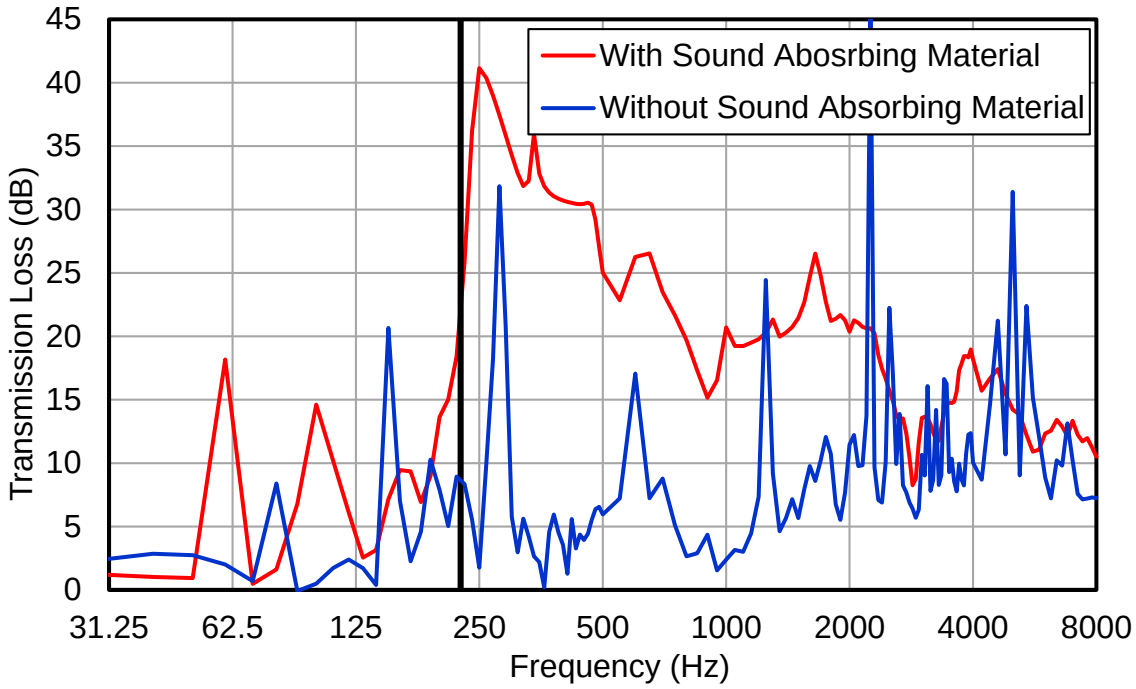

Figure 6.13 TL comparison between with and without sound absorbing material.

6.3.3 Effect of temperature change

Tuned dissipative silencers can accommodate normal fluctuations in operating temperature because of the attached sound absorbing material. Figure 6.14 compares the TL of the tuned dissipative silencer at 20^{o}C to the TL at 500^{o}C. If the sound absorbing material is removed from the pine-tree silencer, the TL comparison between 20^{o}C and 500^{o}C is shown in Figure 6.15.

Because the speed of sound increases when the temperature goes higher, the wavelength at each frequency also becomes longer. It can be found that the TL peaks in both Figure 6.14 and Figure 6.15 shift to higher frequencies. The tuned dissipative silencer is still able to suppress several target frequencies while

providing the broadband attenuation, but the reactive silencer might not attenuate noise at desired frequencies.

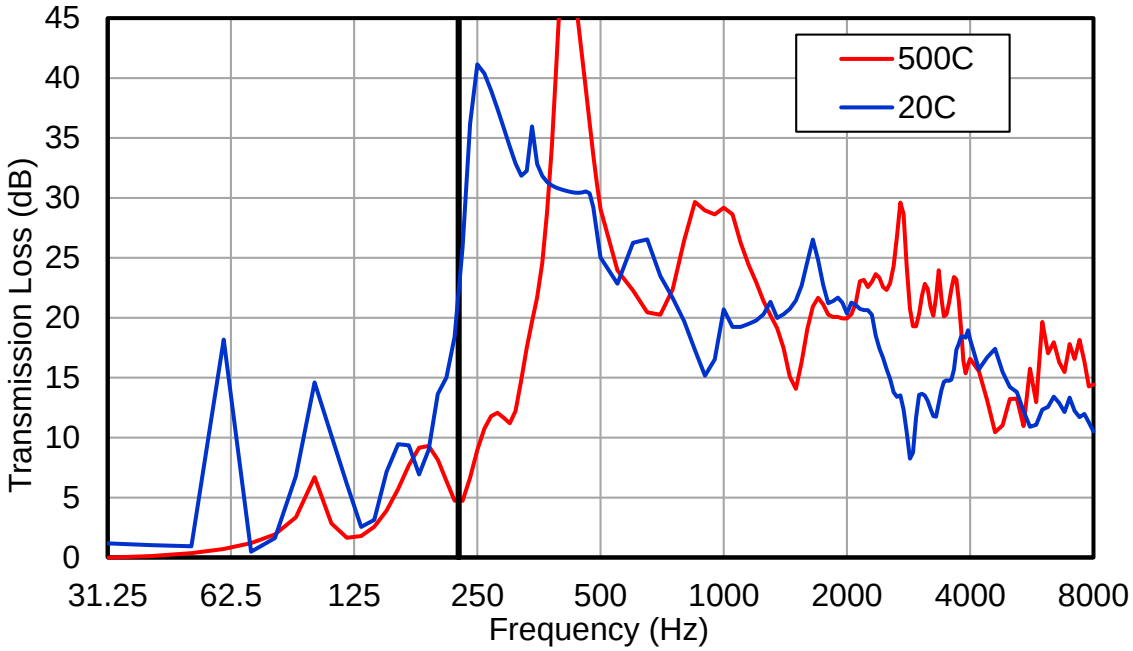

Figure 6.14 TL comparison between 20°C and 500°C.

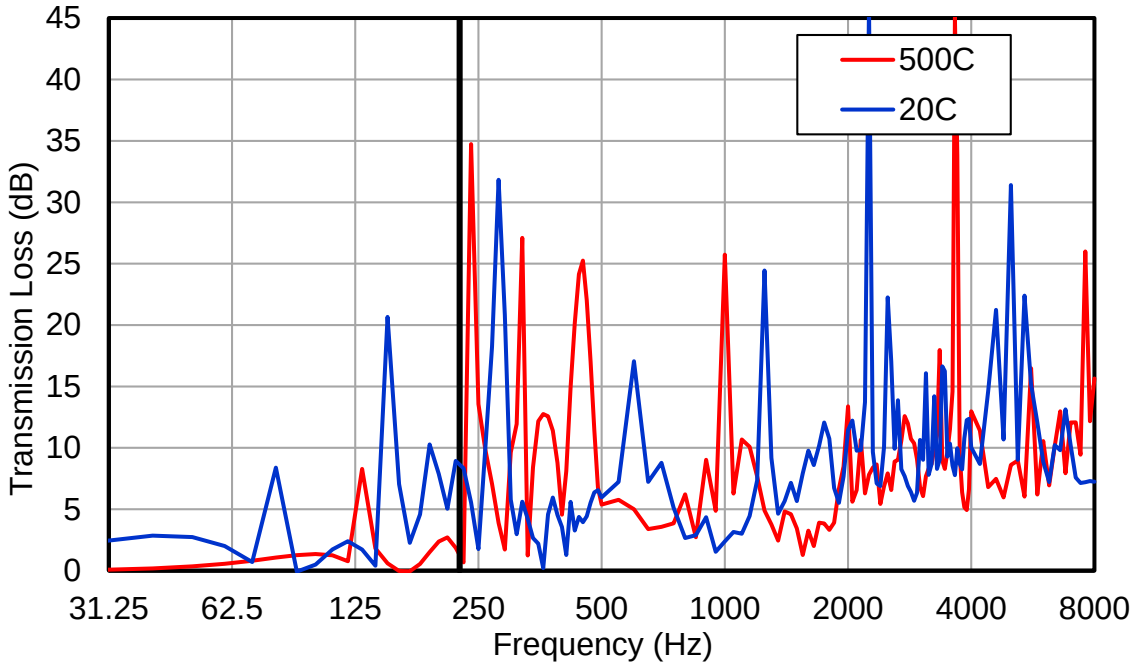

Figure 6.15 TL comparison between 20°C and 500°C.

6.3.4 Effect of non-symmetric design

The tuned dissipative silencer shown in Figure 6.2 has three different cavity sizes. In order to find the benefits of using multiple sizes of cavities in a silencer design, a symmetric tuned dissipative silencer as shown in Figure 6.16, in which all cavities have the same size, is selected to compare to the original non-symmetric design. The TL comparison is shown in Figure 6.17. As expected, the symmetric design at low frequencies has only one peak frequency at around 210 Hz, while the non-symmetric design does provide the attenuation at two more target frequencies at low frequencies. However, the spectrum of attenuation near the target frequency for the symmetric design is wider and the amplitude of attenuation is higher. Above 500 Hz, the performance of both designs is about the same.

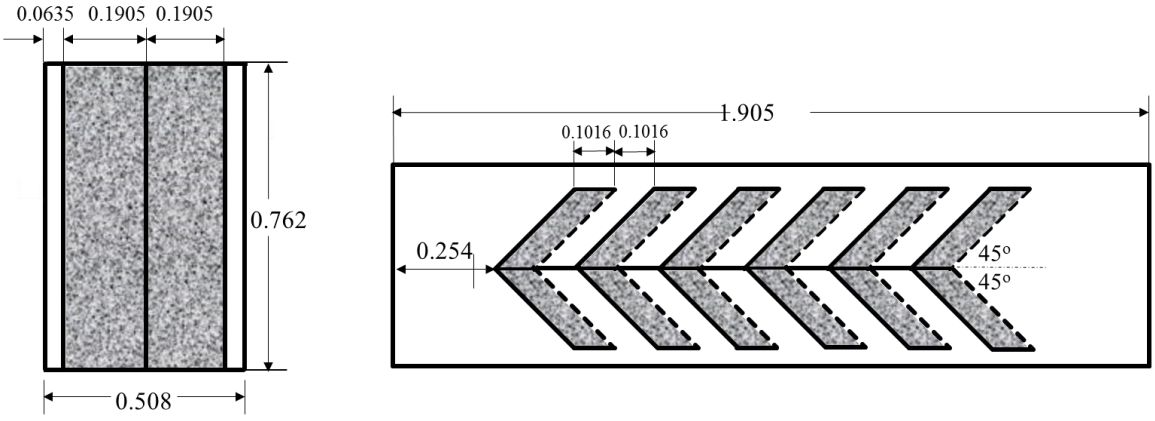

Figure 6.16 A symmetric tuned dissipative silencer (Unit: m).

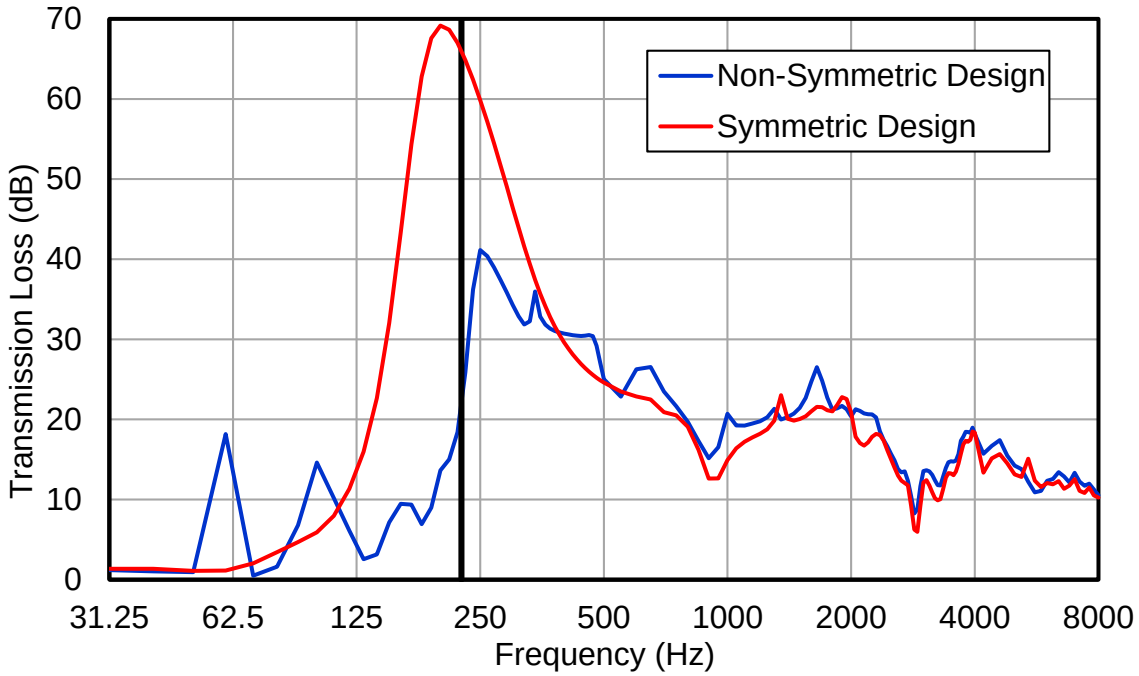

Figure 6.17 TL comparison between non-symmetric and symmetric design.

6.4 Summary

Tuned dissipative silencers are commonly used in the power generation industry to attenuate the broadband noise while suppressing tonal noise. In this chapter, a two dimensional first-mode semi-analytical method is proposed to determine the TL of the dissipative silencer. Given the large size and complex configuration, it is time consuming to model and calculate the TL of the tuned dissipative silencer using 3D FEM or BEM. Therefore, the proposed semi-analytical method can play an important role in the initial design stage by providing a quick assessment of the TL below the plane-wave cutoff frequency. The proposed semi-analytical method matches very well with the BEM and the FEM/AML below the cutoff, and can still provide a decent approximate solution slightly above the cutoff.

To better understand the performance of the tuned dissipative silencer, case study is performed by using the BEM. It is found that the locally reacting modeling of the sound absorbing material is more efficient and it can also provide a similar result compared to the more complex bulk-reacting modelling method. Thanks to the sound absorbing material, the tuned dissipative silencer is able to increase the bandwidth of the attenuation spectrum around the target frequencies, and thus it can accommodate variations in the operating temperature. If there are multiple tonal components in the noise spectrum, several different sizes of cavities can be included in the design to achieve multiple peak frequencies.

Chapter 7 CONCLUSIONS AND RECOMMENDATIONS FOR FUTURE RESERACH

The impedance-to-scattering matrix method is developed for large silencer analysis in this dissertation, which includes a point collocation-based approach and an integral-based approach. Large bar silencers and tuned dissipative silencers are investigated by the BEM in conjunction with the proposed impedance-to-scattering matrix method, and a semi-analytical solution is also developed to quickly assess the performance of tuned dissipative silencers.

7.1 Point collocation-based impedance-to-scattering matrix method

Chapter 2 and Chapter 3 derive the scattering matrix from the BEM impedance matrix for large single-inlet/single-outlet and multi-inlet/multi-outlet silencers, respectively, based on the point collocation approach.

For single-inlet/single-outlet silencers, the derivations are presented for three commonly used inlet/outlet configurations: axisymmetric, non-axisymmetric circular and rectangular. TL above the plane-wave cutoff frequency is defined by assuming a single unit incident plane wave at the inlet and an anechoic termination at the outlet. The proposed method is validated by comparing to available analytical solutions or experimental data. It is also found that adding more evanescent modes barely changes the TL curve.

For large multi-inlet/multi-outlet silencers, it is observed that the scattering matrix of a one-inlet/two-outlet silencer is the same as that of the flipped two-inlet/one-outlet silencer, and the only thing that needs to change is the input from (1,0,0..),

(1,0,00..) and (0,0,0,…) to (0,0,..), (0,0,..) and (1,0,0..). The proposed method is first compared to the lumped impedance matrix method for small mufflers below the plane-wave cutoff. For large silencers, the FEM/AML method is used to validate the proposed method above the plane-wave cutoff.

Recommendations for future work in this area include:

1. Experimental verifications are recommended to further validate the proposed method for large silencers. Since IL is very close to TL for highly absorptive silencers and is easier to measure, comparing the TL from the BEM to the measured IL can further validate the proposed method.
2. More test cases are needed to check if the TL for a two-inlet/one-outlet silencer is identical to the TL of the flipped one-inlet/two-outlet counterpart above the plane-wave cutoff.

7.2 Integral-based impedance-to-scattering matrix method

Chapter 4 demonstrates that the BEM impedance matrix can also be converted to the scattering matrix by using the reciprocal identity integral. Each reciprocal identity integral equation couples a BEM solution with a random boundary condition set at the inlet and outlet to the analytical modal expansion. The motivation to develop this integral-based method is that the collocation-based method always has the uncertainties associated with the “optimal” collocation locations. The integral-based method does not need a collocation point and theoretically can be more stable and accurate.

A few test cases are used to compare the collocation-based method to the integral-based method. It is found that the collocation-based method has the same accuracy and stability as the integral-based method. However, the integral-based method is more computationally intensive due to the need to carry out additional surface integration. Nonetheless, the integral-based method can always serve as a benchmark solution to validate the collocation-based method.

7.3 Bar silencers

Chapter 5 extends the impedance-to-scattering matrix method to large silencers with irregular inlet and outlet configurations. The 2-D FEM is used to extract the cross-sectional modes of the inlet and outlet first, and then the numerical modes are used to expand sound pressure and particle velocity in the impedance-to-scattering matrix method. The proposed method is validated by available analytical/numerical solutions and measurement data. A case study on a triangular unit isolated from a shifted lattice arrangement of round bars is also performed.

The next part of Chapter 5 introduces the Redheffer's star product for combining the scattering matrices of multiple subsystems in series connection. The scattering matrix is a preferred output format than the BEM impedance matrix because it is a system property and is mesh-independent.

The final part of Chapter 5 develops three methods for the determination of TL in one-third octave and octave bands. All three methods are valid for the TL conversion below the plane-wave cutoff frequency at the inlet and outlet, and the direct conversion method is also valid above the plane-wave cutoff frequency.

Several improvements can be done in the future:

1. More irregular inlet and outlet configurations can be tested.
2. Optimization on different bar arrangements can be performed.

7.4 Tuned dissipative silencers

Chapter 6 presents a two-dimensional first-mode semi-analytical solution to determine the TL of tuned dissipative silencers. The semi-analytical solution agrees very well with the 3D BEM solution and the FEM/AML solution below the plane-wave cutoff frequency. The 2D semi-analytical solution can be a useful analysis tool for tuned dissipative silencers in their initial design stage, and it can also serve as a validation tool for the 3D BEM at low frequencies.

A case study on the tuned dissipative silencers is performed using the BEM. It is found that the tuned dissipative silencers can provide broadband noise attenuation while suppressing the tonal noise at low frequencies. With the help of the sound absorbing material, the tuned dissipative silencers can accommodate variations of the operating temperature.

At this point, the semi-analytical solution still requires the BEM to provide two impedance matrices for the inlet and outlet transition ducts. In the future, these two impedance matrices may be approximated by an analytical solution.

APPENDIX NUMERICAL DETERMINATION OF TRANSFER IMPEDANCE

With reference to Figure A.1, a small perforate sample is placed inside a "virtual impedance tube" with an anechoic termination. The wall thickness *t* and the hole spacing *d* of the sample are fully modeled in the BEM. A true anechoic termination is difficult to achieve in the lab, but it is very easy to apply in the numerical model. A unit-amplitude velocity is prescribed at the inlet as the source to drive the virtual measurement system.

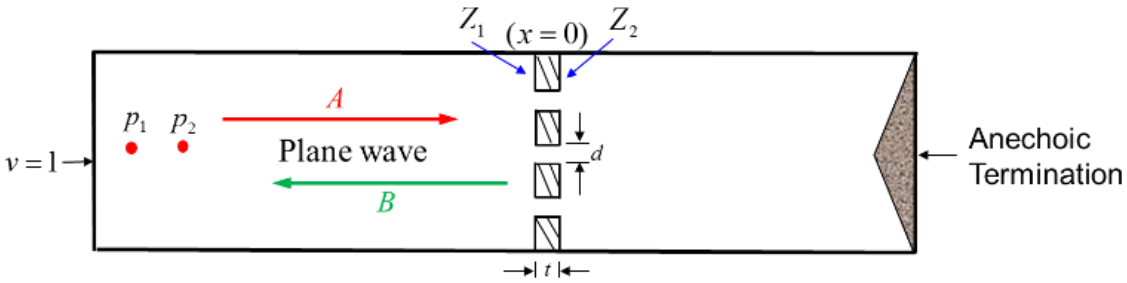

Figure A.1 A perforate sample in a "virtual impedance tube".

According to the plane-wave theory, the sound pressure p and the particle velocity v in the x direction (positive to the right) are

$$p = Ae^{-jkx} + Be^{jkx} \tag{A.1}$$

$$v = (1/\rho c)(Ae^{-jkx} - Be^{jkx}) \tag{A.2}$$

where *A* and *B* are the complex amplitudes of the incident and reflected waves, respectively, *k* is the wavenumber, ρ is the mean density, *c* is the speed of sound, and $j = \sqrt{-1}$. On the front face of the sample, the acoustical impedance is

$$Z_1 = \frac{p}{u} = \rho c(A+B)/(A-B) \tag{A.3}$$

if x=0 is set there. On the back side of the sample, the acoustical impedance is simply the characteristic impedance due to the anechoic termination. In other words,

$$Z_2 = \rho c \tag{A.4}$$

Therefore, the transfer impedance Z_{tr} of the perforate sample is

$$Z_{tr} = Z_1 - Z_2 = \rho c((A+B)/(A-B) - 1) \tag{A.5}$$

The two complex amplitudes, *A* and *B*, can be determined by placing two field points in the BEM model. Let p_1 and p_2 be the sound pressures of the two field points shown in Figure A.1. Use Equation A.1 twice to get

$$p_1 = Ae^{-jkx_1} + Be^{jkx_1} \tag{A.6}$$

$$p_2 = Ae^{-jkx_2} + Be^{jkx_2} \tag{A.7}$$

The matrix form of two equations above is

$$\begin{Bmatrix} p_1 \\ p_2 \end{Bmatrix} = \begin{bmatrix} e^{-jkx_1} & e^{jkx_1} \\ e^{-jkx_2} & e^{jkx_2} \end{bmatrix} \begin{Bmatrix} A \\ B \end{Bmatrix} \tag{A.8}$$

After that, the two unknowns *A* and *B* can be solved by a simple matrix inverse:

$$\begin{Bmatrix} A \\ B \end{Bmatrix} = \begin{bmatrix} e^{-jkx_1} & e^{jkx_1} \\ e^{-jkx_2} & e^{jkx_2} \end{bmatrix}^{-1} \begin{Bmatrix} p_1 \\ p_2 \end{Bmatrix} \tag{A.9}$$

With *A* and *B* solved, the transfer impedance Z_{tr} of the perforate sample is calculated by Equation A.5. This transfer impedance can then be used later in the muffler BEM model that uses the same perforate pattern.

The first test case is a straight-through perforated tube muffler as shown in Figure A.2. The details of the perforated tube are given below. The hole diameter (d_h) is 4.98 mm, the wall thickness (t) is 0.9 mm, the distances between two neighboring holes are b=15.13 mm and h=15.54 mm, respectively, and the porosity (σ) is 8.4%. The total number of holes is 170.

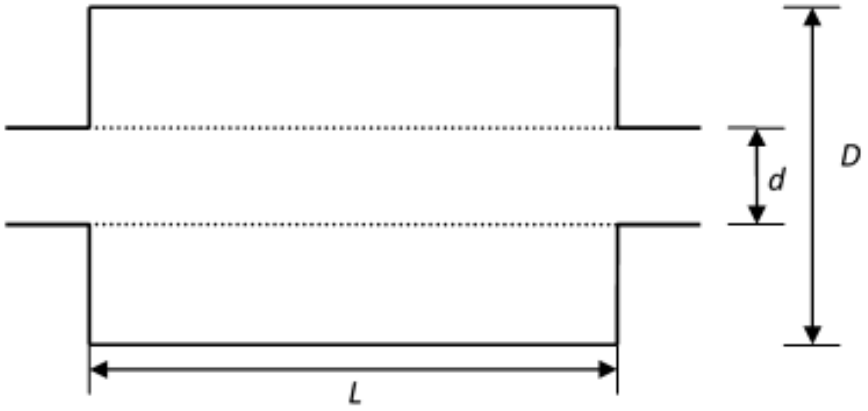

Figure A.2 Straight-through perforated tube muffler test case.

(L=257.2 mm, d=49 mm, D =164.4 mm).

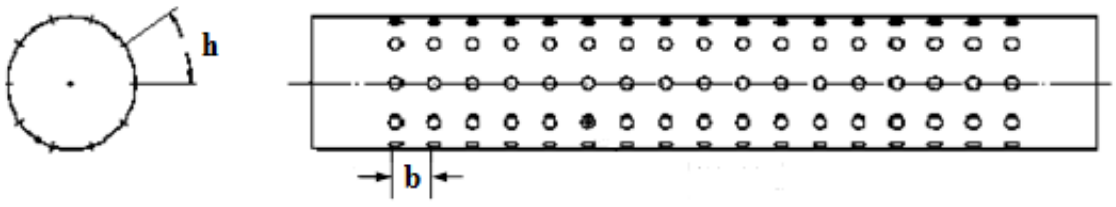

Figure A.3 Definition of *b* and *h*.

In addition to the transfer impedance to model the perforate, we also want to see if a detailed 3D modeling can produce a decent result. After all, our proposed method is based on the same detailed 3D modeling concept, only on a much smaller scale. There are two different kinds of detailed 3D modeling techniques in BEM. The first technique is to model the wall thickness of the perforated tube, which requires two layers of meshes with one on each side of the thin tube (0.9 mm thickness), and a detailed hole modeling with a side mesh along the depth; the second technique is a reduced version that ignores the wall thickness of the tube, but still models every circular hole in a 2D fashion. Figure A.4 and A.5 show the BEM mesh of the detailed 3D modeling with wall thickness. Due to the rotational symmetry nature of this muffler, only a small sector needs to be modeled. The reduced zero-thickness BEM mesh is similar to the one shown in Figure A.4 except that there is only one layer of mesh placed on the mid surface of the perforated tube.

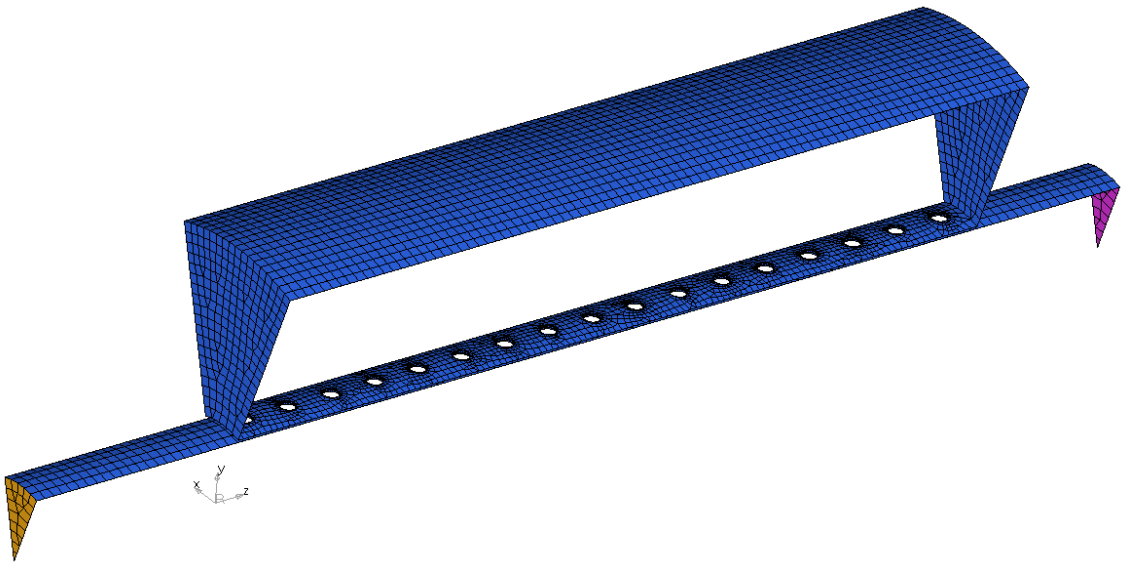

Figure A.4 BEM mesh for the detailed 3D modeling of the muffler.

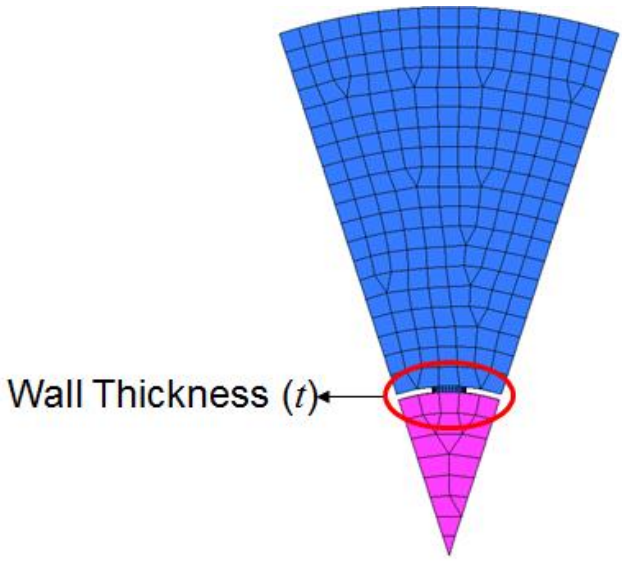

Figure A.5 Side view of the BEM mesh that shows the wall thickness.

To numerically “measure” the transfer impedance, we use the virtual impedance tube setup as demonstrated in Figure A.1. A 75.6mm X 77mm rectangular perforated plate (0.9 mm thickness) is placed in the middle of an 800.9 mm long duct with the same rectangular cross section. The perforate sample has the same porosity and the same perforate pattern as the real perforated tube, except that it is a flat sample without any curvature. A BEM mesh that models the 800.9 mm long duct along with the perforated sample is used to calculate the sound pressures at the two field points shown in Figure A.1. The exact locations of the two field points are not important as long as they are away from the sample to avoid any near-field 3D effect. The (dimensioned) transfer impedance is then calculated by Equation A.5 and sent to the muffler BEM model to determine the TL of the muffler. As one can see, the entire procedure requires two BEM models, one for the measurement setup, and the other for the muffler. Fortunately, the

measurement setup is a small-scale model, and its transfer impedance can be reused in other muffler designs as long as they use the same perforate pattern.

Figure A.6 compares the TL results from the proposed method, the detailed 3D model with wall thickness, and the detailed 3D modeling without wall thickness, to the experimental data. As we can see from the figure, both the proposed method and the detailed 3D modeling with wall thickness match the experimental result very well. The zero-thickness detailed 3D modeling (using only one layer of "T' elements on the tube) falls short at high frequencies.

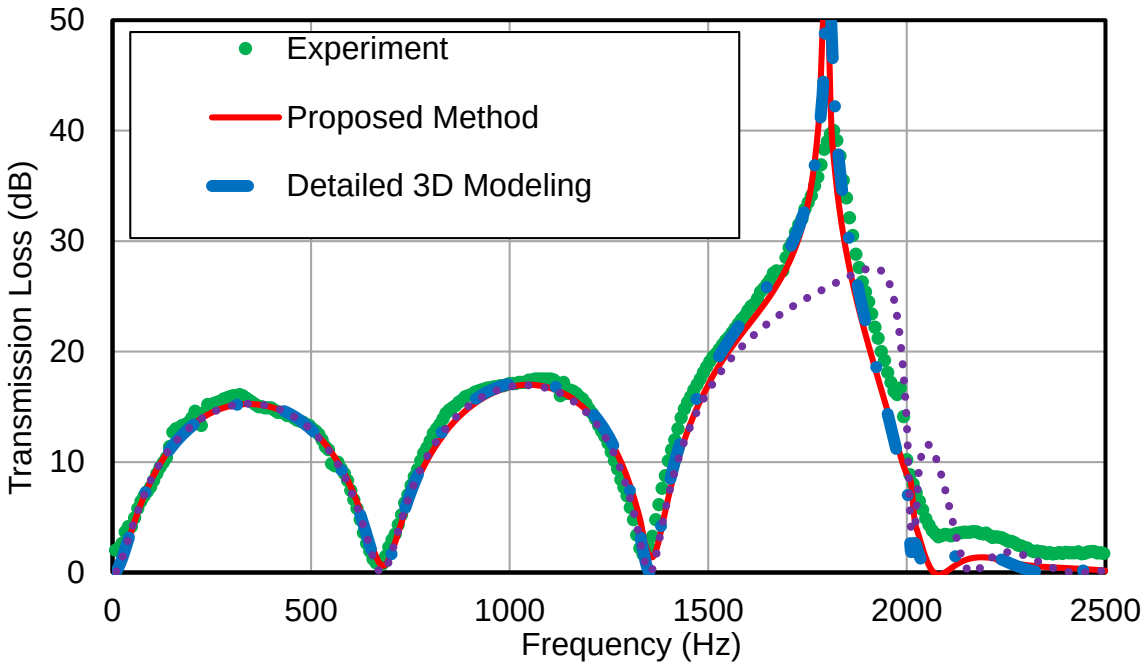

Figure A.6 Performance of the proposed method in test case 1 (circular holes).

In the second test case, we replace each circular hole on the perforated tube by an 8mm X 2.5mm rectangular slot, as shown in Figure A.7. The 8 mm length is arranged along the circumferential direction and the 2.5 mm width is along the axial

direction. The resulting porosity (σ) is 8.6%. The rest of the dimensions, including wall thickness, b, and h, remain the same as in the first test case.

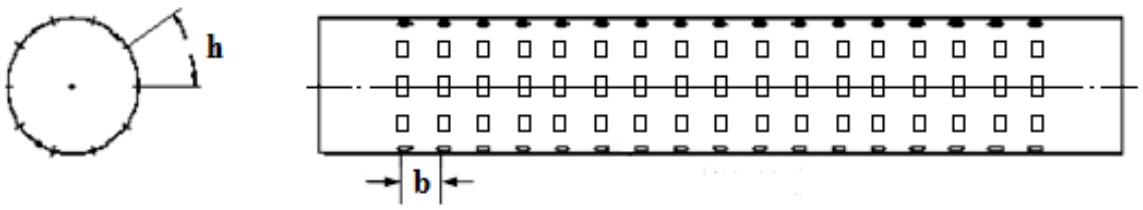

Figure A.7 Perforated tube with rectangular slots.

Figure A.8 shows the comparison of the proposed method along with the zero-thickness detailed 3D modeling to the benchmark solution (detailed 3D modeling with wall thickness). As expected, the proposed method matches the benchmark solution very well because it is basically based on the same 3D modeling concept, but implemented in an indirect, two-step procedure. The zero-thickness detailed 3D modeling falls off at high frequencies, which is the same as the first test case.

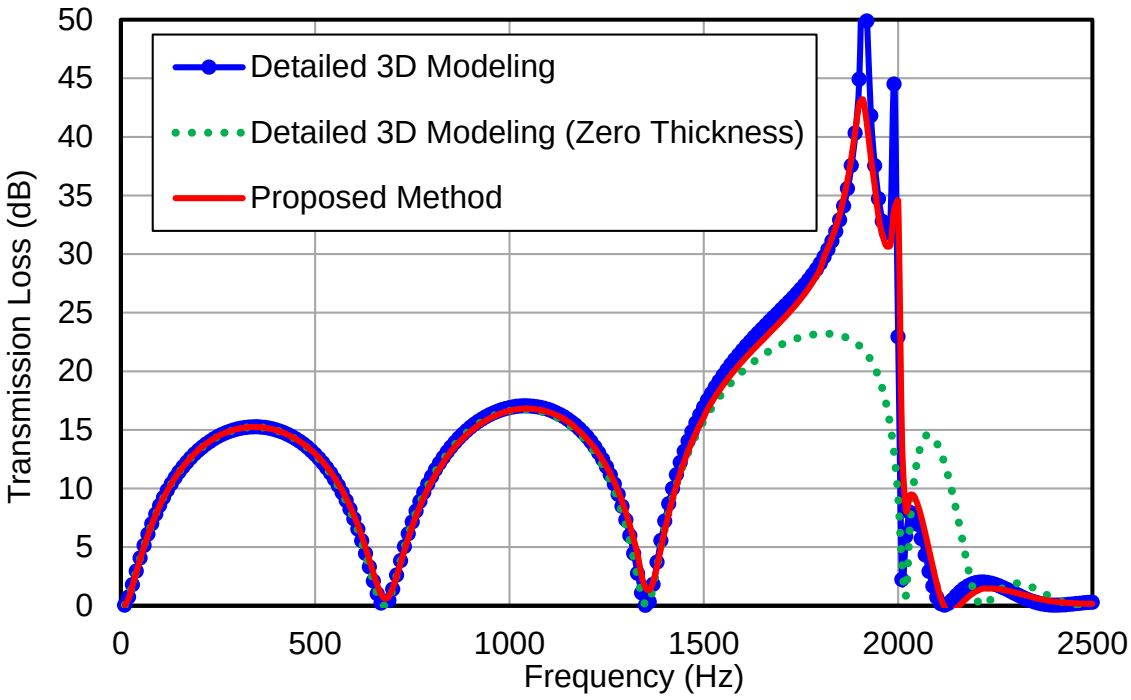

Figure A.8 Performance of the proposed method in test case 2 (rectangular slots).

A simple numerical determination of the transfer impedance of perforated tube is developed to deal with the situation when existing empirical formulas cannot be used with full confidence. The resulting transfer impedance data can also be reused in other designs as long as they use the same perforate pattern. The proposed indirect, two-step procedure can easily match the full-blown 3D modeling of the whole muffler. Therefore, it is recommended to model the perforated tube by determined transfer impedance instead of a 3D detailed modeling on the whole muffler, using either the BEM or the FEM.

REFERENCES

L. Bernek, I. Vér, (2006). Noise and Vibration Control Engineering: Principles and Applications, Wiley.

M.L. Munjal, (2014). Acoustic of Duct and Mufflers, John Wiley & Sons, New York.

H.P. Wallin, U. Carlsson, M. Åbom, H. Bodén, and R. Glav, (2012). Sound and Vibration, Marcus Wallenburg Laboratoriet.

D.A. Harris, (1991). Silencers, In: Harris D.A. (eds) Noise Control Manual. Springer, Boston, MA.

D. Potente, (2005). “General design principles for an automotive muffler”. In Proceedings of ACOUSTICS, 153-158.

T. W. Wu, P. Zhang and C. Y. R. Cheng, (1998). "Boundary element analysis of mufflers with an improved method for deriving the four-pole parameters," Journal of Sound and Vibration, **217**(4), 767-779.

A. Selamet and P. M. Radavich, (1997). “The effect of length on the acoustic attenuation performance of concentric expansion chambers: an analytical, computational and experimental investigation”, Journal of Sound and Vibration, **201**(4), 407-426.

A. D. Pierce, (1981). Acoustics: an introduction to its physical principles and applications (Vol. 678), McGraw-Hill, New York.

G. Lou, T. W. Wu and C. Y. R. Cheng, (2003). “Boundary element analysis of packed silencers with a substructuring technique”, Engineering Analysis with Boundary Elements, **27**(7), 643-653.

T. W. Wu and G. C. Wan, (1996). “Muffler performance studies using a direct mixed-body boundary element method and a three-point method for evaluating transmission loss”, Journal of Vibration and Acoustics, **118**(3), 479-484.

T. W. Wu, C. Y. R. Cheng and P. Zhang, (2002). “A direct mixed-body boundary element method for packed silencers”, The Journal of the Acoustical Society of America, **111**(6), 2566-2572.

C. Jiang, T. W. Wu and C. Y. R. Cheng. (2010). “A single-domain boundary element method for packed silencers with multiple bulk-reacting sound absorbing materials”, Engineering Analysis with Boundary Elements, **34**(11), 971-976.

T. W. Wu, G. Lou and C. Y. R Cheng, (2000). “BEM analysis of exhaust network systems using the impedance matrix synthesis”, WIT Transactions on Modelling and Simulation, 26.

A. Cummings and R. J. Astley, (1996). “Finite element computation of attenuation in bar-silencers and comparison with measured data”, Journal of Sound and Vibration, **196**(3), 351-369.

F.P. Mechel, (2002). Formulas of acoustics, Springer Science & Business Media.

P. Wang and T. W. Wu, (2015). “BEM analysis of large tuned dissipative silencers and bar silencers”, In INTER-NOISE and NOISE-CON Congress and Conference Proceedings (Vol. 250, No. 2, pp. 4767-4776), Institute of Noise Control Engineering.

C. Y. R. Cheng, and A. F. Seybert (1987). “Recent applications of the boundary element method to problems in acoustics”, SAE Technical Paper.

A. F Seybert and T. W. Wu, (1998). Acoustic modeling: Boundary element methods, Wiley, New York.

Z. L. Ji, (2010). “Boundary element acoustic analysis of hybrid expansion chamber silencers with perforated facing”, Engineering Analysis with Boundary Elements, **34**(7), 690-696.

K. S. Peat, (1982). “Evaluation of four-pole parameters for ducts with flow by the finite element method”, Journal of Sound and Vibration, **84**(3), 389-395.

K. S. Peat and K. L. Rathi, (1995). “A finite element analysis of the convected acoustic wave motion in dissipative silencers”, Journal of Sound and Vibration, **184**(3), 529-545.

T. Tsuji, T. Tsuchiya and Y. Kagawa, (2002). “Finite element and boundary element modelling for the acoustic wave transmission in mean flow medium”, Journal of Sound and Vibration, **255**(5), 849-866.

R.Barbieri and N. Barbieri, (2006). “Finite element acoustic simulation based shape optimization of a muffler”, Applied Acoustics, **67**(4), 346-357.

A. Cummings and N. Sormaz, (1993). “Acoustic attenuation in dissipative splitter silencers containing mean fluid flow”, Journal of Sound and Vibration, **168**(2), 209–227

K. U. Ingard, (1994). “Notes on Sound Absorption Technology”, Poughkeepsie, NY: Noise Control Foundation.

S.K. Kakoty and V.K. Roy, (2002). “Bulk reaction modeling of ducts with and without mean flow”, Journal of the Acoustical Society of America **112**(1), 75–83.

R. Kirby, (2003). “Transmission loss predictions for dissipative silencers of arbitrary cross section in the presence of mean flow”, The Journal of the Acoustical Society of America, **114**(1), 200-209.

R. Kirby and J. B. Lawrie, (2005). “A point collocation approach to modelling large dissipative silencers”, Journal of sound and vibration, **286**(1), 313-339.

J. B. Lawrie and R. Kirby, (2006). “Mode-matching without root-finding: Application to a dissipative silencer”, The Journal of the Acoustical Society of America, **119**(4), 2050-2061.

R. Kirby, (2009). “A comparison between analytic and numerical methods for modeling automotive dissipative silencers with mean flow”, Journal of Sound and Vibration, **325**(3), 565-582.

R. Kirby, K. Amott, P. T. Williams and W. Duan, (2014). “On the acoustic performance of rectangular splitter silencers in the presence of mean flow”, Journal of Sound and Vibration, **333**(24), 6295-6311.

L. Zhou, T. W. Wu, D. W. Herrin and C. Y. R. Cheng, (2012). “Analytical and BEM solutions of sound attenuation in bar silencers”, In INTER-NOISE and NOISE-CON Congress and Conference Proceedings (Vol. 2012, No. 4, pp. 7737-7748), Institute of Noise Control Engineering.

L. Zhou, (2013). “Assessing and mitigating airborne noise from power generation equipment”, University of Kentucky.

L. Zhou, T. W. Wu, K. Ruan and D. W. Herrin, (2016). A reciprocal identity method for large silencer analysis. Journal of Sound and Vibration, **364**, 165-176.

P. Wang and T. W. Wu, (2014). “Impedance-to-scattering matrix method for silencer analysis”, In INTER-NOISE and NOISE-CON Congress and Conference Proceedings (Vol. 248, No. 2, pp. 453-460), Institute of Noise Control Engineering.

P. Wang and T. W. Wu, (2016). “Impedance-to-scattering matrix method for large silencer analysis using direct collocation”, Engineering Analysis with Boundary Elements, **73**, 191-199.

S. Marburg and B. Nolte, (2008). Computational acoustics of noise propagation in fluids: finite and boundary element methods (Vol. 578), Springer, Berlin.

R. H. Dicke, (1947). “A computational method applicable to microwave networks”, Journal of Applied Physics, **18**(10), 873-878.

M. Åbom, (1991). “Measurement of the scattering-matrix of acoustical two-ports,” Mechanical Systems and Signal Processing, **5**(2), 89-104.

R. Redheffer, (1962). “On the relation of transmission-line theory to scattering and transfer”, Studies in Applied Mathematics, **41**(1-4), 1-41.

F. P. Mechel, (1990). “Theory of baffle-type silencers”, Acta Acustica united with Acustica, **70**(2), 93-111.

J. Allard and N. Atalla, (2009). “Propagation of sound in porous media: modelling sound absorbing materials”, John Wiley & Sons, New York.

M. E. Delany and E. N. Bazley, (1970). “Acoustical properties of fibrous absorbent materials”, Applied acoustics, **3**(2), 105-116.

X. Hua, (2013). “Advanced Studies on Transfer Impedance with Application to After-treatment Devices and Micro-perforated Panel Absorbers”, University of Kentucky.

P. Bonfiglio and F. Pompoli, (2009). “An Acoustical Finite Element Model of Perforated Elements”, In Proceedings of the COMSOL Conference 2009.

P. Wang, J. Li and T. W. Wu, (2015). “Numerical Determination of Transfer Impedance for Perforates”, SAE International Journal of Passenger Cars-Mechanical Systems, **8**(2015-01-2312), 1003-1008.

J. W. Sullivan and M. J. Crocker, (1978). “Analysis of concentric-tube resonators having unpartitioned cavities”, The Journal of the Acoustical Society of America, **64**(1), 207-215.

A. Selamet, M. B. Xu, I. J. Lee and N. T. Huff, (2004). “Analytical approach for sound attenuation in perforated dissipative silencers”, The Journal of the Acoustical Society of America, **115**(5), 2091-2099.

A. Selamet, Z. L. Ji and P. M. Radavich, (1998). “Acoustic attenuation performance of circular expansion chambers with offset inlet/outlet: II. Comparison with experimental and computational studies”, Journal of Sound and Vibration, **213**(4), 619-641.

A. Selamet and Z. L. Ji, (2000). “Acoustic attenuation performance of circular expansion chambers with single-inlet and double-outlet”, Journal of sound and vibration, **229**(1), 3-19.

F.D. Denia, L. Baeza, J. Albelda and F.J. Fuenmayor, (2003). "Acoustic behavior of elliptical mufflers with single-inlet and double-outlet." In Proceedings of the Tenth International Congress on Sound and Vibration, **6**, 3287-3294.

C. J. Wu, X. J. Wang and H. B. Tang, (2008). “Transmission loss prediction on a single-inlet/double-outlet cylindrical expansion-chamber muffler by using the modal meshing approach”, Applied Acoustics, **69**(2), 173-178.

M. L. Munjal, (1987). “A simple numerical method for three-dimensional analysis of simple expansion chamber mufflers of rectangular as well as circular cross-section with a stationary medium”, Journal of Sound and vibration, **116**(1), 71-88.

C. Jiang, T.W. Wu and C.Y.R. Cheng, (2005). "Evaluation of transmission loss using the boundary element method for mufflers with two inlets." The Journal of the Acoustical Society of America, **118**(3), 1919.

A. Mimani and M.L. Munjal, (2012). "Acoustical analysis of a generaln of multi-port elements—an impedance matrix approach." International Journal of Acoustics and Vibration, **17**(1), 23.

X. Hua, C. Jiang, D.W. Herrin and T.W. Wu, (2014). "Determination of transmission and insertion loss for multi-inlet mufflers using impedance matrix and superposition approaches with comparisons." Journal of Sound and Vibration, **333**(22), 5680-5692.

P. Wang, T. W. Wu and D. W. Herrin, (2016). “Boundary Element Analysis of Large Two-Inlet Silencers”, In INTER-NOISE and NOISE-CON Congress and Conference Proceedings.

P. Wang, K. Ruan, T. W. Wu and D. W. Herrin, (2017). “BEM Analysis of Large Three-Port Silencers with FEM-AML Validation”, In INTER-NOISE and NOISE-CON Congress and Conference Proceedings.

J. P. Berenger, (1994). “A perfectly matched layer for the absorption of electromagnetic waves”, Journal of computational physics, **114**(2), 185-200.

C. K. Tam, L. Auriault and F. Cambuli, (1998). “Perfectly matched layer as an absorbing boundary condition for the linearized Euler equations in open and ducted domains”, Journal of Computational Physics, **144**(1), 213-234.

A. Bermúdez, L. Hervella-Nieto, A. Prieto and R. Rodrı, (2007). “An optimal perfectly matched layer with unbounded absorbing function for time-harmonic acoustic scattering problems”, Journal of Computational Physics, **223**(2), 469-488.

N. A. Nilsson and S. Soderqvist, (1983). “The bar silencer-improving attenuation by constricted two-dimensional wave propagation”, In INTER-NOISE and NOISE-CON Congress and Conference Proceedings (Vol. 1983, No. 4, pp. 351-354). Institute of Noise Control Engineering.

R. Kirby, P. Williams and J. Hill, (2012). “A comparison between the performance of different silencer designs for gas turbine exhaust systems”, In Acoustics 2012.

R. Kirby, P. Williams and J. Hill, (2014). “A three dimensional investigation into the acoustic performance of dissipative splitter silencers”, The Journal of the Acoustical Society of America, **135**(5), 2727-2737.

L. Yang, P. Wang and T. W. Wu, (2017). “Boundary element analysis of bar silencers using the scattering matrix with two-dimensional finite element modes”, Engineering Analysis with Boundary Elements, **74**, 100-106.

Z. Fang and Z. L. Ji, (2013). “Acoustic attenuation analysis of expansion chambers with extended inlet/outlet”, Noise Control Engineering Journal, **61**(2), 240-249.

Y. B. Park, H. D. Ju, and S. B. Lee, (2009). “Transmission loss estimation of three-dimensional silencers by system graph approach using multi-domain BEM”, Journal of Sound and Vibration, **328**(4), 575-585.

L. Yang and Z. L. Ji, (2016). “Acoustic attenuation analysis of network systems by using impedance matrix method”, Applied Acoustics, **101**, 115-121.

G. Kudernatsch, (2000). “Combustion turbine exhaust systems-Low frequency noise reduction”, In Proc. INTER-NOISE.

L. H. Bell and D. H. Bell, (1993). Industrial Noise Control: Fundamentals and Applications, Second Edition, CRC Press.

F. P. Mechel, (1998). Schallabsorber, Vol. III, Ch. 32: Ducts with cross-layered lining and pine tree silencers. Hirzel, Stuttgart.

A. Selamet, M. B. Xu, I. J. Lee and N. T. Huff, (2005). “Helmholtz resonator lined with absorbing material”, The Journal of the Acoustical Society of America, **117**(2), 725-733.

C. Q. Howard and R. A. Craig, (2014). “Noise reduction using a quarter wave tube with different orifice geometries”, Applied Acoustics, **76**, 180-186.

X. Wang and C. M. Mak, (2012). “Acoustic performance of a duct loaded with identical resonators”, The Journal of the Acoustical Society of America, **131(**4), EL316-EL322.

C. Kittel, (1986). Introduction to Solid State Physics, 6th ed, John Wiley & Sons, New York.

S. H. Seo and Y. H. Kim, (2005). “Silencer design by using array resonators for low-frequency band noise reduction”, The Journal of the Acoustical Society of America, **118**(4), 2332-2338.

J. M. Coulon, N.Atalla and A. Desrochers, (2016). Optimization of concentric array resonators for wide band noise reduction. Applied Acoustics, **113**, 109-115.

M. J. Crocker (Ed.), (2007). Handbook of noise and vibration control, John Wiley & Sons.

Z. Tao, D. W. Herrin and A. F. Seybert, (2003). “Measuring bulk properties of sound-absorbing materials using the two-source method”, (No. 2003-01-1586), SAE Technical Paper.

H. Utsuno, T. W. Wu, A. F. Seybert and T. Tanaka, (1990). “Prediction of sound fields in cavities with sound absorbing materials”, AIAA journal, **28**(11), 1870-1876.

D. A. Bies, C. H. Hansen and G. E. Bridges, (1991). “Sound attenuation in rectangular and circular cross-section ducts with flow and bulk-reacting liner”, Journal of sound and vibration, **146**(1), 47-80.

VITA

Peng Wang was born in Zhejiang, China. He studied in the College of Power and Energy Engineering at Harbin Engineering University, and received the degree of Bachelor of Science in 2012. In August 2013, he was admitted in the PhD program in Mechanical Engineering at the University of Kentucky. His research areas include engineering acoustics and noise and vibration control. He was awarded Best Student Paper Award and Hallberg Foundation Award in Noise-Con 2014. In the year of 2016, he received Leo Beranek Student medal for Excellence in the Study of Noise Control from Institution of Noise Control Engineering (INCE), and also received Michiko So Finegold Award in Noise-Con 2016. In 2017, he was awarded Outstanding Graduate Student of the Department of Mechanical Engineering. During his four years in the PhD program, he has published 3 journal papers and 8 conference papers, and has 2 journal papers to be submitted.

Peng Wang